

NUMERICAL ASSESSMENT OF NEGATIVE SKIN FRICTION EFFECTS ON
DIAPHRAGM WALLS

A THESIS SUBMITTED TO
THE GRADUATE SCHOOL OF NATURAL AND APPLIED SCIENCES
OF
MIDDLE EAST TECHNICAL UNIVERSITY

BY

CANSU GENÇOĞLU

IN PARTIAL FULFILLMENT OF THE REQUIREMENTS
FOR
THE DEGREE OF MASTER OF SCIENCE
IN
CIVIL ENGINEERING

JANUARY 2013

Approval of the thesis:

**NUMERICAL ASSESSMENT OF NEGATIVE SKIN FRICTION EFFECTS ON
DIAPHRAGM WALLS**

submitted by **CANSU GENÇOĞLU** in partial fulfillment of the requirements for the degree of
Master of Science in Civil Engineering Department, Middle East Technical University by,

Prof. Dr. Canan Özgen
Dean, Graduate School of **Natural and Applied Sciences**

Prof. Dr. Ahmet Cevdet Yalçiner
Head of Department, **Civil Engineering**

Prof. Dr. Kemal Önder Çetin
Supervisor, **Civil Engineering Dept., METU**

Examining Committee Members

Prof. Dr. Erdal Çokça
Civil Engineering Dept., METU

Prof. Dr. Kemal Önder Çetin
Civil Engineering Dept., METU

Asst. Prof. Dr. Zeynep Gülerce
Civil Engineering Dept., METU

Asst. Prof. Dr. Nejan Huvaj Sarıhan
Civil Engineering Dept., METU

Dr. Özgür Kuruoğlu
Yüksel Proje Uluslararası A.Ş.

Date: **30.01.2013**

I hereby declare that all information in this document has been obtained and presented in accordance with academic rules and ethical conduct. I also declare that, as required by these rules and conduct, I have fully cited and referenced all material and results that are not original to this work.

Name, Last name : Cansu Gençođlu

Signature :

ABSTRACT

NUMERICAL ASSESSMENT OF NEGATIVE SKIN FRICTION EFFECTS ON DIAPHRAGM WALLS

Gençođlu, Cansu
MS, Department of Civil Engineering
Supervisor: Prof. Dr. Kemal Önder Çetin

January 2013, 114 Pages

Within the confines of this study, numerical simulations of time dependent variation of downdrag forces on the diaphragm walls are analyzed for a generic soil site, where consolidation is not completed. As part of the first generic scenario, consolidation of a clayey site due to the application of the embankment is assessed. Then two sets of diaphragm walls, with and without bitumen coating, are analyzed. For comparison purposes, conventional analytical calculation methods (i.e., rigid-plastic and elastic-plastic soil models) are also used, the results of which, establish a good basis of comparison with finite-element based simulation results. Additionally, the same generic cases are also analyzed during the stages of excavation, when diaphragm walls are laterally loaded. As the concluding remark, on the basis of time dependent stress and displacement responses of bitumen coated and uncoated diaphragm walls, it was observed that negative skin friction is a rather complex time-dependent soil-structure and loading interaction problem. This problem needs to be assessed through methods capable of modeling the complex nature of the interaction. Current analytical methods may significantly over-estimate the amount of negative skin friction applied on the system, hence they are judged to be over-conservative. However, if negative skin friction is accompanied by partial unloading as expected in diaphragm walls or piles used for deep excavations, then they may be subject to adverse combinations of axial load and moment, which may produce critical combinations expressed in interaction diagrams. Neglecting the axial force and moment interaction may produce unconservative results.

Keywords –Negative Skin Friction, Diaphragm Wall, Bitumen Coating.

ÖZ

DİYAFRAM DUVARLAR ÜZERİNDEKİ NEGATİF ÇEVRE SÜRTÜNMESİ ETKİLERİNİN NÜMERİK DEĞERLENDİRMESİ

Gençoğlu, Cansu
Yüksek Lisans, İnşaat Mühendisliği Bölümü
Tez Yöneticisi: Prof. Dr. Kemal Önder Çetin

Ocak 2013, 114 Sayfa

Bu çalışma kapsamında, diyafram duvarlar üzerinde, zamana bağlı değişkenlik gösteren ve negatif çevre sürtünmesinden kaynaklanan yüklerin nümerik simülasyonları, konsolidasyonu tamamlamamış tipik bir zemin sahası için analiz edilmiştir. İlk senaryo kapsamında, killi bir zeminde dolgu uygulaması sonucunda gelişen konsolidasyon süreci değerlendirilmiştir. Analizler iki farklı set olarak çalışılmış olup, bitümsüz ve bitümlü olmak üzere iki farklı diyafram duvar modellenmiştir. Söz konusu analiz setleri, karşılaştırma amacıyla analitik modelleme yöntemleri (rijit-plastik, elastik-plastik zemin modelleri) ile de gerçekleştirilmiş olup, nümerik simülasyon sonuçları ile iyi bir karşılaştırma temeli oluşturulmuştur. Bununla birlikte, aynı analiz setleri, diyafram duvarların kazı aşamaları sırasında yanıl olarak yüklendiği durum için de analiz edilmiştir. Sonuç olarak, bitüm kaplamalı olan ve olmayan diyafram duvarların, zamana bağlı stres ve deplasman tepkileri değerlendirildiğinde, negatif çevre sürtünmesi olayının, oldukça karmaşık, zamana bağlı zemin-yapı ve yükleme etkileşimi problemi olduğu gözlenmiştir. Bu problemin, söz konusu etkileşimlerin kompleks yapısını modelleyebilen metodlar ile değerlendirilmesi gerekmektedir. Mevcut analitik metodlar, negatif çevre sürtünmesi miktarını önemli ölçüde fazla tahmin edebilmekte olup, bu nedenle aşırı konservatif olarak değerlendirilmektedir. Bununla birlikte, negatif çevre sürtünmesi olayının, derin kazılar için kullanılan diyafram duvar veya kazıklarda olduğu gibi kısmi olarak yükün boşalttığı sistemlerde gözlenmesi durumunda, diyafram duvar veya kazıkların eksenel yük ve momentin kritik kombinasyonlarına maruz kalabileceği, dolayısıyla eksenel yük ve moment etkileşimini ihmal etmenin güvenli olmayan sonuçlar doğurabileceği değerlendirilmektedir.

Anahtar kelimeler –Negatif Çevre Sürtünmesi, Diyafram Duvar, Bitüm Kaplaması.

To My Parents
My Sister
and My Dear Sir

ACKNOWLEDGMENTS

First of all, I would like to thank my supervisor, Prof. Dr. Kemal Önder Çetin, for his guidance, advice, support and encouragement throughout the study.

I also wish to thank all members of the Geotechnical Group of Yüksel Proje Uluslararası A.Ş. for their support, intimate friendship and for creating an excellent working environment. I especially thank my colleague Volkan Üzeler and my managers Mustafa Kemal Akman, Özgür Kuruoğlu and Atilla Horoz, who have encouraged and supported me throughout the M.S. study.

I wish to express my sincere gratitude to my parents Şebnem - Muharrem Gündüz and my deary sister Birsu Gündüz for their unconditional support, love and encouragement throughout my life.

I would also like to present my special thanks to Fatma - Adil Gençoğlu and Caner Gençoğlu for their kindness, moral support and unshakable faith in me throughout this study.

Finally, I would like to thank Cihangir Gençoğlu, to whom I adore with all my heart, for holding my hand throughout the study as so he does in my life. Thank you for all the beauties you brought to my life dear... With you...

TABLE OF CONTENTS

ABSTRACT	V
ÖZ	VI
ACKNOWLEDGMENTS	VIII
TABLE OF CONTENTS	IX
LIST OF FIGURES	XI
LIST OF TABLES	XIV
CHAPTERS	1
1. INTRODUCTION	1
1.1. Purpose and Scope	1
1.2. Problem Significance	1
2. LITERATURE SURVEY	3
2.1. A Brief Review on Negative Skin Friction Phenomenon	3
2.1.1. Pile Foundations	3
2.1.2. Negative Skin Friction Phenomenon	4
2.1.3. Effects of Negative Skin Friction on Pile Foundations	6
2.1.4. Precautions to Reduce Downdrag	7
2.2. Analytical Methods to Assess a Pile Subjected to Negative Skin Friction	7
2.2.1. Rigid - Plastic Model	8
2.2.2. Elastic - Plastic Model	9
2.2.3. Numerical Iterative Approach	11
2.3. Empirical Methods to Calculate the Unit Negative Skin Friction	11
2.4. Design Approaches and Considerations for the Design of Pile Foundations Subjected to Negative Skin Resistance / Downdrag	14
3. NUMERICAL MODELLING OF NEGATIVE SKIN FRICTION PROBLEMS	23
3.1. Analysis Approach	23
3.2. Numerical Modeling Software	27
3.3. Constitutive Models	28
3.3.1. Elastic - Perfectly Plastic Model	28
3.3.2. Soft-Soil Model	31
3.3.3. Hardening Soil Model	33
3.4. Modeling Scenario and Cases	37
3.4.1. The Soil - Diaphragm Wall Model	37
3.4.1.1. Geometry and Definitions	37
3.4.1.2. Parameter Selection	38
3.4.1.2.1. Silty Sand Layer	38
3.4.1.2.2. Clay Layer	39
3.4.1.2.3. Gravelly Sand Layer	40
3.4.1.2.4. Diaphragm Wall Parameters	40
3.4.2. Analysis Scenario 1: Diaphragm Wall - Soil Interaction Model	41
3.4.2.1. Case 1: Diaphragm Wall - Soil Interaction	41
3.4.2.2. Case 2: Bitumen Coated Diaphragm Wall - Soil Interaction	43
3.4.3. Analysis Scenario 2: Diaphragm Wall - Soil Interaction Model during Excavation	45
3.4.3.1. Case 1: Diaphragm Wall - Soil Interaction during Excavation	45
3.4.3.2. Case 2: Bitumen Coated Diaphragm Wall - Soil Interaction during Excavation	47
4. SIMULATION RESULTS & DISCUSSION	51
4.1. Scenario 1: Diaphragm Wall - Soil Interaction Model	51
4.1.1. Case 1: Diaphragm Wall - Soil Interaction	51
4.1.1.1. Vertical Displacement vs. Axial Position	51
4.1.1.2. Relative Displacement vs. Vertical Position	54
4.1.1.3. Variation of Skin Friction Force Along the Pile Length	55
4.1.2. Case 2: Bitumen Coated Diaphragm Wall - Soil Interaction	56

4.1.2.1.	Vertical Displacement vs. Axial Position	56
4.1.2.2.	Relative Displacement vs. Vertical Position	59
4.1.2.3.	Variation of Skin Friction Force Along the Pile Length	60
4.2.	Scenario 2: Diaphragm Wall - Soil Interaction Model during Excavation	61
4.2.1.	Case 1: Diaphragm Wall - Soil Interaction during Excavation	61
4.2.1.1.	Vertical Displacement vs. Axial Position	61
4.2.1.2.	Relative Displacement vs. Vertical Position	64
4.2.1.3.	Variation of Skin Friction Force Along the Pile Length	65
4.2.2.	Case 2: Bitumen Coated Diaphragm Wall - Soil Interaction during Excavation	66
4.2.2.1.	Vertical Displacement vs. Axial Position	66
4.2.2.2.	Relative Displacement vs. Vertical Position	68
4.2.2.3.	Variation of Skin Friction Force Along the Pile Length	69
4.2.2.4.	Bending Moment vs. Axial Force	70
4.3.	Calculation of Negative Skin Friction by Analytical Methods	73
4.3.1.	Rigid - Plastic Model: Diaphragm Wall - Soil Interaction	75
4.3.2.	Elastic - Plastic Model: Diaphragm Wall - Soil Interaction	76
5.	SUMMARY AND CONCLUSIONS	77
5.1.	Summary	77
5.2.	Conclusions	77
	REFERENCES	79
	APPENDICES	80
	A NUMERICAL SIMULATION OUTPUTS OF ANALYSIS SCENARIO 1	81
	Case 1: Diaphragm Wall - Soil Interaction Model	81
	Case 2: Bitumen Coated Diaphragm Wall - Soil Interaction Model	87
	B NUMERICAL SIMULATION OUTPUTS OF ANALYSIS SCENARIO 2	93
	Case 1: Diaphragm Wall - Soil Interaction Model during Excavation	93
	Case 2: Bitumen Coated Diaphragm Wall - Soil Interaction Model during Excavation	104

LIST OF FIGURES

FIGURES

Figure 1: Types of bearing pile (a) Friction pile (b) End - bearing pile 3 (Tomlinson and Woodward, 2008)	3
Figure 2: Distribution of Axial Forces in a Pile (Briaud & Tucker, 1996).....	5
Figure 3: Negative Skin Friction on a Pile (Briaud & Tucker, 1996)	5
Figure 4: Settlement Profile Under a Pile Group (Briaud & Tucker, 1996).....	6
Figure 5: Negative Skin Friction on a Single Pile (Rigid Plastic Model) (L. Shaw Shong, 2002).....	8
Figure 6: Negative Skin Friction on a Single Pile (Elastic Plastic Model) (Shong, 2002).....	10
Figure 7: Adhesion factors for Driven Piles in Clay (Design and Construction of Driven Pile Foundations, 1998).....	12
Figure 8: Adhesion Values for Piles in Cohesive Soil (Design and Construction of Driven Pile Foundations, 1998).....	13
Figure 9: Negative Skin Friction Factors for Piles Driven into Soft to Firm Clays (Tomlinson and Woodward, 2008).....	14
Figure 10: Evolution of the Load Distribution in a Pile (Briaud & Tucker, 1996)	16
Figure 11: The Geological Profile of the Analyzed Soil Section	24
Figure 12: Construction of Diaphragm Wall.....	24
Figure 13: Application of Bitumen Coating	25
Figure 14: The Excavation Process (2.00 meters of Excavation at Each Step)	26
Figure 15: Application of Bitumen Coating	26
Figure 16: Application of Plates and Interfaces (PLAXIS 2D User's Manual, 2010)	27
Figure 17: Position of Nodes and Stress Points in Soil Elements (PLAXIS 2D User's Manual, 2010).....	28
Figure 18: The Basic Idea of an Elastic Perfectly Plastic Model (PLAXIS 2D User's Manual, 2010).....	29
Figure 19: The Mohr - Coulomb Yield Surface In Principal Stress Space ($c=0$) (PLAXIS 2D User's Manual, 2010)	30
Figure 20: Logarithmic Relation Between Volumetric Strain and Mean Stress (PLAXIS 2D User's Manual, 2010)	31
Figure 21: The Yield Surface of the Soft Soil Model in $p' - q$ Plane.....	32
Figure 22: Representation of the Total Yield Contour of the Soft Soil Model in Principal Stress Space (PLAXIS 2D User's Manual, 2010).....	32
Figure 23: Hyperbolic Stress-Strain Relation in Primary Loading for a Standard Drained Triaxial Test (PLAXIS 2D User's Manual, 2010).....	33
Figure 24: Successive Yield Loci for Various Constant Values of the Hardening Parameter γ^p (PLAXIS 2D User's Manual, 2010).....	35
Figure 25: The Geological Profile of the Analyzed Soil Section	37
Figure 26: The Sequence of Events for Pure Consolidation Assessment.....	42
Figure 27: The Sequence of Events for Pure Consolidation Assessment with Bitumen Application ..	44
Figure 28: Diaphragm Wall Application And Excavation Of The Site.....	45
Figure 29: The Sequence of Excavation Stages	46
Figure 30: The Sequence of Excavation Stages with Bitumen Application.....	48
Figure 31: Selected Axial Cross Sections of the Clay Layer.....	51
Figure 32: Vertical Displacement during 25 %, 40 %, 55 %, 70 % and 85 % of Consolidation Process at the Depth of 5 m.....	52
Figure 33: Vertical Displacement during 25 %, 40 %, 55 %, 70 % and 85 % of Consolidation Process at the Depth of 7 m.....	52
Figure 34: Vertical Displacement during 25 %, 40 %, 55 %, 70 % and 85 % of Consolidation Process	53
at the Depth of 9 m.....	53
Figure 35: Vertical Displacement during 25 %, 40 %, 55 %, 70 % and 85 % of Consolidation Process at the Depth of 10 m.....	53

Figure 36: Vertical Displacement during 25 %, 40 %, 55 %, 70 % and 85 % of Consolidation Process at the Depth of 11 m.....	54
Figure 37: Relative Displacement of the Wall and the Soil	54
Figure 38: Relative Displacement of the Wall and the Soil Close to Neutral Point.....	55
Figure 39: Skin Friction Force Acting on the Wall as a Function of Vertical Position of the Wall.....	55
Figure 40: The Behavior of the Skin Friction Force Acting on the Wall around the Neutral Point.....	56
Figure 41: The Axial Sections of the Clay Layer.....	56
Figure 42: Vertical Displacement during 25 %, 40 %, 55 %, 70 % and 85 % of Consolidation Process at the Depth of 5 m.....	57
Figure 43: Vertical Displacement during 25 %, 40 %, 55 %, 70 % and 85 % of Consolidation Process at the Depth of 7 m.....	57
Figure 44: Vertical Displacement during 25 %, 40 %, 55 %, 70 % and 85 % of Consolidation Process at the Depth of 9 m.....	58
Figure 45: Vertical Displacement during 25 %, 40 %, 55 %, 70 % and 85 % of Consolidation Process at the Depth of 10 m.....	58
Figure 46: Vertical Displacement during 25 %, 40 %, 55 %, 70 % and 85 % of Consolidation Process at the Depth of 11 m.....	59
Figure 47: Relative Displacement of the Wall and the Soil	59
Figure 48: Relative Displacement of the Wall and the Soil Close to Neutral Point.....	60
Figure 49: Skin Friction Force Acting on the Wall as a Function of Vertical Position of the Wall.....	60
Figure 50: The Behavior of the Skin Friction Force Acting on the Wall around the Neutral Point.....	61
Figure 51: The Axial Sections of the Clay Layer.....	61
Figure 52: Vertical Displacement during 25 % and 40 % of Consolidation Process at the Depth of 5 m	62
Figure 53: Vertical Displacement during 25 %, 40 % and 55 % of Consolidation Process at the Depth of 7 m.....	62
Figure 54: Vertical Displacement during 25 %, 40 %, 55 % and 70 % of Consolidation Process at the Depth of 9 m	63
Figure 55: Vertical Displacement during 25 %, 40 %, 55 %, 70 % and 85 % of Consolidation Process at the Depth of 11 m.....	63
Figure 56: Relative Displacement of the Fill Side of the Wall and the Soil	64
Figure 57: Relative Displacement of the Excavation Side of the Wall and the Soil	64
Figure 58: Skin Friction Force Acting on the Fill Side of the Wall as a Function of Vertical Position of the Wall.....	65
Figure 59: Skin Friction Force Acting on the Excavation Side of the Wall as a Function of Vertical Position of the Wall.....	65
Figure 60: The Axial Sections of the Clay Layer.....	66
Figure 61: Vertical Displacement during 25 % and 40 % of Consolidation Process at the Depth of 5 m	66
Figure 62: Vertical Displacement during 25 %, 40 % and 55 % of Consolidation Process	67
Figure 63: Vertical Displacement during 25 %, 40 %, 55 % and 70 % of Consolidation Process.....	67
Figure 64: Vertical Displacement during 25 %, 40 %, 55 %, 70 % and 85 % of Consolidation Process	68
Figure 65: Relative Displacement of the Fill Side of the Wall and the Soil	68
Figure 66: Relative Displacement of the Excavation Side of the Wall and the Soil	69
Figure 67: Skin Friction Force Acting on the Fill Side of the Wall as a Function of Vertical Position of the Wall.....	69
Figure 68: Skin Friction Force Acting on the Excavation Side of the Wall as a Function of Vertical Position of the Wall.....	70
Figure 69: Bending Moment vs. Axial Force Characteristics for Simulation Step 3	70
Figure 70: Bending Moment vs. Axial Force Characteristics for Simulation Steps 3 and 4	71
Figure 71: Bending Moment vs. Axial Force Characteristics for Simulation Steps 3, 4 and 5	71

Figure 72: Bending Moment vs. Axial Force Characteristics for Simulation Steps 3, 4, 5 and 6	72
Figure 73: Bending Moment vs. Axial Force Characteristics for Simulation Steps 3, 4, 5, 6 and 7	72
Figure 74: Flowchart for Analytical Negative Skin Friction Calculation Algorithm	73
Figure 75: Comparison of Total Stress Calculation of PLAXIS TM Simulation and the Analytical Method Utilized	74
Figure 76: Comparison of Water Pressure Calculation of PLAXIS TM Simulation and the Analytical Method Utilized	75
Figure 77: Comparison of Effective Stress Calculation of PLAXIS TM Simulation and the Analytical Method Utilized	75
Figure 78: Comparison of Skin Friction Force Calculation of PLAXIS TM Simulation and	76
the Analytical Method Utilized (Simplified).....	76
Figure 79: Comparison of Skin Friction Force Calculation of PLAXIS TM Simulation and the Analytical Method Utilized	76

LIST OF TABLES

TABLES

Table 1: Approximate Range of Reduction Factor (β) Coefficient	13
Table 2: Negative Skin Friction Design Process	17
Table 3: Parameters of the Mohr - Coulomb Model	31
Table 4: Parameters of the Soft - Soil model	33
Table 5: Parameters of Hardening Soil Model	36
Table 6: Parameters of the Silty Sand Layer for Mohr - Coulomb Model	38
Table 7: Parameters of the Clay Model.....	39
Table 8: Parameters of the Hardening Soil Model	40
Table 9: Parameters of the Diaphragm Wall Model.....	40
Table 10: The Parameters and Corresponding Values Used in Analytical Calculations.....	74

CHAPTER 1

INTRODUCTION

1.1. Purpose and Scope

The purpose of this study is to investigate the negative skin friction phenomenon and interpret its effects on diaphragm walls by means of numerical analyses. The negative skin friction effect is conventionally considered for the design of pile foundations with axial loading, however, in this study, the effect of negative skin friction phenomenon is assessed for laterally loaded diaphragm walls. For this purpose, numerical assessment of time dependent variation of downdrag forces on the diaphragm walls are analyzed via consolidation analysis for the following cases;

- Analysis Scenario 1: Diaphragm Wall - Soil Interaction Model
 - Case 1: Diaphragm Wall - Soil Interaction
 - Case 2: Bitumen Coated Diaphragm Wall - Soil Interaction
- Analysis Scenario 2: Diaphragm Wall - Soil Interaction Model during Excavation
 - Case 1: Diaphragm Wall - Soil Interaction
 - Case 2: Bitumen Coated Diaphragm Wall - Soil Interaction

"Analysis Scenario 1: Diaphragm Wall - Soil Interaction Model" illustrates the consolidation dynamics of the clay layer due to the application of the embankment. This scenario breaks down into two sub scenarios, which comparatively illustrate the effect of bitumen utilization to reduce downdrag forces in detail. Those analyses are also carried out by conventional analytical calculation methods (i.e. Rigid - Plastic and Elastic Plastic Soil Models) and the corresponding results are presented comparatively.

"Analysis Scenario 2: Diaphragm Wall - Soil Interaction Model during Excavation" illustrates the consolidation of the clay layer due to the application of the embankment and excavation of the soil consecutively. Similarly, this scenario also breaks down into two sub scenarios, to comparatively analyze the effect of negative skin friction on diaphragm walls in detail.

In this study, PLAXIS™ software is utilized to perform numerical analyses, which is a two - dimensional finite element analysis software, developed specifically for deformation and stability studies in geotechnical engineering projects.

As a result of comparison of time dependent stress and displacement responses of bitumen coated and uncoated diaphragm walls, obtained from the analytical models and numerical simulations, it is concluded that downdrag forces develop as part of a complex interaction among the soil, pile and the applied load, which requires a complete assessment of soil-pile-load interaction with proper models.

The details of this finite element analysis software, together with the utilized constitutive models and the analysis scenarios with the corresponding cases are explained within the following sections, respectively.

1.2. Problem Significance

The negative skin friction/downdrag phenomenon is observed particularly in soft soils as a result of consolidation settlement by means of dissipation of excess pore pressure induced by surcharge loading. Negative skin friction is the most common problem in the design and construction of pile foundations in compressible soils due to induced excessive and differential settlements of the pile foundations. According to Briaud & Tucker (1996), it is stated that downdrag phenomenon has caused significant damage in various structures. In addition to this, negative skin friction produces a dragload which can exceed the rated capacity of the pile itself as indicated in Fellenius (1984).

In pile foundation design, the design load is composed of sustained (i.e., permanent or dead) load and of temporary (i.e., transient or live) load. The design aims to ensure that the design load does not exceed the allowable load, by also considering the safety factors.

There are principally two design approaches used for the design of pile foundations subjected to negative shaft resistance in the literature and fundamental specifications. The traditional method is rather conservative, which assumes that negative shaft resistance will occur on the pile shaft through the portion of a soil layer with a settlement greater than 10 mm, determines the magnitude of negative shaft resistance and considers this resistance as an additional load to the pile supports.

On the other hand, recent methods to determine the negative shaft resistance loads are based on the relative pile - soil movement such as explained in Briaud & Tucker (1996). The method of analysis that Briaud & Tucker (1996) recommends is based on the static equilibrium of the pile and on the compatibility of the relative pile-soil movement and is limited to vertical piles. The above mentioned study states that, in order to design the piles subject to downdrag, the settlement of the pile due to downdrag and structural load, the maximum load in the pile due to downdrag and structural loads and the ultimate capacity of the pile are the input parameters of the problem. According to Briaud & Tucker (1996), transient live loads should not be considered at the neutral point because they only reverse the negative skin friction caused by downdrag temporarily.

Additionally, Fellenius (1984) states that, the dragload, which should be considered as a beneficial force prestressing the pile and reducing the deformation that occurs from live loads will not have any influence on the pile bearing capacity. The dragload must not be subtracted from the pile capacity when determining the allowable load, as long as the pile structural strength is not exceeded. Neither must the dragload be added to the design loads when checking whether the loads from the structure exceed the allowable load or not.

Although above mentioned two opinions appear to be contradictory, both approaches are utilized in the state of the art pile design procedures, as discussed in "Design Approaches and Considerations for the Design of Pile Foundations Subjected to Negative Skin Resistance / Downdrag" section.

CHAPTER 2

LITERATURE SURVEY

2.1. A Brief Review on Negative Skin Friction Phenomenon

2.1.1. Pile Foundations

Pile foundations are frequently required to transfer the load from the superstructure through weak compressible strata onto stiffer or more compact less compressible soils or onto rock. They are implemented to prevent uplift forces when used to support tall structures subjected to lateral loads in the form of wind, earthquake, etc. Pile foundations are also preferred to reduce excessive settlement to an acceptable level (Tomlinson and Woodward, 2008).

Piles are classified as large displacement piles, small displacement piles and replacement piles according to the method of installation (British Standard Code of Practice for Foundations (BS 8004: 1986)). Large displacement piles comprise solid-section piles or hollow-section piles with a closed end, which are driven or jacked into the ground and thus displace the soil. Small displacement piles are also driven or jacked into the ground but have a relatively small cross-sectional area. They include rolled steel H- or I-sections and pipe or box sections driven with an open end such that the soil enters the hollow section. Replacement piles are formed by first removing the soil by boring using a wide range of drilling techniques. Concrete may be placed into an unlined or lined hole, or the lining may be withdrawn as the concrete is placed. Preformed elements of timber, concrete or steel may be placed in drilled holes.

The basis of the 'soil mechanics approach' to calculating the ultimate capacity of piles is that the total resistance of the pile to compression loads is the sum of two components, namely shaft friction and base resistance. A pile can be basically classified as a friction pile or an end-bearing pile on the basis of how they develop the support (i.e., response to the load). A pile in which the shaft-frictional component predominates is known as a friction pile (Figure 1 - a), while a pile bearing on rock or some other hard incompressible material is known as an end-bearing pile (Figure 1 - b). On the other hand, many piles carry loads by a combination of friction and end bearing.

Additionally, Fellenius (1984) emphasizes a distinction between the terms 'shaft resistance' and 'skin friction'. It is reported that the term 'shaft resistance' is used to intend the shear stress induced in the pile due to loading of the pile. On the other hand, the term 'skin friction' is used when the shear stress is induced due to settling or swelling of the soil.

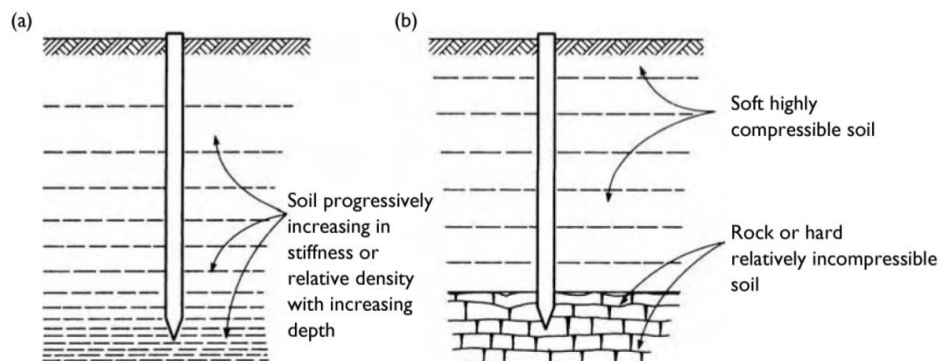


Figure 1: Types of bearing pile (a) Friction pile (b) End-bearing pile (Tomlinson and Woodward, 2008)

2.1.2. Negative Skin Friction Phenomenon

In almost all practical applications of pile foundations, there exists a finite displacement between the soil layer and the pile as a consequence of the dynamics of soil and pile interaction.

The displacement of a pile occurs due to:

- The own weight of the pile itself
- The total load on the pile

The settlement of the soil layer may be caused by:

- Self-weight of unconsolidated recent overburden and fill
- Surcharge-induced consolidation settlement
- Consolidation settlement after dissipation of excess pore pressure induced due to pile driving
- Lowering of groundwater level
- Thawing of frozen soils
- Collapse settlements due to wetting of unsaturated fill
- Construction work adjacent to the site
- Reconsolidation of soft soils disturbed during driving
- Crushing of subsoil under sustained loading

The empirical results show that only a few millimeters of relative displacement between the settling soil and the pile shaft surfaces is sufficient to mobilize the shaft resistance in either upward or downward directions.

In most of the applications, the structural load applied to the top of the pile causes the pile to move downwards with respect to the soil. Thus, the relative movement between the pile and the soil produces shear resistance, which acts upwards along the corresponding interface and contributes to the bearing capacity of the pile.

On the other hand, if a pile is driven through a layer of soft compressible soil such as soft clay, soft silt, peat, recent fill, or collapsible soil, it is possible for the embedding soil to move downwards with respect to the pile. This causes opposite (i.e., negative) shear stress, which acts in the same direction with the relative movement of soil and imposes dragload on the pile, as compared to previously discussed case.

In Figure 2, the axial forces on the pile for both cases are illustrated, where:

F_p	the positive skin friction force
F_n	the downdrag force
Q_t	the load carried at the top of the pile
Q_p	the load carried by the pile point
R_{ut}	the ultimate load to be carried at the top of the pile
R_{up}	the ultimate load to be carried by the pile point

As can be seen from the figure, for the case without downdrag, i.e., where the relative movement of the pile is downward, the mobilized shear stress along the pile - soil interface acts upward and contributes to the bearing capacity of the pile. However, in the case of downdrag, i.e., where the relative movement of the soil is downward, the mobilized shear stress along the pile - soil interface acts downwards and produces a dragload which increases the load applied to the pile. For this case, it is observed that the dragload is produced down to a certain point along the pile. This point is called as the neutral point. In Figure 3 - a, it is shown that above the neutral point negative shaft resistance, and beyond the neutral point positive shaft resistance occurs.

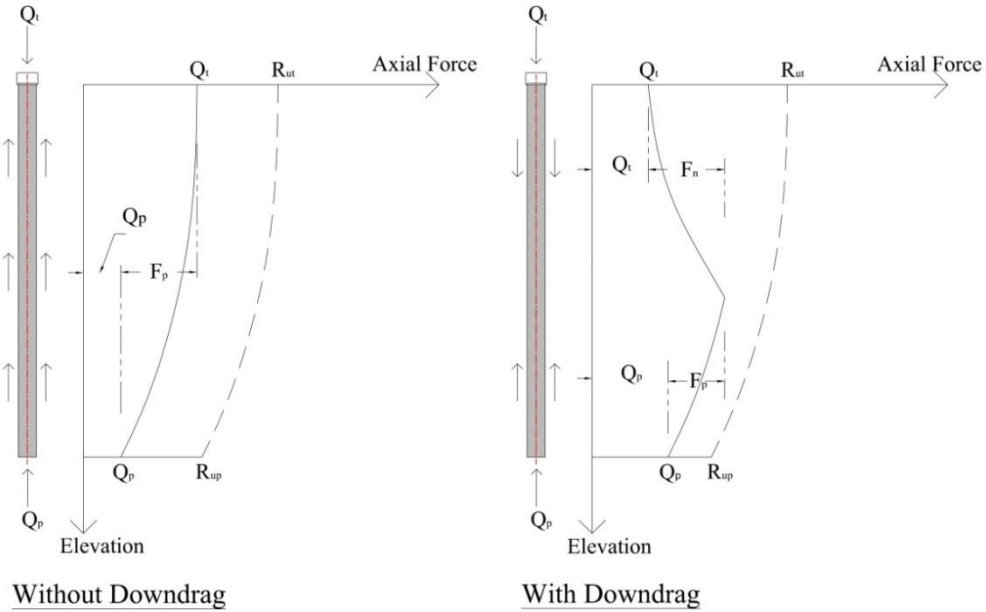


Figure 2: Distribution of Axial Forces in a Pile (Briaud & Tucker, 1996)

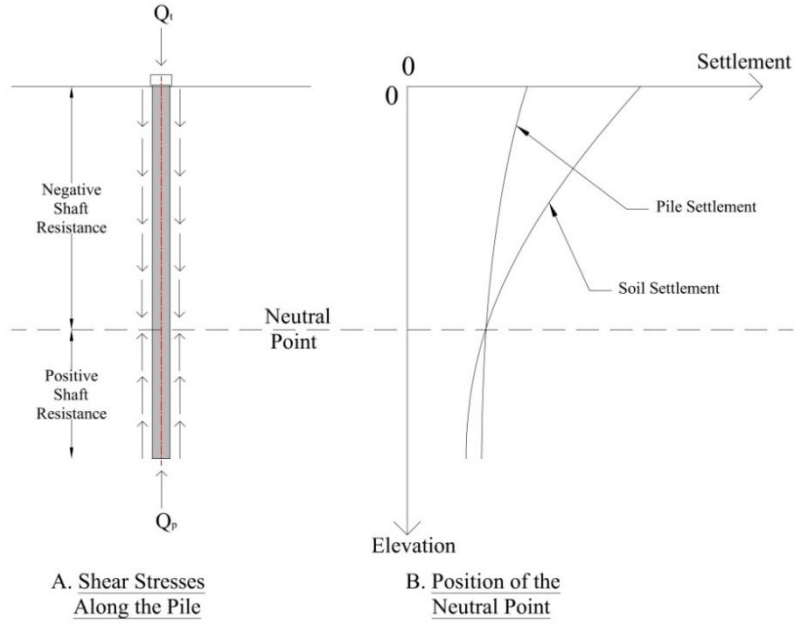


Figure 3: Negative Skin Friction on a Pile (Briaud & Tucker, 1996)

"Neutral plane" is a term used to define the location of the force equilibrium in the pile. It also describes location where there exists no relative movement between the pile and the soil, i.e., at where the pile and the soil settle equal amounts as demonstrated in Figure 3 - b. The location of the neutral plane depends on the soil profile through the pile and loading conditions. In the case of a pile resting on a hard layer, the neutral point has a tendency to be located closer to the bottom of the compressible layer. This phenomenon is clarified with an extreme case where a pile rests on a rock in Fellenius (1984). It is reported that, for such a case, the location of the neutral point is expected to be

at the bedrock elevation. On the other hand, if the pile is embedded in a deformable layer, the neutral point tends to be located above the bottom of the compressible layer. In this case, the position of the neutral point depends on the settlement profile for the compressible layer and the movement profile for the pile (Briaud & Tucker, 1996).

2.1.3. Effects of Negative Skin Friction on Pile Foundations

Negative skin friction is the most common problem in the design and construction of pile foundations in compressible soils where the relative movement of the pile is upward with respect to the soil. In this case, the main problem is the excessive and differential settlements of the pile foundations due to downdrag phenomenon. According to Briaud & Tucker (1996), it is stated that downdrag phenomenon has caused significant damage in various structures. In addition to this, negative skin friction produces a dragload which can exceed the rated capacity of the pile itself as indicated in Fellenius (1984).

In frictional piles, the neutral plane is closer to the surface level and the corresponding dragload applied to the pile shaft is smaller. On the other hand, in the case of end - bearing piles, the neutral plane is lower (i.e., closer to the competent soil layer) and the corresponding dragload on the pile shaft is larger.

In addition to these, frictional piles result in larger foundation settlement compared to the end - bearing piles. Therefore, serviceability of the foundations becomes important in the design of frictional piles, however, for the end - bearing piles, the safety factor on pile structure becomes more of an issue (Shong, 2002).

Piles are usually installed in groups for the support of structures. Briaud & Tucker (1996) reports that according to instrumented full - scale history (Okabe, 1977), laboratory scale test (Koerner and Mukhopadhyay, 1972) and an extensive numerical analysis with a three dimensional element computer program using a non - linear soil model (Jeong and Briaud, 1992), it is proven that the downdrag force on a group of "n" closely spaced piles is less than "n" times the downdrag force on an isolated single pile due to soil settlement profile of group piles as shown in Figure 4.

As can be seen from the Figure 4, group piles disturb the free field settlement profile and there exists a "hanging" effect. It is also observed that especially around the interior piles, the soil settlement is reduced compared to external piles, thus interior piles are subjected to lesser negative skin friction compared to the external piles (external piles are also subjected to lesser negative skin friction compared to an isolated single pile).

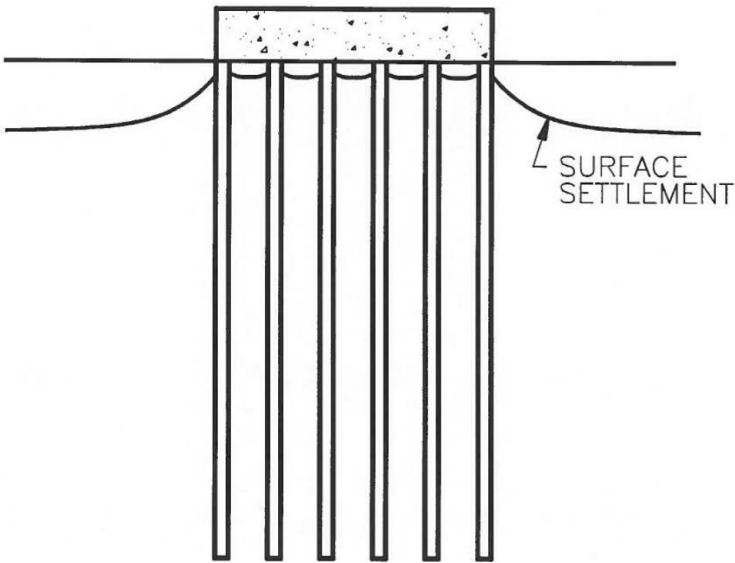


Figure 4: Settlement Profile Under a Pile Group (Briaud & Tucker, 1996)

It should be emphasized here that " the total negative skin friction on the pile or group piles should not be greater than the total imposed fill weight inducing the subsoil settlement within the effective coverage of the pile or group piles" (Shong, 2002).

2.1.4. Precautions to Reduce Downdrag

In order to overcome the engineering problems generated by downdrag, some precautions can be considered. The reduction of downdrag can be achieved by:

- Preloading the subsoil to reduce or eliminate the subsoil settlement before pile installation
- Using group piles which takes the advantage of the "hanging" effect
- Utilizing frictional piles considering larger settlement in the design
- Using double - tube pile method where the outer pile carries the dragload and the inner pile carries the structural load
- Increasing the capacity of piles by means of increasing cross section, length or number of piles, thus reducing impact of downdrag on each pile
- Reducing the pile - soil interaction by means of electro - osmosis
- Coating the piles with a friction reducer such as bitumen

Even though individual cases may differ, the most cost effective method is the bitumen coating of piles among the methods mentioned above. Bitumen is 'a class of amorphous, black or dark-colored (solid, semi solid, or viscous) cementitious substances, natural or manufactured, composed principally of high molecular weight hydrocarbons, soluble in carbon disulfide, and found in asphalts, tars, pitches, and asphaltites' as defined in ASTM D 1079 - 87a. The bitumen is a predominating component of the asphalt which occur in nature or obtained by refining petroleum. The bituminous coatings such as certain types of asphalts or other viscous coatings has been used as friction reducer between the pile and soil interface before the installation. Bitumen is a non – linear viscous material and the shearing response of bitumen can be modeled by:

$$\tau = \eta x \dot{\gamma} \quad (1)$$

where τ is the shear stress, $\dot{\gamma}$ is the shear strain rate and η is the secant viscosity here after referred to as viscosity (Briaud & Tucker, 1996). This practically means that the applied bitumen is effective during the transient settling process, when the settlement rate of the soil is relatively high. During the previously mentioned process, the bitumen will act to reduce the frictional forces between the pile and the soil and thus will reduce the downdrag forces through the pile. However, in the steady state the bitumen will lose its effectiveness.

The design criteria for the bitumen involves criterion for storage, driving, downdrag and particle penetration. The bitumen must be designed so that it does not deform excessively under the gravity stresses during the storage period (design for storage), so that it does not deform excessively under the dynamic stresses present during driving (design for driving), so that it offers little shearing resistance so as to reduce downdrag during the soil settlement process (design for downdrag reduction), and so that it allows the soil particles to penetrate only an allowable amount into the coating (design for particle penetration) (Briaud & Tucker, 1996).

2.2. Analytical Methods to Assess a Pile Subjected to Negative Skin Friction

There are several methodologies in assessing piles subjected to downdrag/negative skin friction. The primary step to assess the negative skin friction is to determine the location of the neutral plane and afterwards to estimate the dragload on the pile shaft. Shong (2002) presents basic analytical closed form equations to determine the location of the neutral plane and dragload on the pile shaft. These analytical methods, namely, "Rigid - Plastic Model" and "Elastic - Plastic Model" include the effect of soil-structure interaction and differ in the load transfer behavior between the pile and the soil. On the other hand, "Numerical Iterative Method " can also be implemented which is enhanced by elaborating the computational methodology compared to the basic analytical methods and provides more accurate results, however, computer programs are required to overcome the computational burden. The details of the analytical methods, "Rigid - Plastic Model" and "Elastic - Plastic Model" and "Numerical Iterative Method " are explained in detail in this section.

2.2.1. Rigid - Plastic Model

The rigid plastic model is a relatively more simplified method among the closed form equations. This model does not consider load transfer behavior and the compressibility of the pile which results in over-prediction of the negative skin friction. However, it will be explained for the sake of completeness, since it forms the basis of elastic plastic model.

The assumptions of the rigid - plastic model can be summarized as below;

- The pile - soil friction is fully mobilized to ultimate condition
- The unit shaft and toe resistances exhibits a linear behavior with respect to depth
- The positive (q_n) and negative (r_s) unit shaft resistances are assumed to be equal at the same depth.

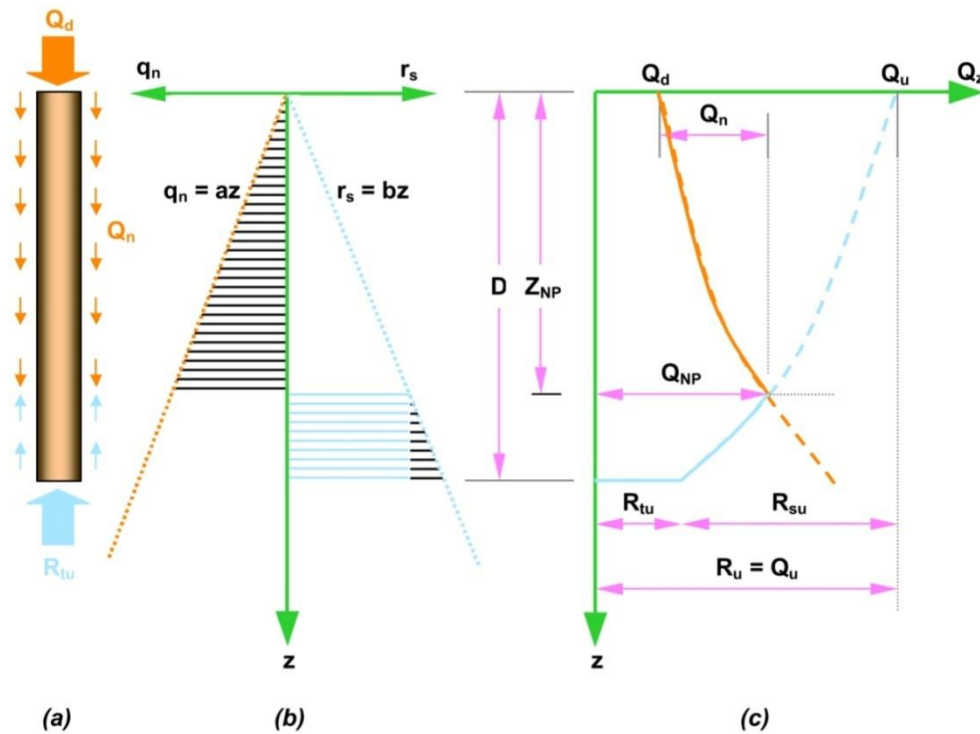


Figure 5: Negative Skin Friction on a Single Pile (Rigid Plastic Model) (L. Shaw Shong, 2002)

In Figure 5 (a), a single pile subjected to negative skin friction is given. The distribution of the assumed positive and negative unit shaft resistances and the resultant axial forces in the pile are represented in Figure 5 (b) and (c), respectively, where:

q_n	the negative unit shaft resistance
r_s	the positive unit shaft resistance
D	the pile penetration length
Z_{NP}	the depth of neutral plane
Q_d	the imposed load at pile top
Q_n	the negative skin friction on pile above neutral plane
Q_{NP}	the pile axial load at neutral plane
R_{tu}	the ultimate pile toe resistance
R_{su}	the ultimate pile shaft resistance over the whole shaft length
Q_u	is equal to $R_u =$ ultimate pile capacity = $R_{tu} + R_{su}$

In this method two unitless parameters, α and F_s are defined as follows:

$$\alpha = \frac{R_u}{R_{su}} \quad (2)$$

and

$$F_s = \frac{R_u}{Q_d} \quad (3)$$

The static equilibrium equation at the neutral point:

$$Q_{NP} = Q_d + \int_0^{Z_{NP}} A_s q_n dz = R_{tu} + \int_{Z_{NP}}^D A_s r_s dz \quad (4)$$

By taking the integral and substituting the unitless parameters, α and F_s :

$$\frac{Z_{NP}}{D} = \sqrt{\left[\frac{1}{2} \left(\frac{R_u - \frac{R_u}{F_s}}{R_{su}} \right) \right]} = \sqrt{\frac{\alpha}{2}} \left[1 - \frac{1}{F_s} \right] \quad (5)$$

and

$$\frac{Q_{NP}}{R_u} = \frac{1}{2} \left(1 + \frac{1}{F_s} \right) \quad (6)$$

2.2.2. Elastic - Plastic Model

The elastic plastic model is a relatively more enhanced method compared to the rigid plastic model. This model considers relative pile - soil displacement and defines a transition zone to calculate the location of the neutral point.

The assumptions of the elastic - plastic model can be summarized as below;

- The pile is rigid and incompressible
- The soil settlement profile is assumed to be linear
- The pile - soil friction is fully mobilized to ultimate condition except the transition zone
- The positive(q_n) and negative(r_s) unit shaft resistances are assumed to be equal at the same depth.

In the Figure 6 (a), the relative displacement between the pile and the soil is represented. Here, the midpoint of the transition zone gives the location of the neutral point and the defined unitless parameters to make use of in the equations are stated as follows:

$$\psi = \frac{\delta_{ty}}{S} \quad (7)$$

where δ_{ty} is the relative displacement between the pile toe and the soil at the pile toe that is required to yield the toe resistance.

$$\omega = \frac{\delta_{sy}}{S} \quad (8)$$

where δ_{sy} is the relative displacement between the pile and the soil around the pile shaft that is required to yield the shaft resistance.

$$\lambda = \frac{\delta_h}{S} = \frac{Z_{NP}}{D} \quad (9)$$

where δ_h is the relative settlement between the pile head and the settled ground surface.

The distribution of the positive and negative unit shaft resistances and the resultant axial forces in the pile are represented in Figure 6 (b) and (c) considering the elastic plastic model. The relation between the unit shaft resistance and displacement is given in the Figure 6 (d) which is utilized to calculate the mobilized unit shaft resistance through the transition zone. The pile toe settlement and the corresponding toe resistance is given in Figure 6 (e) which is referred to calculate the mobilized toe resistance in the system.

The static equilibrium equation at the neutral point:

$$Q_{NP} = Q_d + \int_0^{(\lambda-\omega)D} A_s q_{ny} dz + \int_{(\lambda-\omega)D}^{\lambda D} A_s q_{nz} dz = \int_{\lambda D}^{(\lambda+\omega)D} A_s r_{szm} dz + \int_{(\lambda+\omega)D}^D A_s r_{sy} dz + R_{tm} \quad (10)$$

By taking the integral and substituting the unitless parameters, α and F_s :

$$\lambda = \frac{Z_{NP}}{D} = \frac{\sqrt{(\alpha - 1)^2 + 8\psi(\alpha - 1) + 8\psi^2 \left(1 - \frac{2}{3}\omega^2 - \frac{\alpha}{F_s}\right) - (\alpha - 1)}}{4\psi} \quad (11)$$

$$\frac{Q_{NP}}{R_u} = \frac{1}{F_s} + \frac{1}{\alpha} \left(\lambda^2 - \omega\lambda + \frac{\omega^2}{3} \right) \quad (12)$$

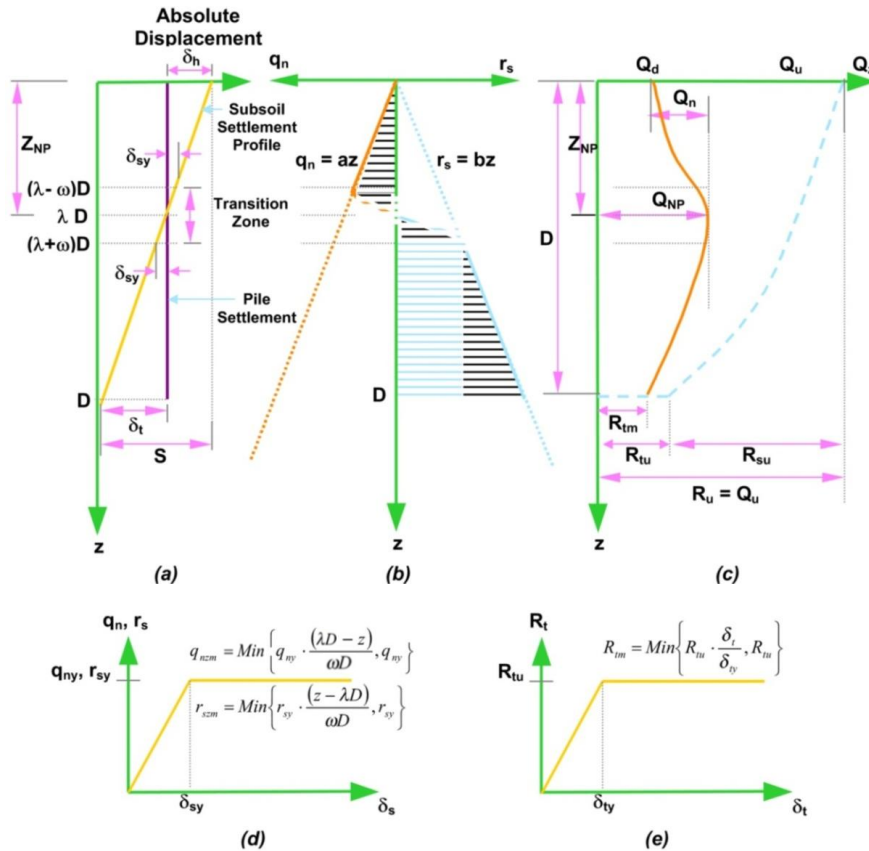


Figure 6: Negative Skin Friction on a Single Pile (Elastic Plastic Model) (Shong, 2002)

2.2.3. Numerical Iterative Approach

It should be noted here that the accuracy of the Elastic Plastic Model can be enhanced by slightly elaborating the computation methodology with:

- Appropriate constitutive soil models
- Consolidation settlement profile for the soil
- Elastic compression dynamics of the pile
- Elastic punch dynamics in the bearing soil layer

However, the above mentioned improvements require utilization of numerical iterative methods, which are handled by software to overcome the computational burden. In this study, PLAXISTM software is utilized for the purpose. The detailed pile and soil models used in this study are explained in detail in the next chapter.

2.3. Empirical Methods to Calculate the Unit Negative Skin Friction

There are two basic empirical methods to estimate the unit negative skin friction at the corresponding depth, namely the Total Stress Approach (α -Method) and the Effective Stress Approach (β -Method):

- Total Stress Approach (α - Method): This method makes use of the undrained shear strength (c_u) in the analysis to calculate the negative skin friction. The negative skin friction ($f_{s \text{ neg}}$), which is equal to adhesion (c_a), is calculated by:

$$f_{s \text{ neg}} = c_a = \alpha \times c_u \quad (13)$$

where α is an empirical adhesion factor and c_u is the undrained shear strength.

The adhesion factor, depends the nature and shear strength of the soil, besides pile dimension, method of pile installation and time effects. Design and Construction of Driven Pile Foundations (1998), offers Figure 7 for determination of adhesion factor, which represents the relation between adhesion factor and undrained shear strength depending on pile diameter (b) and clay thickness (D) for the mentioned sites. On the other hand, Figure 8 is also provided for the selection of adhesion when the special soil stratigraphy cases identified in Figure 7 are not existing at the site.

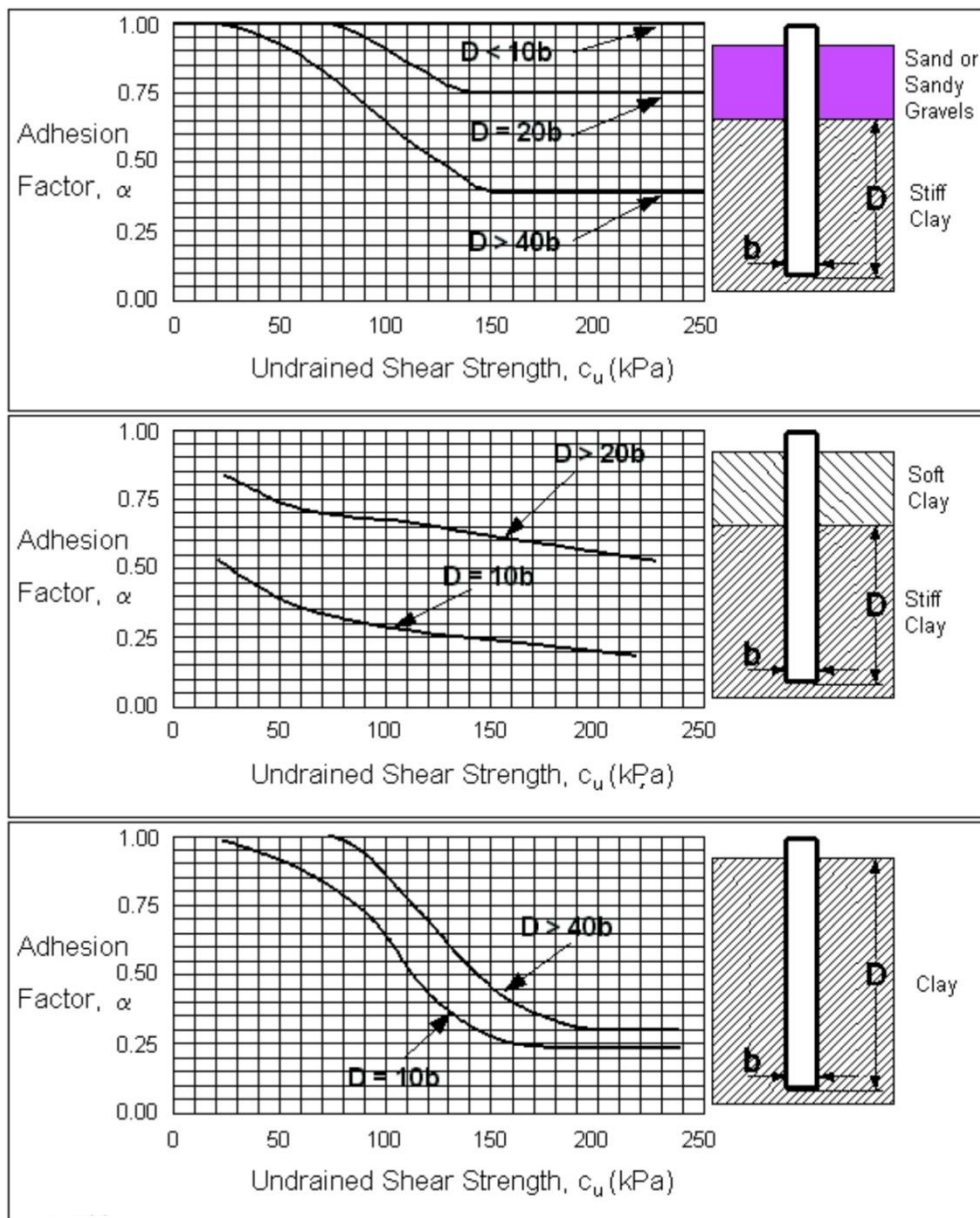


Figure 7: Adhesion factors for Driven Piles in Clay
 (Design and Construction of Driven Pile Foundations, 1998)

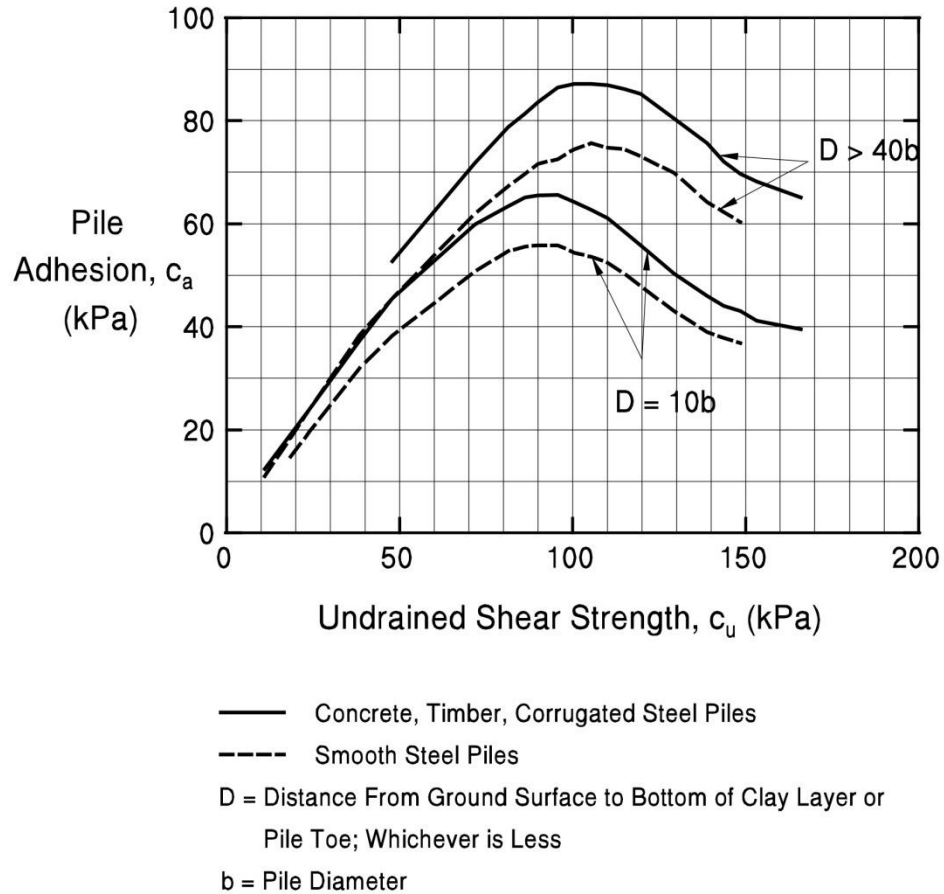


Figure 8: Adhesion Values for Piles in Cohesive Soil
 (Design and Construction of Driven Pile Foundations, 1998)

- Effective Stress Approach (β - Method) : This method assumes that the negative skin friction is proportional to the effective over-burden pressure and can be computed from the equation:

$$f_{s\text{ neg}} = \beta \times \sigma'_v \quad (14)$$

where β is a reduction factor and σ'_v is the effective over-burden pressure at the depth of interest.

Design and Construction of Driven Pile Foundations (1998) represents recommended ranges of reduction factor dependent on the soil type and angle of friction (ϕ), as given in Table 1.

Table 1: Approximate Range of Reduction Factor (β) Coefficient
 (Design and Construction of Driven Pile Foundations, 1998)

Soil Type	ϕ (Degree)	β
Clay	25 ~ 30	0,25 ~ 0,35
Silt	28 ~ 34	0,27 ~ 0,50
Sand	32 ~ 40	0,30 ~ 0,60
Gravel	35 ~ 45	0,35 ~ 0,80

In addition, Tomlinson and Woodward (2008), offers negative skin friction factors for piles driven into soft to firm clays as a function of depth of penetration as demonstrated in Figure 9.

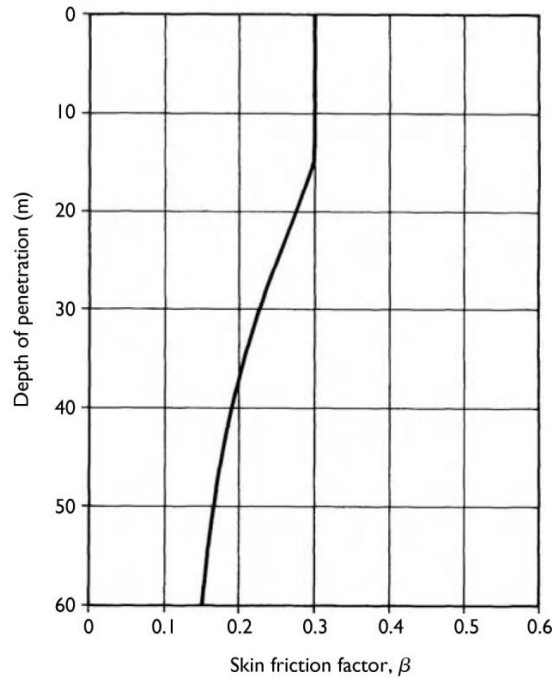


Figure 9: Negative Skin Friction Factors for Piles Driven into Soft to Firm Clays (Tomlinson and Woodward, 2008)

In the literature, there exists contradicting arguments; since very little relative displacement is enough to mobilize the full friction and settlement starts just after the installation of the piles or due to reconsolidation of soft soils disturbed during driving, Total Stress Approach (α -Method) should be used for clay to design the foundations in the short term. However, consolidation is a long term process and thus, Effective Stress Approach (β - Method) should be used for clay to design the foundations in the long term. Therefore, according to Briaud & Tucker (1996), "the pile must be designed for both short term and long term cases, with the worst case governing the design". On the other hand, Fellenius (1984) states that " Load-transfer from a pile to the soil or from soil to a pile is primarily governed by the effective stress in the soil, and both shaft and toe resistances are proportional to the effective overburden stress. That is, the load transfer is best analyzed using the "beta method" of analysis."

2.4. Design Approaches and Considerations for the Design of Pile Foundations Subjected to Negative Skin Resistance / Downdrag

In pile foundation design, the design load is composed of sustained (i.e., permanent or dead) load and of temporary (i.e., transient or live) load. The design aims to ensure that the design load does not exceed the allowable load, by also considering the safety factors.

There are principally two design approaches used for the design of pile foundations subjected to negative shaft resistance in the literature and fundamental specifications. The traditional method is a conservative one, which assumes that negative shaft resistance will occur on the pile shaft through the portion of a soil layer with a settlement greater than 10 mm, determines the magnitude of negative shaft resistance and adds this resistance as a load to the pile supports. On the other hand, recent methods to determine the negative shaft resistance loads are based on the relative pile - soil movement such as explained in Briaud & Tucker (1996). The method of analysis that Briaud & Tucker (1996) recommends is based on the static equilibrium of the pile and on the compatibility of the relative pile-soil movement and is limited to vertical piles. This study states that in order to design the piles subjected to downdrag, the settlement of the pile due to downdrag and structural load, the maximum load in the pile due to downdrag and structural loads and the ultimate capacity of the pile are the input parameters of the problem.

The settlement of a pile, hence the amount of the relative movement between the soil and the pile, is mostly determined by the amount and characteristics (i.e., permanent or transient) of the load applied. According to Briaud & Tucker (1996) these phenomena are illustrated in Figure 10, where the evolution of load distribution on a pile due to transient and permanent loading is given for the cases with and without negative skin friction. As can be observed from the figure, transient live loads should not be considered at the neutral point because they only reverse the negative skin friction caused by downdrag temporarily (Briaud & Tucker (1996)).

In addition to this, Fellenius (1984) also states that, the dragload, which constitutes a beneficial force prestressing the pile and reducing the deformation that occurs from live loads will not have any influence on the pile bearing capacity and the dragload must not be subtracted from the pile capacity when determining the allowable load, as long as the pile structural strength is not exceeded. Neither must the dragload be added to the design loads when checking that the loads from the structure do not exceed the allowable load.

Eurocode 7 (2004) also proposes two "contradictory" design approaches for piles subjected to ground displacement, such as consolidation, which can affect the piles by causing downdrag. The first approach, evaluates this phenomenon as an "indirect action" and soil-structure interaction analysis is performed to determine the relative displacements and forces. It is also emphasized that, the displacement of the pile relative to the surrounding moving ground, the shear resistance of the soil along the shaft of the pile, the weight of the soil and the expected surface loads around each pile should be considered for interaction calculations.

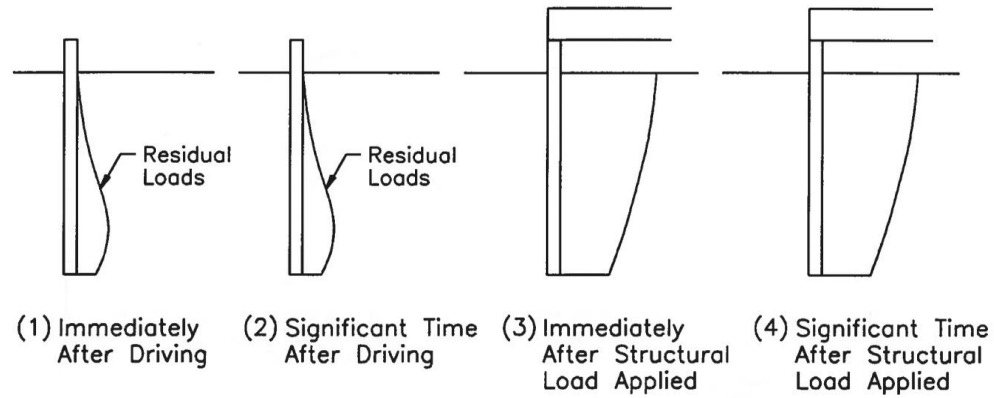
On the other hand, the second approach proposed in Eurocode 7 (2004) evaluates this phenomenon as an "equivalent direct action" and an upper-bound action for downdrag force is defined. In order to define an/a appropriate/maximum upper-bound action, the shear resistance at the interface between the soil and the pile shaft and downward movement of the ground due to self-weight compression and any surface load around the pile should be considered. Total Stress Approach (α -Method) is utilized to calculate downdrag force induced by consolidation of cohesive layer. Then, the characteristic vertical compressive action applied to the pile is calculated by addition of axial load applied to the pile, the pile weight and the downdrag force. In addition, an exception for transient loads are also defined for this approach and it is stated that downdrag and transient loading need not be considered simultaneously in load combinations.

The design approaches and considerations of

- Design and Construction Guidelines for Downdrag on Uncoated and Bitumen-Coated Piles (1996)
- Design and Construction of Driven Pile Foundations (1998)
- AASHTO LRFD Bridge Design Specification (2007)
- Drilled Shafts: Construction Procedures and LRFD Design Methods (2010)

are comparatively summarized in Table 2.

(a) Evolution of Load Distribution Without Downdrag



(b) Evolution of Load Distribution With Downdrag

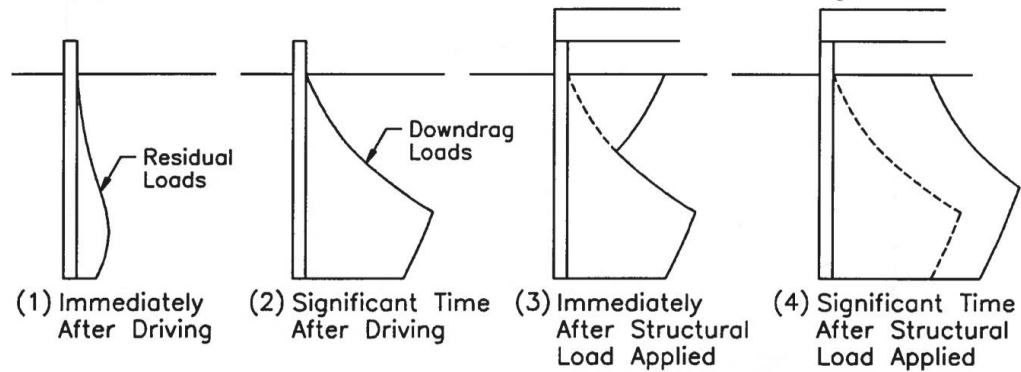


Figure 10: Evolution of the Load Distribution in a Pile (Briaud & Tucker, 1996)

Table 2: Negative Skin Friction Design Process

Technical Document		Design and Construction Guidelines for Downdrag on Uncoated and Bitumen-Coated Piles (1996)	Design and Construction of Driven Pile Foundations (1998)	AASHTO LRFD Bridge Design Specification (2007)	Drilled Shafts: Construction Procedures and LRFD Design Methods (2010)
Step #					
1	Initialization	Establish the idealized soil profile and estimate the pile load (dead loads, permanent and transient live loads) and pile length (L).	Establish the idealized soil profile and soil properties for computing settlement.	Establish the idealized soil profile and soil properties for computing settlement.	Establish the idealized soil profile and soil properties for computing settlement.
2	Preliminary works to calculate consolidation settlement	Determine the variation of vertical stress ($\Delta\sigma_v$) beneath the center of embankment vs. ratio of depth to embankment depth (Z/B).	Determine the overburden pressure increase (Δp) vs. depth due to the fill.	Determine the overburden pressure increase (Δp) vs. depth due to the fill.	For the time-dependent settlement (consolidation) assume end of consolidation settlement.
3	Perform consolidation settlement computations	Perform settlement computations to estimate total ground surface settlement and check the clues to know when to consider downdrag in design ¹ to decide whether or not downdrag may be	Perform settlement computations for the soil layers along the embedded pile length (L).	Perform settlement computations for the soil layers along the embedded pile length (L) or shaft.	Assume that consolidation settlement varies linearly with depth.

¹

i	The total settlement of the ground surface will be larger than 100 mm
ii	The settlement of the ground surface after the piles are driven will be larger than 10 mm
iii	The height of the embankment to be placed on the ground surface exceeds 2 m
iv	The thickness of the soft compressible layer is larger than 10 m
v	The water table will be drawn down by more than 4 m
vi	The piles will be longer than 25 m

Step #	Technical Document	Design and Construction Guidelines for Downdrag on Uncoated and Bitumen-Coated Piles (1996)	Design and Construction of Driven Pile Foundations (1998)	AASHTO LRFD Bridge Design Specification (2007)	Drilled Shafts: Construction Procedures and LRFD Design Methods (2010)
		a problem.			
4	Determination of transition zone characteristics (if applicable)	Establish the settlement profiles down to a depth where settlement is negligible by calculating the time factor and thus the percent consolidation at the times of pile driving, significant time after pile driving, immediately after load application on the piles and significant time after load application on the piles.	Determine the pile length (L) that will be subjected to negative shaft resistance; assuming that negative shaft resistance will occur on the pile shaft through the portion of a soil layer with a settlement greater than 10 mm.	Determine the pile length (L) or shaft that will be subjected to downdrag; assuming that downdrag fully develops, if the settlement in the soil layer is 0.4 in. or greater relative to the pile or shaft.	Select load transfer curves for all of the layers. For the sake of simplicity, a linear curve is selected for load transfer in base resistance and fully plastic curves are selected for load transfer in side resistance. <u>Note:</u> Alternatively, nonlinear curves can be used, but a numerical computer solution is required.
5	Determination of the negative shaft resistance / downdrag	Determination of maximum friction between pile and soil and maximum point resistance . <u>Note:</u> a) Both total and effective stress analysis for clay and effective stress analysis for sand are performed and the pile must be designed with the worst case governing the design. b) The point resistance is assumed to follow an elastic -	Determine the magnitude of negative shaft resistance (Q_s^-) by using Total Stress Approach (α - Method).	Determine the magnitude of downdrag, DD, by using static analysis. <u>Note:</u> For the case of piles, downdrag can be estimated using α , λ and β (when the long term conditions after consolidation is considered) methods for cohesive soils. In the case of cohesionless soils that will be subjected to downdrag due to overlying	Calculate nominal unit side resistances applicable to the downdrag problem. <u>Note:</u> In the case of cohesive soils, the α method for short term undrained conditions and effective stress analysis for long term conditions is applied. For cohesionless soils β method is applied to calculate the nominal unit side resistance.

Step #	Technical Document	Design and Construction Guidelines for Downdrag on Uncoated and Bitumen-Coated Piles (1996)	Design and Construction of Driven Pile Foundations (1998)	AASHTO LRFD Bridge Design Specification (2007)	Drilled Shafts: Construction Procedures and LRFD Design Methods (2010)
	Determination of the negative shaft resistance / downdrag	plastic model.		<p>consolidating layers effective stress method should be used to estimate negative skin resistance.</p> <p>For shafts, downdrag loads may be estimated using the α method for cohesive soils and β method for granular soils.</p>	
6	Determination of the neutral point location	Determine the location of neutral point by comparing the soil settlement profile with the pile settlement profile (See Figure 3).	N/A	N/A	<p>Apply an iterative procedure to define the location of the neutral plane.</p> <p>1) Assume that the initial neutral plane is at the interface between the compressible soil layer and the underlying dense or stiff layer.</p> <p>2) Calculate the nominal head load (Q_T) as the difference between the nominal side resistance (R_{SN}), nominal base resistance (R_{BN}) and downdrag.</p> $Q_T = R_{SN} + R_{BN} - Q_D$ <p>3) Considering the static</p>

Step #	Technical Document	Design and Construction Guidelines for Downdrag on Uncoated and Bitumen-Coated Piles (1996)	Design and Construction of Driven Pile Foundations (1998)	AASHTO LRFD Bridge Design Specification (2007)	Drilled Shafts: Construction Procedures and LRFD Design Methods (2010)
	Determination of the neutral point location				<p>equilibrium of pile, calculate the maximum load which occurs at the neutral plane.</p> $Q_{max} = Q_T + Q_D$ <p>4) Calculate the settlement at the neutral plane considering the elastic compression of pile and base settlement (select a random value for the base settlement)</p> <p>5) If the required condition for neutral plane is not met, update Q_T and repeat the steps 2-4.</p>
7	Evolution of the load distribution	The PILENEG program is run for evolution of the load distribution in the pile during downdrag for the specified four steps in Figure 10.	N/A	N/A	N/A
8	Constitution of load - sett. envelope	A Load - Settlement Envelope resulting from equilibrium conditions under rapid top load application and long term downdrag is obtained.	N/A	N/A	N/A

Step #	Technical Document	Design and Construction Guidelines for Downdrag on Uncoated and Bitumen-Coated Piles (1996)	Design and Construction of Driven Pile Foundations (1998)	AASHTO LRFD Bridge Design Specification (2007)	Drilled Shafts: Construction Procedures and LRFD Design Methods (2010)
9	<p align="center">Design Considerations</p>	<p>The design of pile foundation is carried out by considering the drivability of the pile, the allowable settlement of the pile, the safety against structural failure of the pile material, the safety against soil failure by the use of load and resistance factors.</p> <p><u>Note:</u> At the top of the pile dead loads, permanent live loads and transient live loads are considered, however, at the neutral point dead loads, permanent loads and downdrag loads are considered. The transient live loads are not taken into consideration at the neutral point since they only reverse the negative skin friction caused by downdrag temporarily.</p>	<p>Calculate ultimate pile capacity (Q_u^+) by the positive shaft and toe resistance and afterwards the net ultimate pile capacity (Q_u^{NET}), available to resist imposed loads.</p> $Q_u^{NET} = Q_u^+ - Q_s^-$	<p>AASHTO LRFD specifications (2007) are utilized for the evaluation of limit states under downdrag based on the followings;</p> <p>1) The downdrag force (DD) is a component of the permanent load with a load factor $\gamma=0.35$ (minimum) and $\gamma =1.25$ (maximum)</p> <p>2) Each strength limit state is evaluated acc. to the basic LRFD equation which is,</p> $\sum \eta_i \gamma_i F_i + \gamma_p (DD) \leq \sum_{i=1}^n \phi_{S,i} R_{SN,i} + \phi_B R_{BN}$ <p>For the geotechnical strength limit state, soil layers that undergo settlement exceeding 4% of shaft diameter, the downdrag forces are likely to remain and should be included with the maximum load factor. In the case of application of non-permanent (transient) loads,</p>	<p>AASHTO LRFD specifications (2007) are utilized for the evaluation of limit states under downdrag.</p>

<div style="text-align: center;">Technical Document</div> <div style="text-align: center;">Step #</div>	<div style="text-align: center;">Design and Construction Guidelines for Downdrag on Uncoated and Bitumen-Coated Piles (1996)</div>	<div style="text-align: center;">Design and Construction of Driven Pile Foundations (1998)</div>	<div style="text-align: center;">AASHTO LRFD Bridge Design Specification (2007)</div>	<div style="text-align: center;">Drilled Shafts: Construction Procedures and LRFD Design Methods (2010)</div>
Design Considerations			<p>which cause a downward movement of the pile and reduce the downdrag over the period of application, strength limit states in compression should be performed under the full load combination with the non-permanent components of load excluding downdrag.</p> <p>For the structural strength limit state, the maximum axial force effect in the shaft which occurs at the neutral plane, resulting from all load components, including full downdrag with the maximum load factor should be checked.</p>	

CHAPTER 3

NUMERICAL MODELLING OF NEGATIVE SKIN FRICTION PROBLEMS

3.1. Analysis Approach

The negative skin friction/downdrag phenomenon is observed particularly in soft soils as a result of consolidation settlement by means of dissipation of excess pore pressure induced by surcharge loading. Negative skin friction is the most common problem in the design and construction of pile foundations in compressible soils due to excessive and differential settlements of the pile foundations. In addition to this, negative skin friction produces dragload, that can exceed the rated capacity of the pile itself as indicated in Fellenius (1984).

Although, the negative skin friction effect is generally considered for design of pile foundations with axial loading, in this study, the effect of negative skin friction phenomenon is assessed for laterally loaded diaphragm walls. This study aims to observe the negative skin friction phenomenon and interpret its effects by means of numerical analyses on diaphragm walls. In order to analyze the effects of frictional forces through the wall-soil interface, considering the retaining structure and soil dynamics in a coupled manner, time dependent variation of downdrag forces on the diaphragm walls are analyzed via consolidation analysis. For this purpose, the analyzed scenarios within the scope of this study are summarized below:

- Analysis Scenario 1: Diaphragm Wall - Soil Interaction Model
 - Case 1: Diaphragm Wall - Soil Interaction
 - Case 2: Bitumen Coated Diaphragm Wall - Soil Interaction
- Analysis Scenario 2: Diaphragm Wall - Soil Interaction Model during Excavation
 - Case 1: Diaphragm Wall - Soil Interaction
 - Case 2: Bitumen Coated Diaphragm Wall - Soil Interaction

The geological profile of the digital model utilized to perform analyses are represented in Figure 11. As can be observed from the figure, the geological profile of the soil section consists of silty sand (indicated by blue), clay (indicated by yellow) and gravelly sand (indicated by green) layers. The properties of the corresponding soil layers, together with their mathematical model parameters is explained in detail in the "Modeling Scenario and Cases" section.

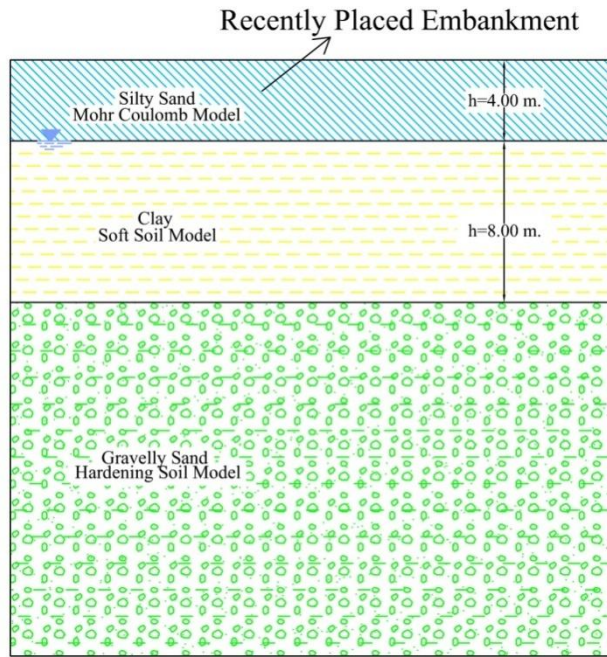


Figure 11: The Geological Profile of the Analyzed Soil Section

"Analysis Scenario 1: Diaphragm Wall - Soil Interaction Model" illustrates consolidation dynamics of the clay layer due to the application of the embankment, as illustrated in Figure 11. In this scenario, the degree of consolidation prior to construction of the diaphragm wall is assumed to be 10 % and time dependent variation of the neutral point and downdrag forces through the consolidation process on the diaphragm wall illustrated in Figure 12 are studied.

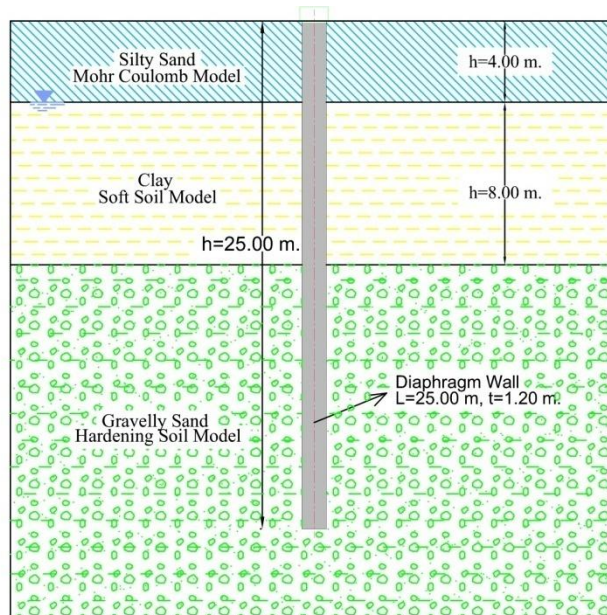


Figure 12: Construction of Diaphragm Wall

"Analysis Scenario 1" breaks down into two sub scenarios, which comparatively illustrate the effect of bitumen utilization to reduce downdrag forces in detail. The application of bitumen coating is illustrated in Figure 13. In order to be able to observe the effect of bitumen coating, soil-structure interaction is modeled by defining the roughness of the interaction. Those analyses are also carried out by conventional analytical calculation methods (i.e. Rigid - Plastic and Elastic Plastic Soil Models) and the corresponding results are presented comparatively.

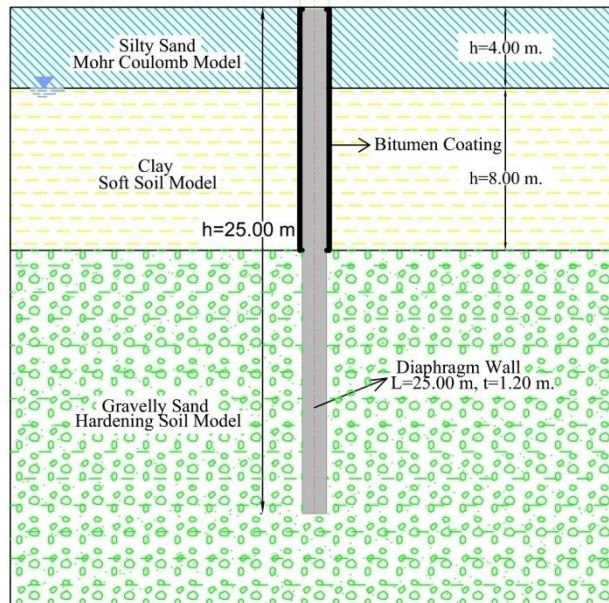


Figure 13: Application of Bitumen Coating

"Analysis Scenario 2: Diaphragm Wall - Soil Interaction Model during Excavation" illustrates the consolidation of the clay layer due to the application of the embankment and excavation of the soil consecutively. Similar to the first scenario, the degree of consolidation prior to construction of the diaphragm wall is assumed to be 10 % and time dependent variation of downdrag forces, induced axial force, moment and shear through the consolidation process on diaphragm wall illustrated in Figure 12 are studied, as the excavation process is carried out as illustrated in Figure 14.

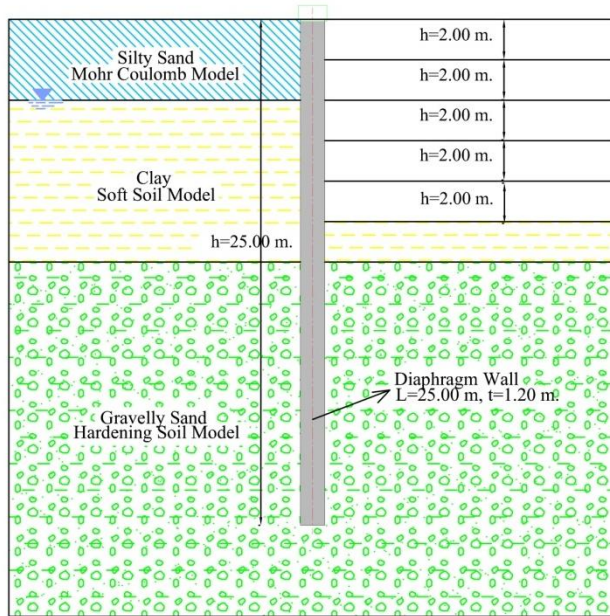


Figure 14: The Excavation Process (2.00 meters of Excavation at Each Step)

"Analysis Scenario 2" also breaks down into two sub scenarios, to comparatively analyze the effect of negative skin friction on diaphragm walls in detail. The application of bitumen coating is illustrated in Figure 15. In order to be able to observe the effect of bitumen coating, soil-structure interaction is modeled by defining the roughness of the interaction.

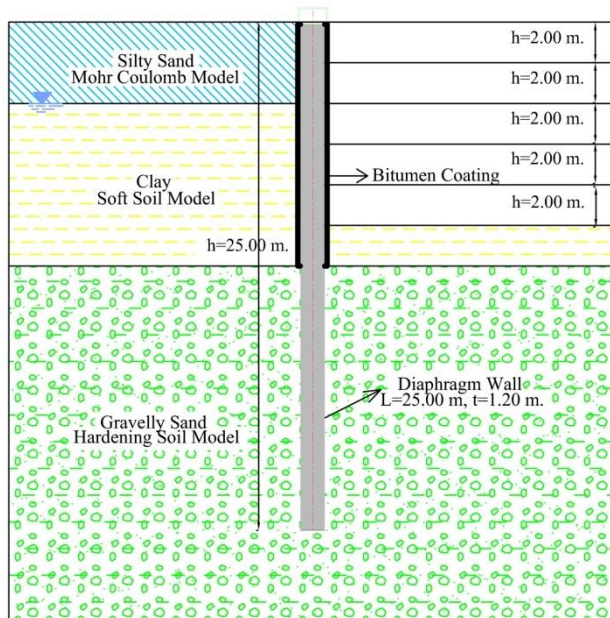


Figure 15: Application of Bitumen Coating

The details of the finite element analysis software, the utilized constitutive models and the analysis scenarios with the corresponding cases are explained in detail within the following sections, respectively.

3.2. Numerical Modeling Software

In this study, numerical analyses are performed by PLAXIS 2D, which is a two - dimensional finite element analysis software, developed specifically for the analysis of deformation and stability in geotechnical engineering projects. PLAXIS 2D enables the user to handle non - linear finite element computations by robust and theoretically sound computational procedures. Even though, there exists similar finite element programs (e.g., Flac and Phase), due to its availability and ease of use PLAXIS 2D is utilized for this study, under the license of Yüksel Proje Uluslararası A.Ş. In the proceeding paragraphs a brief description of the program will be given.

In the case of 2D analysis, the diaphragm wall or pile section is defined as per - meter equivalent with infinite length (into the plane), which can not exactly represent the actual conditions on site for a pile (or pile group), since the surrounding effect of the soil around the pile (or pile group) is not considered in this model. Therefore, 3D models should be utilized for the analysis of piles (or pile groups).

PLAXIS 2D consists of mainly four parts, namely, Input, Calculation, Output and Curves. The geometry of the problem, structures, interfaces, soil data and boundary conditions are defined in the input program. Excavation boundaries and boundaries of the soil layers are defined by using point and line objects. The structural elements may be defined by plates, anchors or geogrids according to the type of the element. In this study, plate elements are used in order to simulate the diaphragm walls. The interface feature of the program enables the user to model soil-structure interaction. In order to define the roughness of the interaction, a suitable value should be assigned as a strength reduction factor (R_{inter}) which relates the interface strength. In Figure 16, the application of plates and interfaces for different structures are illustrated. In this study, interface elements are defined through the diaphragm wall section. The strength reduction factor, (R_{inter}), is defined such that the interface strength to the soil strength is in the order of 2/3 of the soil strength as recommended in the PLAXIS User's Manual. In this way, relative displacements and induced shear stresses between the wall and the soil elements are realistically modeled by interface elements.

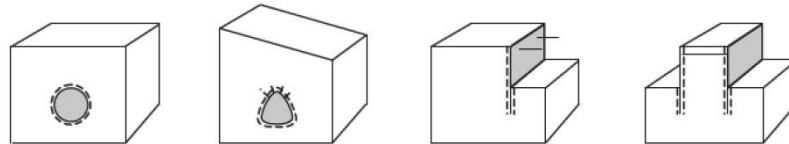


Figure 16: Application of Plates and Interfaces (PLAXIS 2D User's Manual, 2010)

The constitutive models available in PLAXIS 2D which are used to model the soil/rock behavior are Mohr – Coulomb model, hardening soil model, soft soil model and jointed rock model. For these models, three types of drainage responses, drained behavior, undrained behavior and non-porous behavior can be defined in the analysis in order to simulate the pore pressure behavior in the soil. Mohr Coulomb model, soft soil model and hardening soil model will be described briefly in the next section since, these type of soil models are used in the analyses.

PLAXIS 2D finite element program allows the user to create automatic mesh generation, which is performed based on the input of the geometry model after the definition of the geometry, the assignment of the soil and material properties and the boundary conditions. Standard fixities can be used to define the boundary conditions which restrain the horizontal displacement of vertical outer boundaries and vertical and horizontal displacements of bottom boundary. PLAXIS 2D finite element program performs mesh generation by using 6-node triangular or 15-node triangular soil elements. Positions of nodes and stress points in these soil elements is given in Figure 17. The 6-node triangular

element type provides a second order interpolation for displacements and integration involves three stress points. On the other hand, 15-node triangular element type provides a fourth order interpolation for displacements and integration involves twelve stress points, thus 15-node triangular element type is selected for this study, since this element type is more accurate.

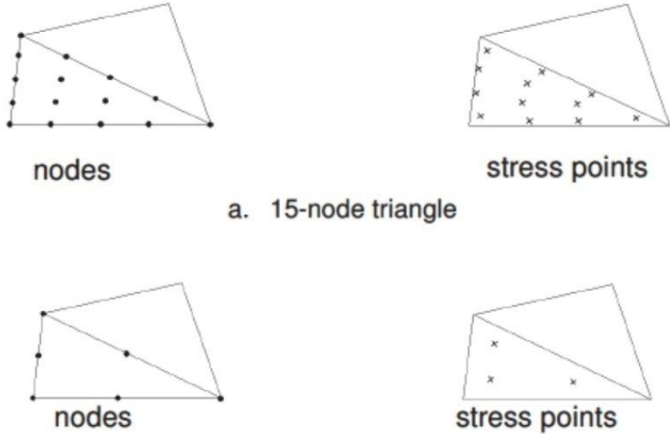


Figure 17: Position of Nodes and Stress Points in Soil Elements (PLAXIS 2D User’s Manual, 2010)

After the mesh generation of the 2D finite element model, calculations window appears, where the user defines the intended construction stages which will take place at site. PLAXIS 2D finite element program offers different types of analysis in this part, basically, plastic calculation, consolidation analysis, safety (ϕ/c reduction) analyses and dynamic analyses. In this study, consolidation analysis will be utilized in order to analyze the development and dissipation of excess pore pressures in a saturated clay-type soil as a function of time. In this way, time dependent variation of the neutral point and downdrag forces on the diaphragm wall will be observed.

Following the execution of the calculation phases defined in calculation program, the program allows the user to view the finite element solution of the selected phases. In the output program, it is possible to view all numerical calculation results like deformed meshes, total displacements, incremental displacements, total strains, effective stresses, total stresses, plastic points, active and excess pore pressures and internal forces of the structural elements. The internal forces of structural elements may be viewed both for the selected phase and envelope of the sectional forces up to selected phase.

3.3. Constitutive Models

3.3.1. Elastic - Perfectly Plastic Model

Elastic - perfectly plastic model also widely referred to Mohr - Coulomb model is a constitutive model which expresses the mechanical behavior of soils as linearly elastic perfectly plastic soil response. The model defines a fixed yield function beyond where, perfectly plastic behavior is monitored that causes irreversible strain.

The basic idea of a linearly elastic perfectly plastic model is decomposition of the elastic and plastic parts of the strain rates as shown in Figure 18.

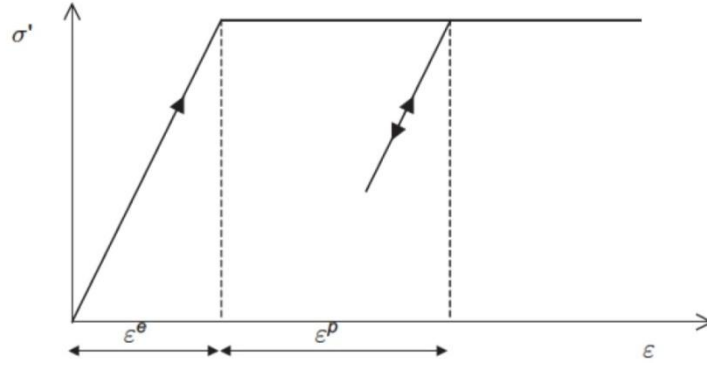


Figure 18: The Basic Idea of an Elastic Perfectly Plastic Model (PLAXIS 2D User's Manual, 2010)

Within the scope of this study, the corresponding 'Silty Sand' layer explained in section 3.3 is modeled by the above mentioned linearly elastic perfectly plastic model. This mathematical model is governed in PLAXISTM by the following set of equations from (15) to (30), where

- $\dot{\sigma}'$ the effective stress rate
- $\dot{\epsilon}$ the strain rate
- $\dot{\nu}'$ the effective Poisson's ratio
- \dot{E}' the effective Young's modulus
- $\underline{\underline{D}}^e$ the elastic material stiffness matrix
- f the yield function
- g the plastic potential function
- α the switch parameter
- φ the friction angle
- c the cohesion
- ψ the dilatancy angle

$$\underline{\dot{\epsilon}} = \underline{\dot{\epsilon}}^e + \underline{\dot{\epsilon}}^p \quad (15)$$

$$\underline{\underline{D}}^e = \frac{E'}{(1-2\nu')(1+\nu')} \begin{bmatrix} (1-\nu') & \nu' & \nu' & 0 & 0 & 0 \\ \nu' & (1-\nu') & \nu' & 0 & 0 & 0 \\ \nu' & \nu' & (1-\nu') & 0 & 0 & 0 \\ 0 & 0 & 0 & (\frac{1}{2}-\nu') & 0 & 0 \\ 0 & 0 & 0 & 0 & (\frac{1}{2}-\nu') & 0 \\ 0 & 0 & 0 & 0 & 0 & (\frac{1}{2}-\nu') \end{bmatrix} \quad (16)$$

$$\underline{\dot{\sigma}}' = \left(\underline{\underline{D}}^e - \frac{\alpha}{d} \underline{\underline{D}}^e \frac{\partial g}{\partial \underline{\sigma}'} \frac{\partial f^T}{\partial \underline{\sigma}'} \underline{\underline{D}}^e \right) \underline{\dot{\epsilon}} \quad (17)$$

$$d = \frac{\partial f^T}{\partial \underline{\sigma}'} \underline{\underline{D}}^e \frac{\partial g}{\partial \underline{\sigma}'} \quad (18)$$

The Mohr - Coulomb yield function (f) is formulated in terms of principal stresses as explained in (19) - (24) and illustrated in Figure 19.

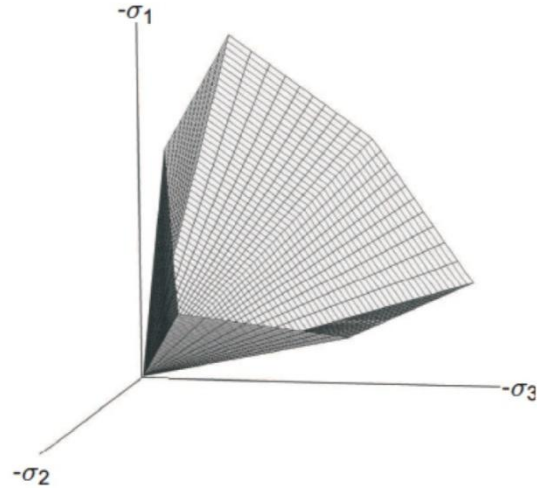


Figure 19: The Mohr - Coulomb Yield Surface In Principal Stress Space ($c=0$) (PLAXIS 2D User's Manual, 2010)

$$f_{1a} = \frac{1}{2}(\sigma'_2 - \sigma'_3) + \frac{1}{2}(\sigma'_2 + \sigma'_3) \sin \varphi - c \cos \varphi \leq 0 \quad (19)$$

$$f_{1b} = \frac{1}{2}(\sigma'_3 - \sigma'_2) + \frac{1}{2}(\sigma'_3 + \sigma'_2) \sin \varphi - c \cos \varphi \leq 0 \quad (20)$$

$$f_{2a} = \frac{1}{2}(\sigma'_3 - \sigma'_1) + \frac{1}{2}(\sigma'_3 + \sigma'_1) \sin \varphi - c \cos \varphi \leq 0 \quad (21)$$

$$f_{2b} = \frac{1}{2}(\sigma'_1 - \sigma'_3) + \frac{1}{2}(\sigma'_1 + \sigma'_3) \sin \varphi - c \cos \varphi \leq 0 \quad (22)$$

$$f_{3a} = \frac{1}{2}(\sigma'_1 - \sigma'_2) + \frac{1}{2}(\sigma'_1 + \sigma'_2) \sin \varphi - c \cos \varphi \leq 0 \quad (23)$$

$$f_{3b} = \frac{1}{2}(\sigma'_2 - \sigma'_1) + \frac{1}{2}(\sigma'_2 + \sigma'_1) \sin \varphi - c \cos \varphi \leq 0 \quad (24)$$

The plastic potential function (g) which contains dilatancy angle (ψ) is also defined to model plastic volumetric strain increments (dilatancy) as observed for dense soils.

$$g_{1a} = \frac{1}{2}(\sigma'_2 - \sigma'_3) + \frac{1}{2}(\sigma'_2 + \sigma'_3) \sin \psi \quad (25)$$

$$g_{1b} = \frac{1}{2}(\sigma'_3 - \sigma'_2) + \frac{1}{2}(\sigma'_3 + \sigma'_2) \sin \psi \quad (26)$$

$$g_{2a} = \frac{1}{2}(\sigma'_3 - \sigma'_1) + \frac{1}{2}(\sigma'_3 + \sigma'_1) \sin \psi \quad (27)$$

$$g_{2b} = \frac{1}{2}(\sigma'_1 - \sigma'_3) + \frac{1}{2}(\sigma'_1 + \sigma'_3) \sin \psi \quad (28)$$

$$g_{3a} = \frac{1}{2}(\sigma'_1 - \sigma'_2) + \frac{1}{2}(\sigma'_1 + \sigma'_2) \sin \psi \quad (29)$$

$$g_{3b} = \frac{1}{2}(\sigma'_2 - \sigma'_1) + \frac{1}{2}(\sigma'_2 + \sigma'_1) \sin \psi \quad (30)$$

The basic input parameters of the linearly elastic perfectly plastic Mohr - Coulomb model for digital simulation are given in Table 3.

Table 3: Parameters of the Mohr - Coulomb Model

Parameter	Explanation	Unit
E	Young's modulus	kN/m^2
ν	Poisson's ratio	$[-]$
c	Cohesion	kN/m^2
φ	Friction angle	$[^\circ]$
ψ	Dilatancy angle	$[^\circ]$

3.3.2. Soft-Soil Model

Soft soils (e.g. normally consolidated clays, clayey silts and peat) have a common feature of high degree of compressibility, which is confirmed by oedometer test data by Janbu (1985). Therefore, the soft soil model considers logarithmic compression behaviour and defines stress dependent soil stiffness. In addition to this, the model defines a distinction between primary loading and unloading - reloading. The pre-consolidation pressure which is the largest stress level experienced by the soil, remains constant during unloading - reloading. However, in primary loading, the pre-consolidation pressure increases resulting in plastic (irreversible) volumetric strains.

Within the scope of this study, the corresponding 'Clay' layer explained in section 3.4 is modeled by the above mentioned soft soil model. The soft soil model makes use of the following equations to define the isotropic ($\sigma'_1 = \sigma'_2 = \sigma'_3$) states of stress and strain where

- ε_v the volumetric strain
- p' the mean effective stress
- λ^* the modified compression index
- κ^* the modified swelling index
- E_{ur} the unloading / reloading elastic Young's modulus
- K_{ur} the unloading / reloading elastic bulk modulus

$$\varepsilon_v - \varepsilon_v^0 = -\lambda^* \ln \frac{p'}{p^0} \quad (31)$$

$$\varepsilon_v^e - \varepsilon_v^{e0} = -\kappa^* \ln \frac{p'}{p^0} \quad (32)$$

$$K_{ur} = \frac{E_{ur}}{3(1 - 2\nu_{ur})} = \frac{p'}{\kappa^*} \quad (33)$$

The logarithmic relation between volumetric strain (ε_v) and mean stress (p') is represented in Figure 20 together with the modified compression and swelling indexes.

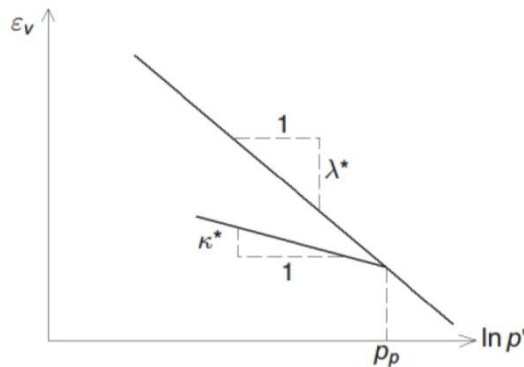


Figure 20: Logarithmic Relation Between Volumetric Strain and Mean Stress (PLAXIS 2D User's Manual, 2010)

The yield function of the soft soil model in PLAXISTM is explained for the triaxial loading case, where $\sigma'_2 = \sigma'_3$ as follows:

$$f = \bar{f} - p_p \quad (34)$$

where \bar{f} is the function of the stress state (p', q) and p_p is the pre-consolidation stress obtained by the following equations:

$$\bar{f} = \frac{q^2}{M^2(p' + c \cot \varphi)} + p' \quad (35)$$

$$p_p = p_p^0 \exp\left(\frac{-\varepsilon_v^p}{\lambda^* - k^*}\right) \quad (36)$$

where M is the parameter which determines the height of the ellipse in the yield surface of the soft soil model in $p' - q$ plane as illustrated in Figure 21.

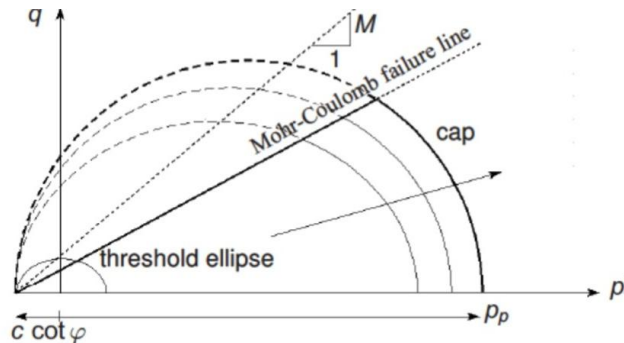


Figure 21: The Yield Surface of the Soft Soil Model in $p' - q$ Plane

As a summary, the plastic behaviour of the soft soil model is defined by compression yield functions and Mohr-Coulomb yield functions. The resulting total yield contour in principal stress state is illustrated in Figure 22.

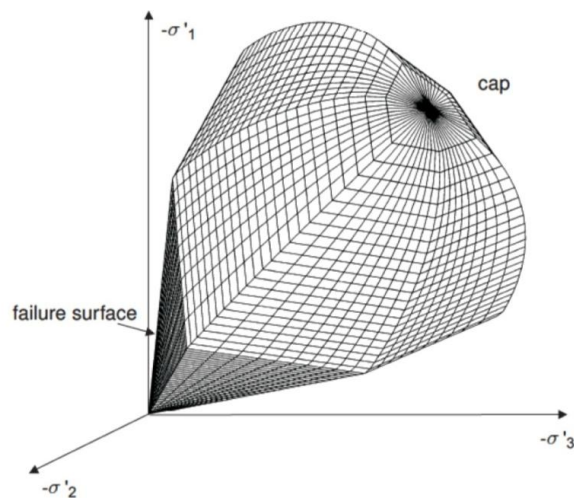


Figure 22: Representation of the Total Yield Contour of the Soft Soil Model in Principal Stress Space (PLAXIS 2D User's Manual, 2010)

The basic parameters of the soft soil model for digital simulation are given in Table 4.

Table 4: Parameters of the Soft - Soil model

Parameter	Explanation	Unit
λ^*	Modified compression index	[-]
\bar{k}^*	Modified swelling index	[-]
c	Cohesion	kN/m ²
φ	Friction angle	[⁰]
Ψ	Dilatancy angle	[⁰]

3.3.3. Hardening Soil Model

The hardening soil model is an advanced constitutive model which is used to model both soft soils and stiff soils as stated in Schanz (1998). The essential characteristic of the hardening soil model is the stress dependency of soil stiffness. As well known, soil shows a decreasing stiffness and irreversible plastic strain when subjected to deviatoric loading. Konder (1963) studied this relationship between the axial strain and deviatoric stress and approximated it by a hyperbola which is used in Duncan & Chang (1970) hyperbolic model. However, hardening soil model is a more sophisticated model compared to the hyperbolic model by means of considering the theory of plasticity, including soil dilatancy and introducing yield cap. Within the scope of this study, the corresponding 'Gravelly Sand' layer explained in section 3.4 is modeled by the above mentioned hardening soil model.

The hyperbolic stress-strain relationship in primary loading for a standard drained triaxial test (Figure 23) are defined by the following equations, where,

- ε_1 the vertical strain
- q the deviatoric stress
- q_f the ultimate deviatoric stress
- q_a the quantity
- R_f the failure ratio
- E_i the initial stiffness
- E_{50} the confining stress dependent stiffness modulus for primary loading
- p^{ref} the reference confining pressure
- E_{50}^{ref} the reference stiffness modulus corresponding to the p^{ref}
- m the power
- σ'_3 the minor principal stress
- φ the friction angle
- c the cohesion

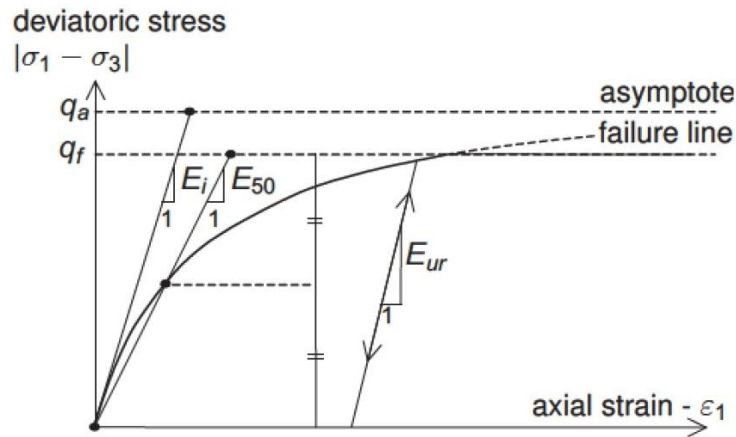


Figure 23: Hyperbolic Stress-Strain Relation in Primary Loading for a Standard Drained Triaxial Test (PLAXIS 2D User's Manual, 2010)

$$-\varepsilon_1 = \frac{1}{E_i} \frac{q}{1 - \frac{q}{q_a}} \quad \text{for } q < q_f \quad (37)$$

$$E_i = \frac{2E_{50}}{2 - R_f} \quad (38)$$

$$E_{50} = E_{50}^{ref} \left(\frac{c \cos \varphi - \sigma'_3 \sin \varphi}{c \cos \varphi + p^{ref} \sin \varphi} \right)^m \quad (39)$$

$$q_f = (c \cot \varphi - \sigma'_3) \frac{2 \sin \varphi}{1 - \sin \varphi} \quad \text{and} \quad q_a = \frac{q_f}{R_f} \quad (40)$$

$$E_{ur} = E_{ur}^{ref} \left(\frac{c \cos \varphi - \sigma'_3 \sin \varphi}{c \cos \varphi + p^{ref} \sin \varphi} \right)^m \quad (41)$$

The approximation of the hyperbola by the hardening soil model is represented below for triaxial loading conditions, where $\sigma'_2 = \sigma'_3$ and σ'_1 being the major compressive stress. Primarily, a shear hardening yield function is formed considering the plastic strains. The set of mathematical equations are represented below, where,

\bar{f} the function of stress
 γ^p the function of plastic strains
 ε_v^p the plastic volume change

$$f = \bar{f} - \gamma^p \quad (42)$$

$$\bar{f} = \frac{2}{E_i} \frac{q}{1 - \frac{q}{q_a}} - \frac{2q}{E_{ur}} \quad (43)$$

$$\gamma^p = -(2\varepsilon_1^p - \varepsilon_v^p) \approx 2\varepsilon_1^p \quad (44)$$

For primary loading, the yield condition $f = 0$ results in;

$$\varepsilon_1^p \approx \frac{1}{2} \bar{f} = \frac{1}{E_i} \frac{1}{1 - \frac{q}{q_a}} - \frac{q}{E_{ur}} \quad (45)$$

For drained triaxial stress paths with $\sigma'_2 = \sigma'_3 = \text{constant}$, the elastic Young's modulus E_{ur} remains constant. In this case, the elastic strain phenomenon is expressed via the following equations below in the hardening soil model.

$$-\varepsilon_1^e = \frac{q}{E_{ur}} \quad (46)$$

$$-\varepsilon_2^e = -\varepsilon_3^e = -v_{ur} \frac{q}{E_{ur}} \quad (47)$$

$$-\varepsilon_1 = -\varepsilon_1^e - \varepsilon_1^p \approx \frac{1}{E_i} - \frac{1}{1 - \frac{q}{q_a}} \quad (48)$$

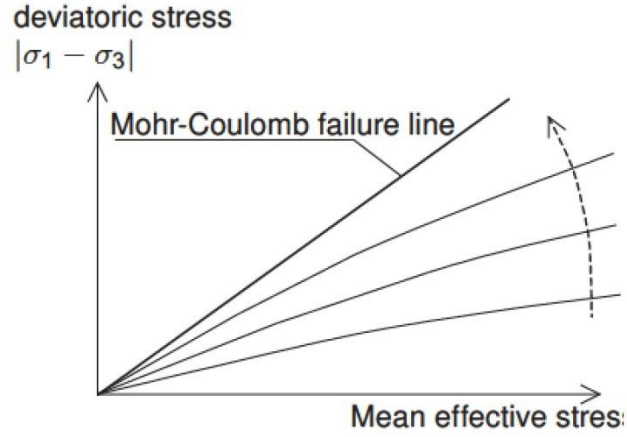


Figure 24: Successive Yield Loci for Various Constant Values of the Hardening Parameter γ^p (PLAXIS 2D User's Manual, 2010)

The relationship between plastic shear strain, $\dot{\gamma}^p$, and plastic volumetric strain, $\dot{\varepsilon}_v^p$, is obtained by the following equation.

$$\dot{\varepsilon}_v^p = \sin \psi_m \dot{\gamma}^p \quad (49)$$

The mobilized dilatancy angle, ψ_m is specified by the following cases.

For $\sin \varphi_m < 3/4 \sin \varphi$:

$$\psi_m = 0$$

For $\sin \varphi_m \geq 3/4 \sin \varphi$ and $\psi > 0$:

$$\sin \psi_m = \max \left(\frac{\sin \varphi_m - \sin \varphi_{cv}}{1 - \sin \varphi_m \sin \varphi_{cv}}, 0 \right) \quad (50)$$

For $\sin \varphi_m \geq 3/4 \sin \varphi$ and $\psi \leq 0$:

$$\psi_m = \psi$$

If $\varphi = 0$

$$\psi_m = 0$$

where φ_{cv} is the critical state friction angle which is a material constant and not dependent of the density and the mobilized friction angle is calculated by the following equation.

$$\sin \varphi_m = \frac{\sigma'_1 - \sigma'_3}{\sigma'_1 + \sigma'_3 - 2c \cot \varphi} \quad (51)$$

The above equations are a small adaptation of stress - dilatancy theory and the main property of the stress - dilatancy theory is that "the material contracts for small stress ratios $\varphi_m < \varphi_{cv}$, whilst dilatancy occurs for high stress ratios $\varphi_m > \varphi_{cv}$. At the failure, when the mobilized friction angle, φ_m , equals to the failure angle, φ , it is found from equation (52) that:

$$\sin \psi = \frac{\sin \varphi - \sin \varphi_{cv}}{1 - \sin \varphi \sin \varphi_{cv}} \quad (52)$$

The basic parameters of the hardening soil model for digital simulation are given in Table 5.

Table 5: Parameters of Hardening Soil Model

Parameter	Explanation	Unit
c	(Effective) cohesion	kN/m ²
φ	(Effective) angle of internal friction	[⁰]
Ψ	Angle of dilatancy	[⁰]
E_{50}	Secant stiffness in standard drained triaxial test	kN/m ²
E_{oed}	Tangent stiffness for primary oedometer loading	kN/m ²
m	Power for stress-level dependency of stiffness	[–]
E_{ur}	Unloading-reloading stiffness ($E_{ur}=3E_{50}$)	kN/m ²
ν_{ur}	Poisson's ratio for unloading-reloading ($\nu_{ur}=0.2$)	[–]
K_0	K_0 value for normal consolidation ($K_0=1-\sin\varphi$)	[–]

3.4. Modeling Scenario and Cases

3.4.1. The Soil - Diaphragm Wall Model

3.4.1.1. Geometry and Definitions

The geological profile of the analyzed soil section is represented in Figure 25. As can be observed from the corresponding figure, the geological profile of the soil section consists of silty sand (indicated by blue), clay (indicated by yellow) and gravelly sand (indicated by green) layers. Geotechnical properties of the corresponding soil layers, together with their mathematical model parameters is explained in detail in the following section.

In addition to the soil layers, the per unit model of the analyzed diaphragm wall section is also illustrated in Figure 25. The properties of the corresponding wall section, together with its mathematical model parameters is also explained in detail in the following section.

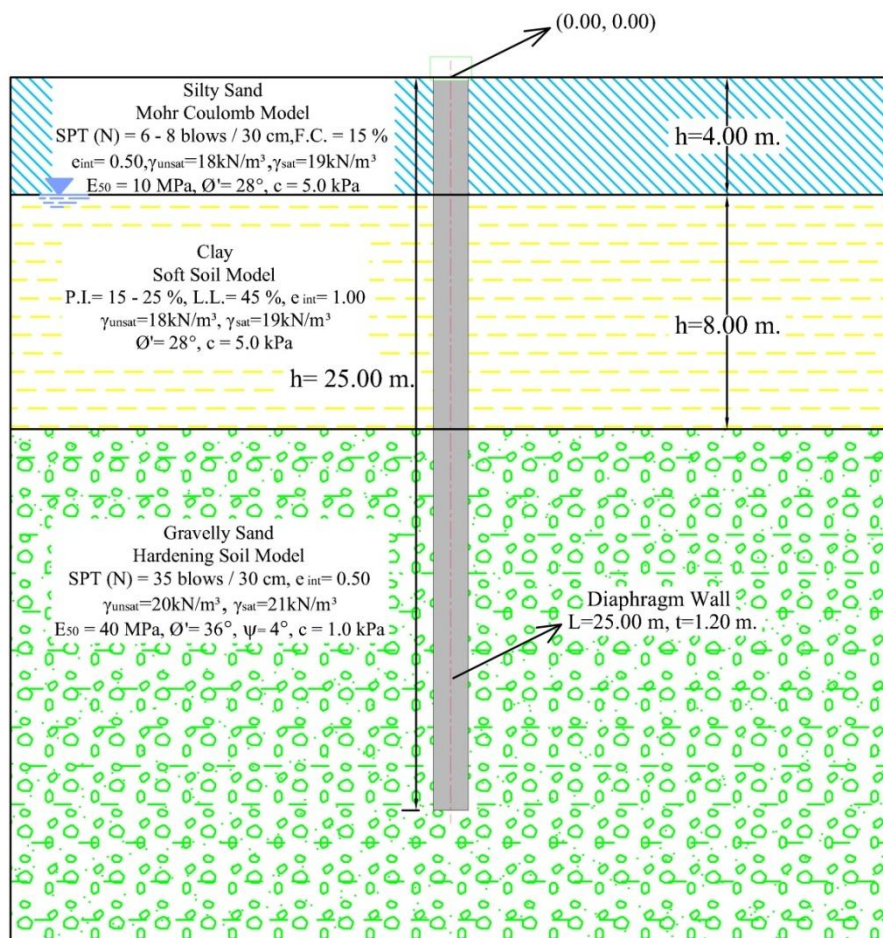


Figure 25: The Geological Profile of the Analyzed Soil Section

3.4.1.2. Parameter Selection

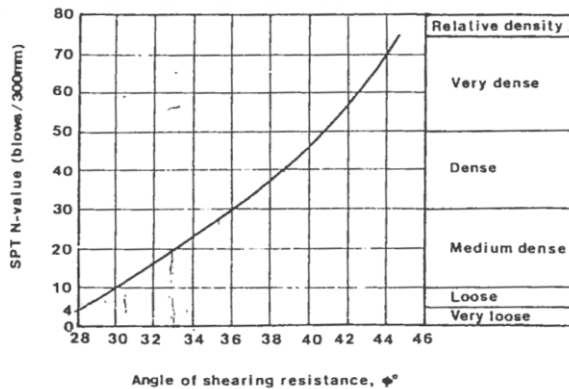
3.4.1.2.1. Silty Sand Layer

In this study, the 'Silty Sand' layer is modeled by the Mohr-Coulomb model. Representative parameters for this soil section is summarized in Table 6 (Carter & Bentley, 1991, Bowles, 1997, PLAXIS 2D User's Manual, 2010).

Table 6: Parameters of the Silty Sand Layer for Mohr - Coulomb Model

Parameter	Symbol	Reference	Value	Unit
Fines Content	FC	-	15	%
Standard Penetration Test Result	N	-	6 - 8	[-]
Drained Unit Weight	γ_{unsat}	Carter & Bentley (1991) Page 40, Table 3.1	18	kN/m ³
Saturated Unit Weight	γ_{sat}	Carter & Bentley (1991) Page 40, Table 3.1	19	kN/m ³
Initial Void Ratio	e_{int}	-	0,5	[-]
Young's Modulus	E_{50}	Bowles, J.E. (1997) Page 316, Table 5.6	10 000 ²	kN/m ²
Poisson's Ratio	ν	Bowles, J.E. (1997) Page 125, Table 2.7	0,3	[-]
Cohesion	c'	-	5,0	kN/m ²
Friction Angle	φ'	Carter & Bentley (1991) Page 92, Figure 6.14	28 - 30 ³	[⁰]
Dilatancy Angle	Ψ	Bolton M.D. (1986)	0	[⁰]
Coefficient of Permeability	$k_x = k_y$	Carter & Bentley (1991) Page 52, Table 4.1	0,086 ⁴	m/day
Strength Reduction Factor in the Interface	R_{inter}	Acc. to PLAXIS 2D User's Manual, 2010	0,635 ⁵	[-]

²According to (Bowles, 1997); $E_{50} = 500(N + 15)$, which gives $E_{50} = 500(6+15) = 10500$ kPa. Therefore, Young's Modulus (E_{50}) is chosen as 10000 kPa as referring to the value calculated.



³

⁴For silty sand, typical permeability values are in the range of 10^{-6} m/s - 10^{-8} m/s according to Carter & Bentley (1991). In this case, for the silty sand layer permeability value is assumed to be 10^{-6} m/s which is equal to 0.086m/day.

⁵The strength reduction factor, (R_{inter}), is defined such that the interface strength to the soil strength is in the order of 2/3 of the soil strength as recommended in the Plaxis User's Manual. In this case, for the silty sand layer where angle of friction (φ') is equal to 28°, the strength reduction factor, R_{inter} , is calculated as; $R_{inter} = \frac{\tan \frac{2\varphi'}{3}}{\tan \varphi} = 0,635$

3.4.1.2.2. Clay Layer

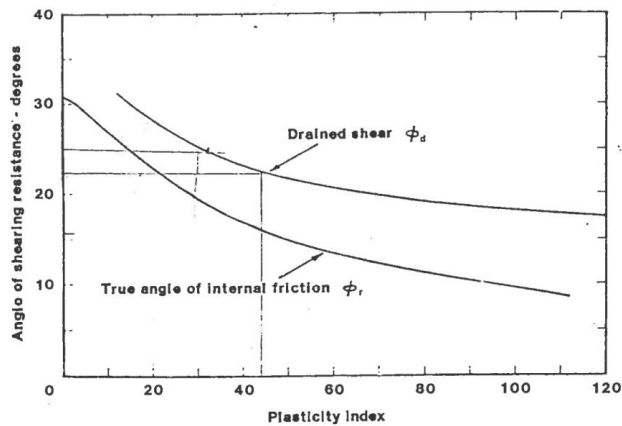
In this study, the 'Clay' layer is modeled by the Soft Soil model. Representative parameters for this soil section is summarized in Table 7 (Carter & Bentley, 1991, Bowles, 1997, PLAXIS 2D User's Manual, 2010).

Table 7: Parameters of the Clay Model

Parameter	Symbol	Reference	Value	Unit
Plasticity Index	PI	-	15 - 25	%
Liquid Limit	LL	-	45	%
Drained Unit Weight	γ_{unsat}	Carter & Bentley (1991) Page 40, Table 3.1	18	kN/m ³
Saturated Unit Weight	γ_{sat}	Carter & Bentley (1991) Page 40, Table 3.1	19	kN/m ³
Initial void ratio	e_{int}	-	1,0	[-]
Modified compression index	λ^*	Acc. to PLAXIS 2D User's Manual, 2010	0,068 ⁶	[-]
Modified swelling index	κ^*	Acc. to PLAXIS 2D User's Manual, 2010	0,027 ⁷	[-]
Cohesion	c'	-	5,0	kN/m ²
Friction angle	φ'	Carter & Bentley (1991) Page 89, Figure 6.12	28 ⁸	[°]
Dilatancy angle	ψ	-	0	[°]
Coefficient of permeability	$k_x = k_y$	Carter & Bentley (1991) Page 52, Table 4.1	4,75x10 ⁻⁴ ⁹	m/day
Strength reduction factor in the interface	R_{inter}	Acc. to PLAXIS 2D User's Manual, 2010	0,635 ⁵	[-]

⁶ For Liquid Limit (L.L.) = 45 %, Compression Index (C_c) is calculated as; $C_c = 0.009 (LL - 10) = 0,315$. Therefore, the modified compression index (λ^*) is calculated as; $\lambda^* = \frac{C_c}{2.3(1+e)} = 0,068$.

⁷ $C_r = 0.20 C_c = 0,063$. Therefore, the modified swelling index (κ^*) is calculated as; $\kappa^* = \frac{2C_r}{2.3(1+e)} = 0,027$.



⁸

⁹ For clay, the typical permeability values are in the range of 10⁻⁸m/s - 10⁻⁹ m/s according to the Carter & Bentley (1991). Therefore, in this case, for the clay layer, the permeability value is assumed to be average of the range given above that is 0.5x10⁻⁸m/s which is equal to 4.75x10⁻⁴ m/day.

3.4.1.2.3. Gravelly Sand Layer

In this study, the 'Gravelly Sand' layer is modeled by the Hardening Soil model. The properties of the corresponding gravelly sand layer are as follows: Standard Penetration Test Result (N) = 35 and initial void ratio (e_{int}) = 0.50. Representative parameters for this soil section is summarized in Table 8 (Carter & Bentley, 1991, Bowles, 1997, PLAXIS 2D User's Manual, 2010).

Table 8: Parameters of the Hardening Soil Model

Parameter	Symbol	Reference	Value	Unit
Standard Penetration Test Result	N	-	35	[-]
Drained Unit Weight	γ_{unsat}	Carter & Bentley (1991) Page 40, Table 3.1	20	kN/m ³
Saturated Unit Weight	γ_{sat}	Carter & Bentley (1991) Page 40, Table 3.1	21	kN/m ³
Initial void ratio	e_{int}	-	0,5	[-]
(Effective) cohesion	c'	-	1,0	kN/m ²
(Effective) angle of internal friction	φ'	Carter & Bentley (1991) Page 92, Figure 6.14	36 ²	[°]
Angle of dilatancy	Ψ	Bolton M.D. (1986)	2 - 4	[°]
Secant stiffness in standard drained triaxial test	E_{50}	Bowles, J.E. (1997) Page 316, Table 5.6	40 000 ¹⁰	kN/m ²
Tangent stiffness for primary oedometer loading	E_{oed}	Acc. to PLAXIS 2D User's Manual, 2010	40 000	kN/m ²
Power for stress-level dependency of stiffness	M	Acc. to PLAXIS 2D User's Manual, 2010	0,5	[-]
Unloading-reloading stiffness ($E_{ur}=3E_{50}$)	E_{ur}	Acc. to PLAXIS 2D User's Manual, 2010	120 000	kN/m ²
Poisson's ratio for unloading-reloading ($\nu_{ur}=0.2$)	ν_{ur}	Bowles, J.E. (1997) Page 123, Table 2.7	0,2	[-]
K_0 value for normal consolidation ($K_0=1-\sin\varphi$)	K_0	Carter & Bentley (1991) Page 95	0,41	[-]
Coefficient of permeability	$k_x = k_y$	Carter & Bentley (1991) Page 52, Table 4.1	0,864 ¹¹	m/day
Strength reduction factor in the interface	R_{inter}	Acc. to PLAXIS 2D User's Manual, 2010	0,613 ⁵	[-]

3.4.1.2.4. Diaphragm Wall Parameters

In this study, per unit of the diaphragm wall section is modeled by the plate elements. Elastic material model is used in the analyses which requires the elastic modulus, (E) and Poisson's ratio, (ν) of the wall section. The required parameters are obtained by TS500, 2000 for concrete class of C20. The material properties of the wall section are summarized in Table 9.

Table 9: Parameters of the Diaphragm Wall Model

Parameter	Symbol	Value	Unit
Thickness	t	120	cm
Unit Weight	γ	24	kN/m ³
Elastic Modulus	E	28 500 000	kPa
Poisson's ratio	ν	0,2	[-]

¹⁰ According to (Bowles, 1997); $E_{50} = 1200(N + 6)$, which gives $E_{50} = 1200(35+6) = 49200$ kPa. Therefore, Young's Modulus (E_{50}) is chosen as 40000 kPa as referring to the value calculated.

¹¹ For gravelly sand, typical permeability values are in the range of 10^{-4} m/s - 10^{-5} m/s according to Carter & Bentley (1991). In this case, for the silty sand layer, the permeability value is assumed to be 10^{-3} m/s which is equal to 0.864 m/day.

3.4.2. Analysis Scenario 1: Diaphragm Wall - Soil Interaction Model

In order to assess the effect of negative skin friction on diaphragm walls two scenarios are analyzed. The first scenario is quite similar to the theoretical "single pile-soil model", considering per unit length approach. Therefore, this scenario is valuable from the point of view of illustrating the basic concepts and effectiveness of the utilized diaphragm wall, soil layer and bitumen models, modeling approach and assumptions.

The above mentioned "Analysis Scenario 1" breaks down into two sub scenarios, which comparatively illustrate the effect of bitumen utilization to reduce downdrag in very detail.

3.4.2.1. Case 1: Diaphragm Wall - Soil Interaction

The digital model illustrated in Figure 25 is simulated with the soil parameters explained in "The Soil - Diaphragm Wall Model" section. The strength reduction factor, (R_{inter}), is defined as $R_{inter}=0,635$ for silty sand and clay layers and $R_{inter}=0,612$ for the gravelly sand layer which relates the interface strength to the soil strength in the order of 2/3 of the soil strength as recommended in the PLAXIS User's Manual.

The above mentioned model illustrated in Figure 26 is numerically assessed with the following sequence of events (i.e., phases):

- Construction of embankment (Step 1)
- Assess until the average degree of consolidation (U) is reached to 10 % (Represents the time elapsed until the construction of the wall) and construct the diaphragm wall (Step 2)
- Assess until the average degree of consolidation of the clay layer reaches to U=25 % (Step 3)
- Assess until the average degree of consolidation of the clay layer reaches to U=40 % (Step 4)
- Assess until the average degree of consolidation of the clay layer reaches to U=55 % (Step 5)
- Assess until the average degree of consolidation of the clay layer reaches to U=70 % (Step 6)
- Assess until the average degree of consolidation of the clay layer reaches to U=85 % (Step 7)
- Assess until "long term" (i.e.: $P_{max} < 1,0$ kPa, U=99%)

The results of this simulation case are presented and evaluated in "Case 1: Diaphragm Wall - Soil Interaction" section.

Analysis Scenario 1

Case 1: Diaphragm Wall - Soil Interaction Model

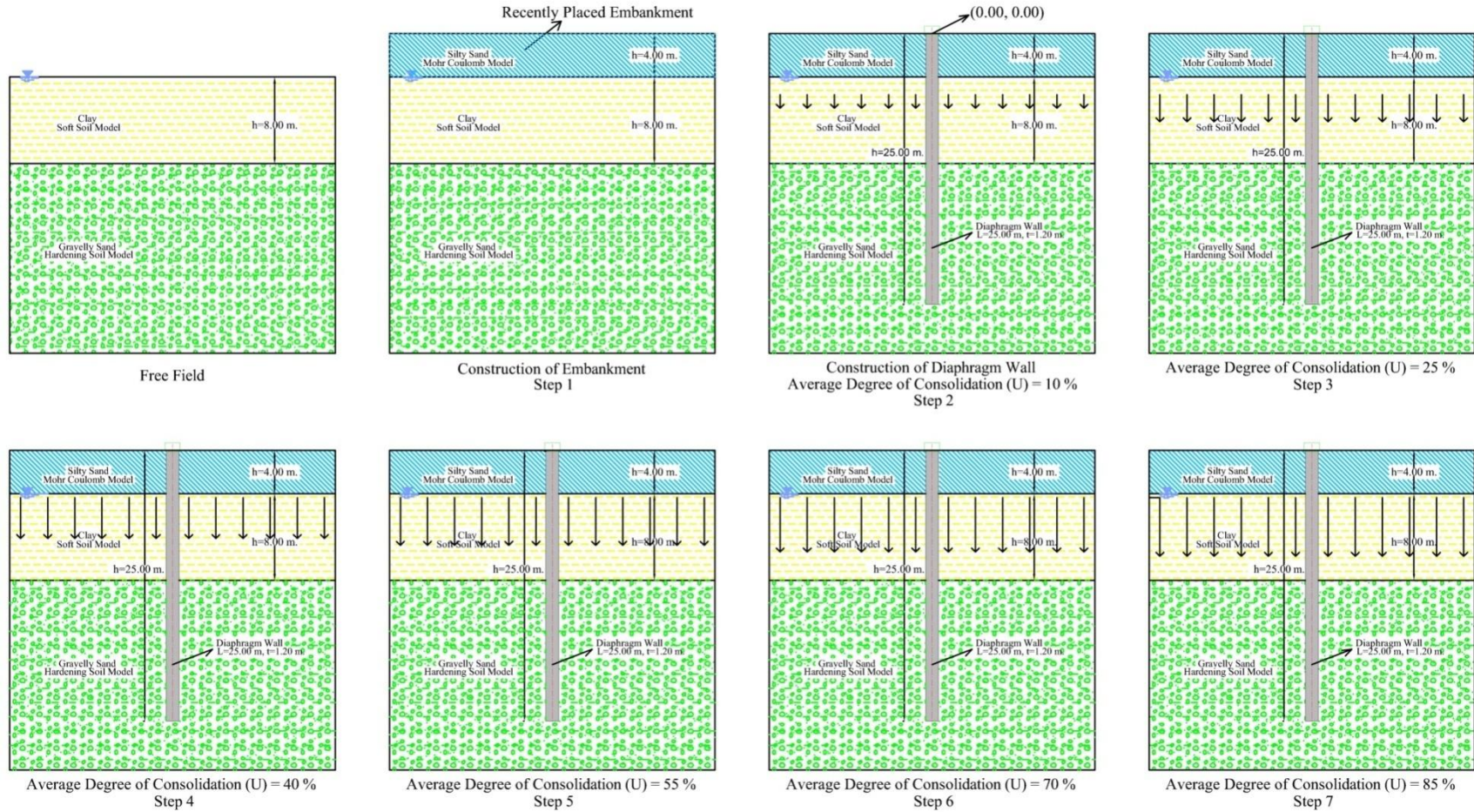


Figure 26: The Sequence of Events for Pure Consolidation Assessment

3.4.2.2. Case 2: Bitumen Coated Diaphragm Wall - Soil Interaction

In this case, the effect of the coating on the wall section is studied by means of reducing the strength reduction factor (R_{inter}). As explained in Briaud & Tucker (1996), case histories have shown that bitumen can reduce the friction to about 5 % to 30 % of the original soil shear strength. Since only the transient consolidation phenomenon is analyzed, which means there always exists sufficient displacement (i.e., strain) rate to fully increase the shear stress of the bitumen (see Equation (1)), this modeling assumption suits well to digital simulation approach. Therefore, in this study, the effect of bitumen is modeled by taking the soil-wall interface friction coefficient R_{inter} as 20 % of its de-facto value so that the value of strength reduction factors are defined as $R_{inter}=0,127$ for silty sand and clay layers.

The digital model illustrated in Figure 25 with the soil parameters explained in "The Soil - Diaphragm Wall Model" section is numerically assessed with the following sequence of events (i.e., phases) illustrated in Figure 27:

- Construction of embankment (Step 1)
- Assess until the average degree of consolidation (U) is reached to 10 % (Represents the time elapsed until the construction of the wall) and construct the diaphragm wall (Step 2)
- Assess until the average degree of consolidation of the clay layer reaches to U=25 % (Step 3)
- Assess until the average degree of consolidation of the clay layer reaches to U=40 % (Step 4)
- Assess until the average degree of consolidation of the clay layer reaches to U=55 % (Step 5)
- Assess until the average degree of consolidation of the clay layer reaches to U=70 % (Step 6)
- Assess until the average degree of consolidation of the clay layer reaches to U=85 % (Step 7)
- Assess until "long term" (i.e.: $P_{max} < 1,0$ kPa, U=99%)

The results of this simulation case are presented and evaluated in "Case 2: Bitumen Coated Diaphragm Wall - Soil Interaction" section.

Analysis Scenario 1

Case 2: Bitumen Coated Diaphragm Wall - Soil Interaction Model

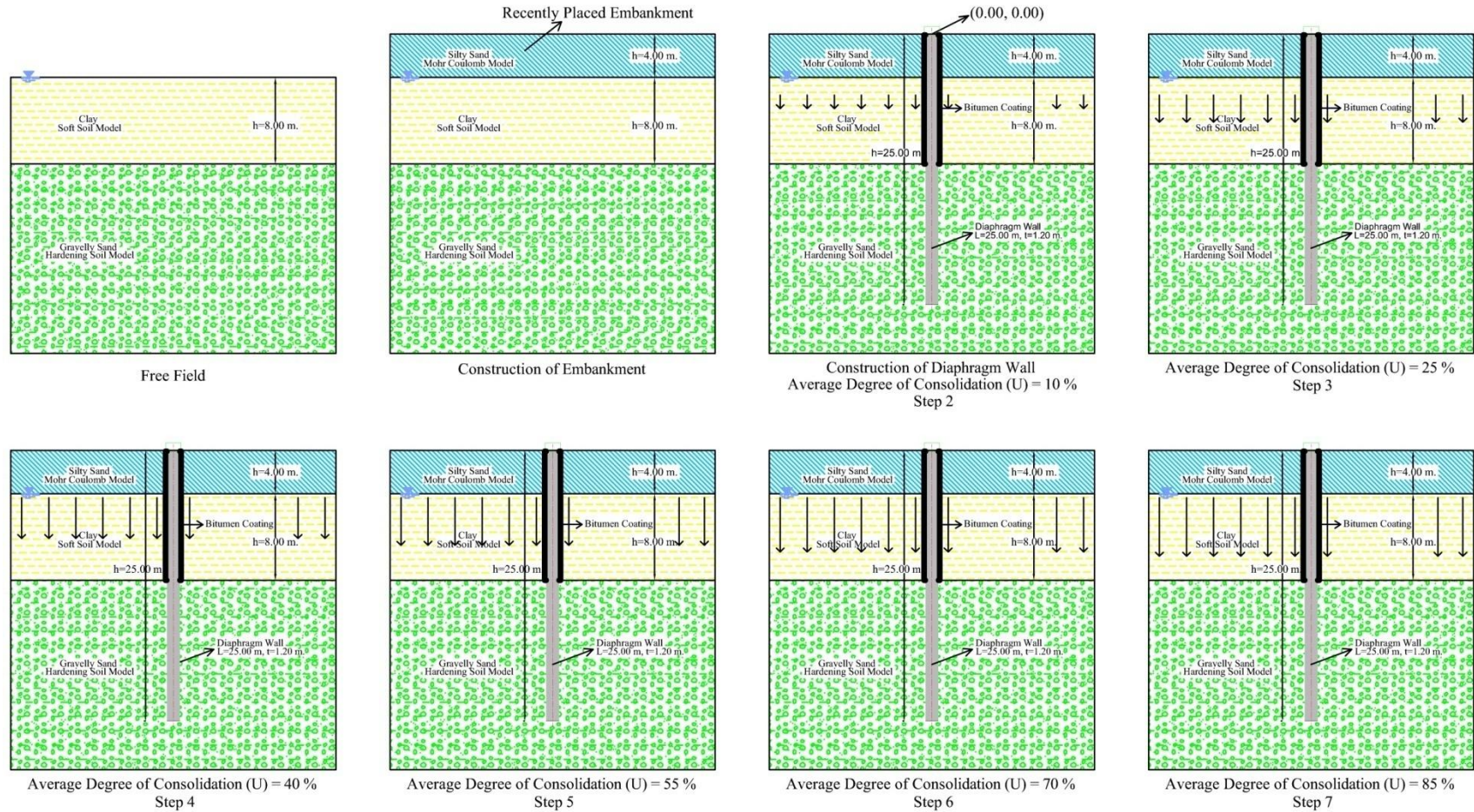


Figure 27: The Sequence of Events for Pure Consolidation Assessment with Bitumen Application

3.4.3. Analysis Scenario 2: Diaphragm Wall - Soil Interaction Model during Excavation

This model intends to assess the time dependent variation of downdrag forces and induced axial force, moment and shear on diaphragm wall during excavation stages illustrated in Figure 28.

The above mentioned "Analysis Scenario 2" breaks down into two hypothetical sub-scenarios to comparatively analyze the effect of negative skin friction on diaphragm walls in very detail.

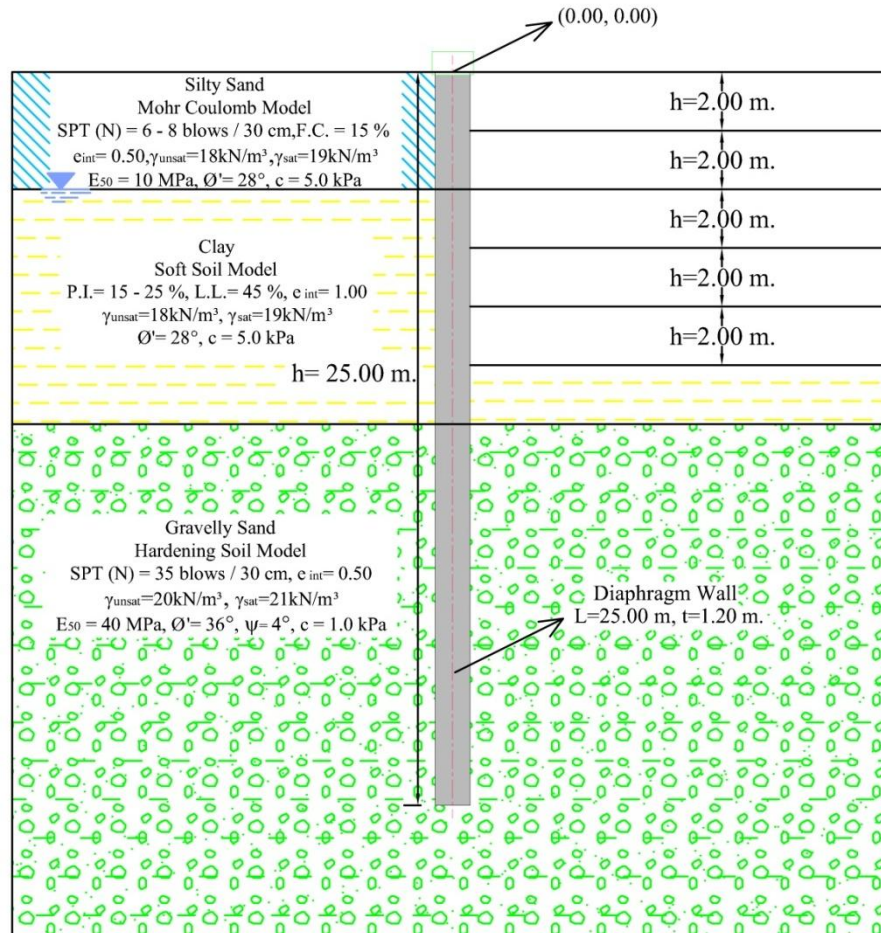


Figure 28: Diaphragm Wall Application And Excavation Of The Site

3.4.3.1. Case 1: Diaphragm Wall - Soil Interaction during Excavation

The digital model illustrated in Figure 28 is simulated with the soil parameters explained in "The Soil - Diaphragm Wall Model" section. The strength reduction factor, (R_{inter}), is defined as $R_{inter}=0,635$ for silty sand and clay layers and $R_{inter}=0,612$ for the gravelly sand layer which relates the interface strength to the soil strength in the order of 2/3 of the soil strength, as recommended in the PLAXIS User's Manual.

Analysis Scenario 2

Case 1: Diaphragm Wall - Soil Interaction Model during Excavation

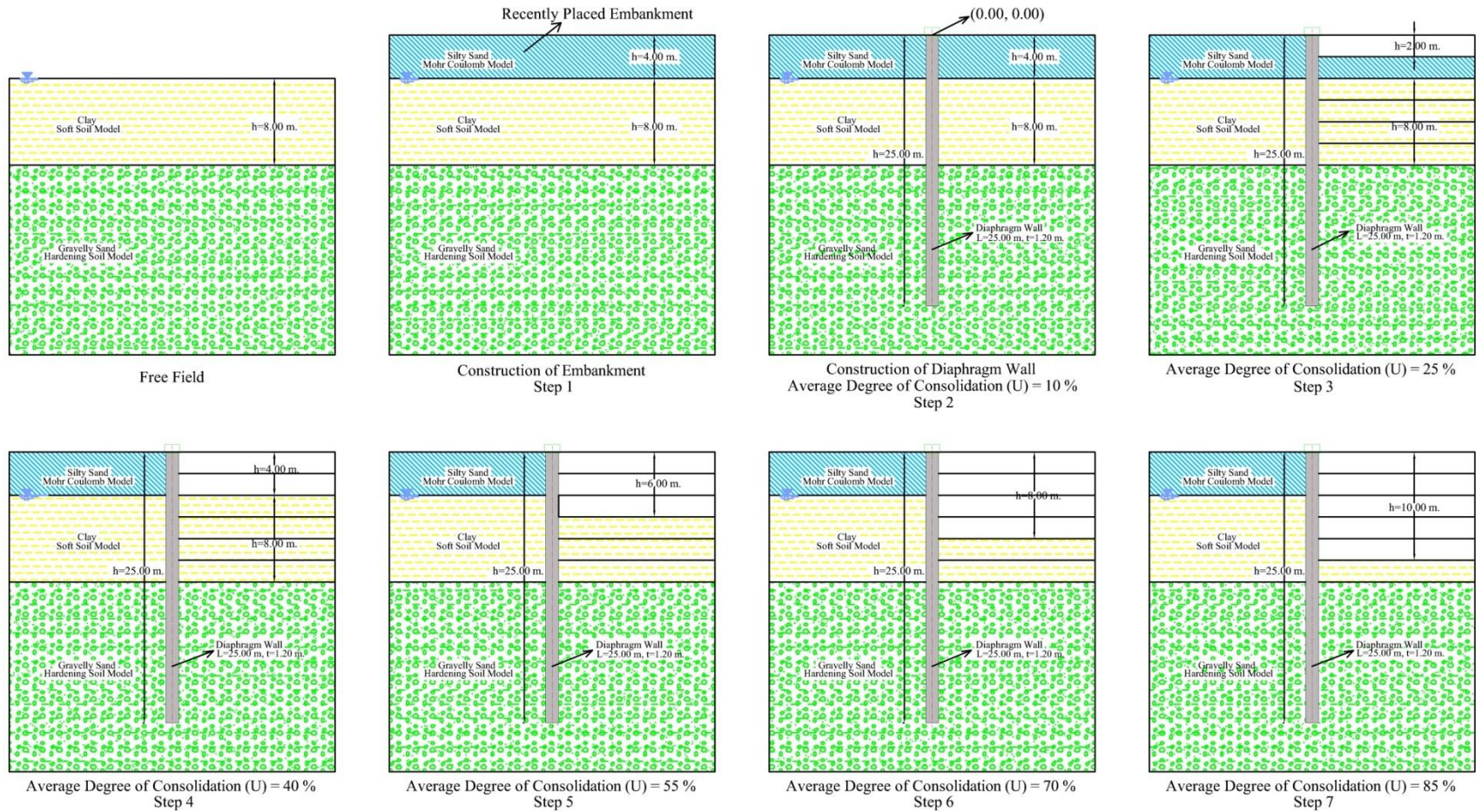


Figure 29: The Sequence of Excavation Stages

The digital model illustrated in Figure 29 is numerically assessed with the following sequence of events (i.e., phases):

- Construction of embankment (Step 1)
- Assess until the average degree of consolidation (U) is reached to 10 % (Represents the time elapsed until the construction of the wall) and construct the diaphragm wall (Step 2)
- 2.00 meters of excavation at the right side of the wall in 2 days where consolidation of clay layer continues and assess until the average degree of consolidation of the clay layer reaches to U=25 % (Step 3)
- 2.00 meters of excavation at the right side of the wall in 2 days where consolidation of clay layer continues and assess until the average degree of consolidation of the clay layer reaches to U=40 % (Step 4)
- 2.00 meters of excavation at the right side of the wall in 2 days where consolidation of clay layer continues and assess until the average degree of consolidation of the clay layer reaches to U=55 % (Step 5)
- 2.00 meters of excavation at the right side of the wall in 2 days where consolidation of clay layer continues and assess until the average degree of consolidation of the clay layer reaches to U=70 % (Step 6)
- 2.00 meters of excavation at the right side of the wall in 2 days where consolidation of clay layer continues and assess until the average degree of consolidation of the clay layer reaches to U=85 % (Step 7)
- Assess until "long term" (i.e.: $P_{\max} < 1,0 \text{ kPa}$, U=99%)

The results of this simulation case are presented and evaluated in "Case 1: Diaphragm Wall - Soil Interaction during Excavation" section.

3.4.3.2. Case 2: Bitumen Coated Diaphragm Wall - Soil Interaction during Excavation

In this case, the strength reduction factor (R_{inter}) is chosen as 20 % of its de-facto value to analyze the effect of negative skin friction on diaphragm walls. Therefore, the value of strength reduction factors are defined as $R_{\text{inter}}=0,127$ for silty sand and clay layers.

Analysis Scenario 2

Case 2: Bitumen Coated Diaphragm Wall - Soil Interaction Model during Excavation

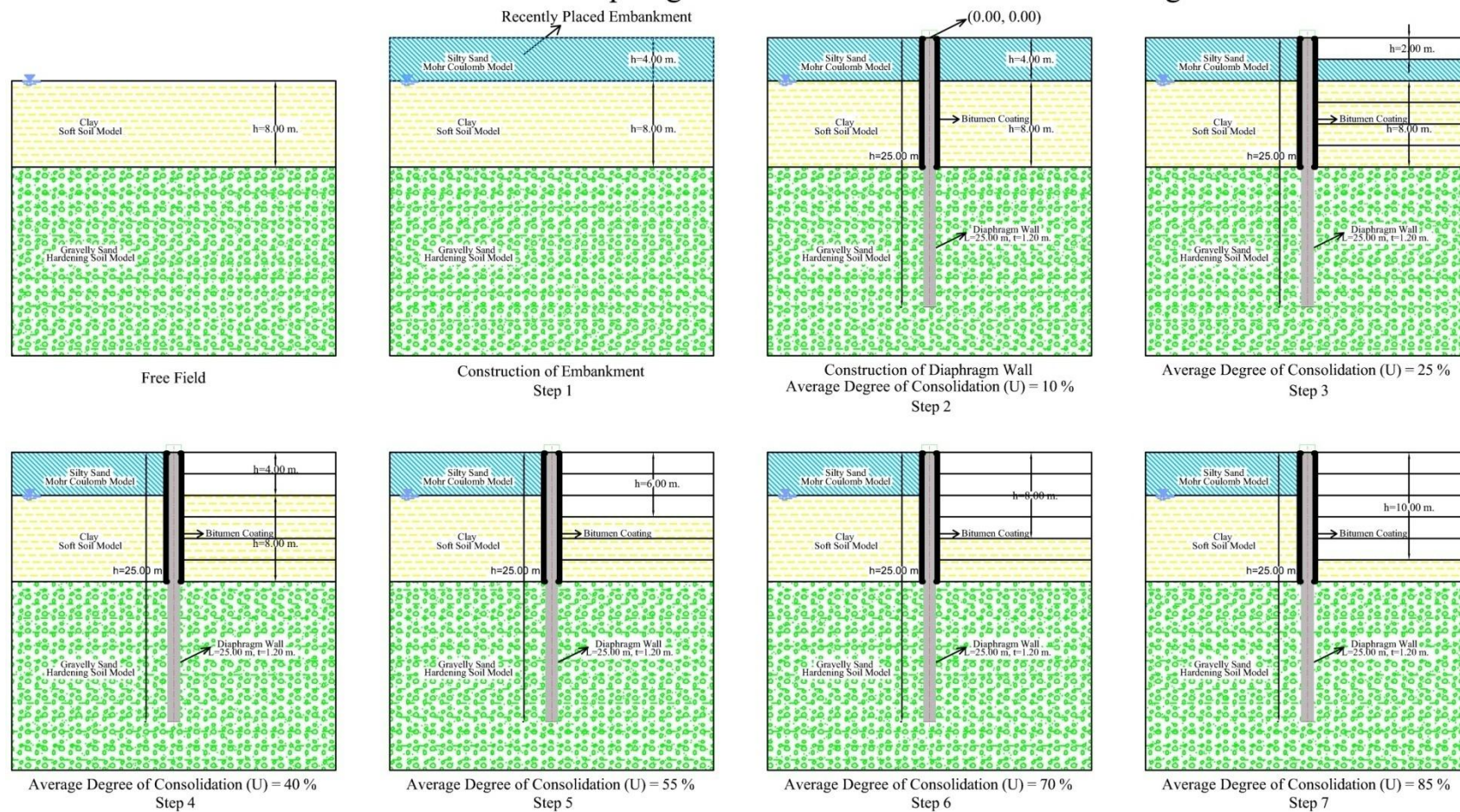


Figure 30: The Sequence of Excavation Stages with Bitumen Application

The digital model illustrated in Figure 28 with the soil parameters explained in "The Soil - Diaphragm Wall Model" section is numerically assessed with the following sequence of events (i.e., phases) illustrated in Figure 30:

- Construction of embankment (Step 1)
- Assess until the average degree of consolidation (U) is reached to 10 % (Represents the time elapsed until the construction of the wall) and construct the diaphragm wall (Step 2)
- 2.00 meters of excavation at the right side of the wall in 2 days where consolidation of clay layer continues and assess until the average degree of consolidation of the clay layer reaches to U=25 % (Step 3)
- 2.00 meters of excavation at the right side of the wall in 2 days where consolidation of clay layer continues and assess until the average degree of consolidation of the clay layer reaches to U=40 % (Step 4)
- 2.00 meters of excavation at the right side of the wall in 2 days where consolidation of clay layer continues and assess until the average degree of consolidation of the clay layer reaches to U=55 % (Step 5)
- 2.00 meters of excavation at the right side of the wall in 2 days where consolidation of clay layer continues and assess until the average degree of consolidation of the clay layer reaches to U=70 % (Step 6)
- 2.00 meters of excavation at the right side of the wall in 2 days where consolidation of clay layer continues and assess until the average degree of consolidation of the clay layer reaches to U=85 % (Step 7)
- Assess until "long term" (i.e.: $P_{\max} < 1,0 \text{ kPa}$, U=99%)

The results of this simulation case are presented and evaluated in "Case :2 Bitumen Coated Diaphragm Wall - Soil Interaction during Excavation" section.

CHAPTER 4

SIMULATION RESULTS & DISCUSSION

As discussed in the previous sections, the generic numerical assessments regarding the analysis of negative skin friction on diaphragm walls are performed for two analysis scenarios which break down into two sub-scenarios to comparatively analyze the effect of negative skin friction on diaphragm walls in detail, the results of which will be explained in the following sub-sections, respectively.

4.1. Scenario 1: Diaphragm Wall - Soil Interaction Model

The first scenario illustrates the interaction of the diaphragm wall and the soil, with respect to the following considerations:

- The soil dynamics, as a consequence of which, negative skin friction is observed on a retaining structure,
- The compression characteristics of the retaining structure,
- The additional shear force acting on the retaining structure due to negative skin friction and the effectiveness of the counter measures.

4.1.1. Case 1: Diaphragm Wall - Soil Interaction

4.1.1.1. Vertical Displacement vs. Axial Position

In order to analyze the vertical displacement of the analyzed soil section, axial slices of various depths illustrated in Figure 31 are taken through the clay layer. The settlement profile of axial slices taken from the sections (AA, BB, CC, DD and EE), during different average degrees of consolidation ($U=25\%$, $U=40\%$, $U=55\%$, $U=70\%$ and $U=85\%$) of the clay layer, are illustrated in Figure 32 - Figure 36.

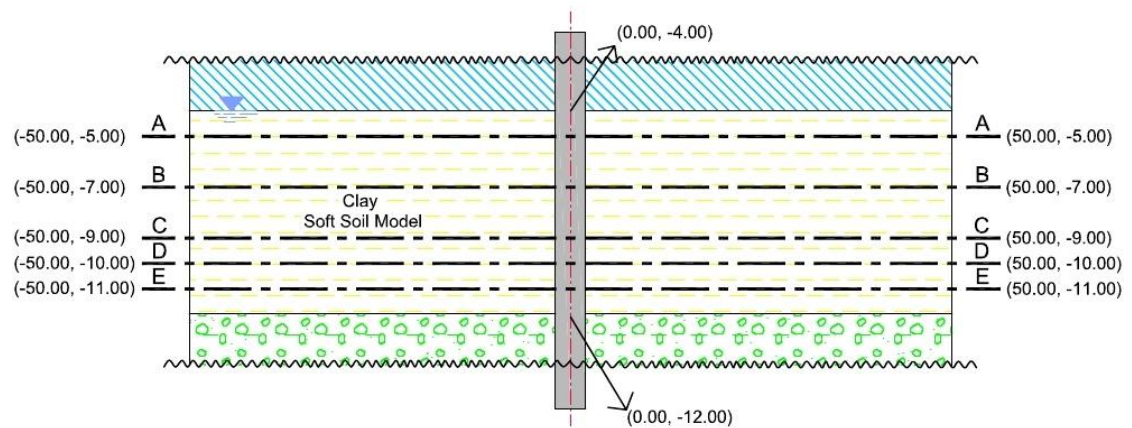


Figure 31: Selected Axial Cross Sections of the Clay Layer

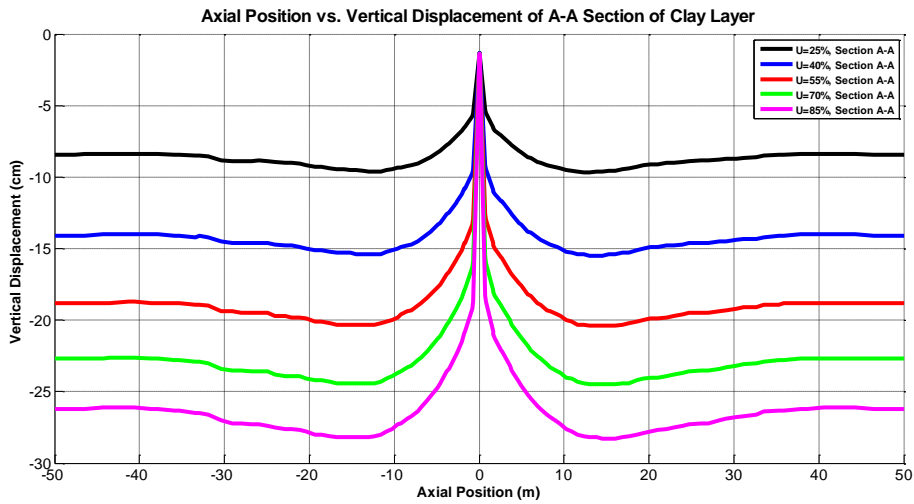


Figure 32: Vertical Displacement during 25 %, 40 %, 55 %, 70 % and 85 % of Consolidation Process at the Depth of 5 m

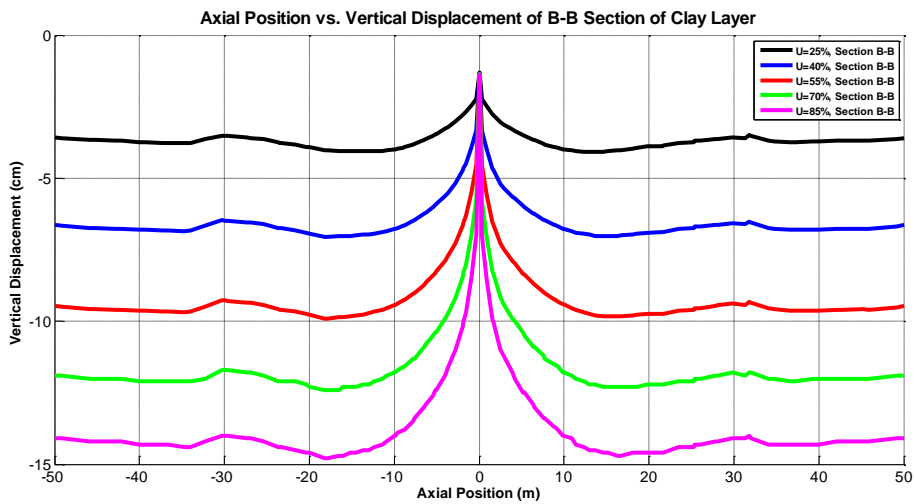


Figure 33: Vertical Displacement during 25 %, 40 %, 55 %, 70 % and 85 % of Consolidation Process at the Depth of 7 m

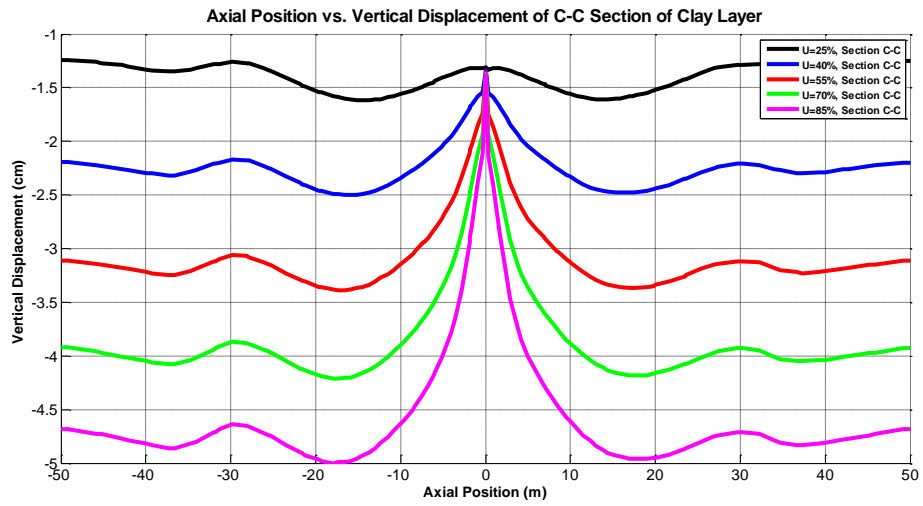


Figure 34: Vertical Displacement during 25 %, 40 %, 55 %, 70 % and 85 % of Consolidation Process at the Depth of 9 m

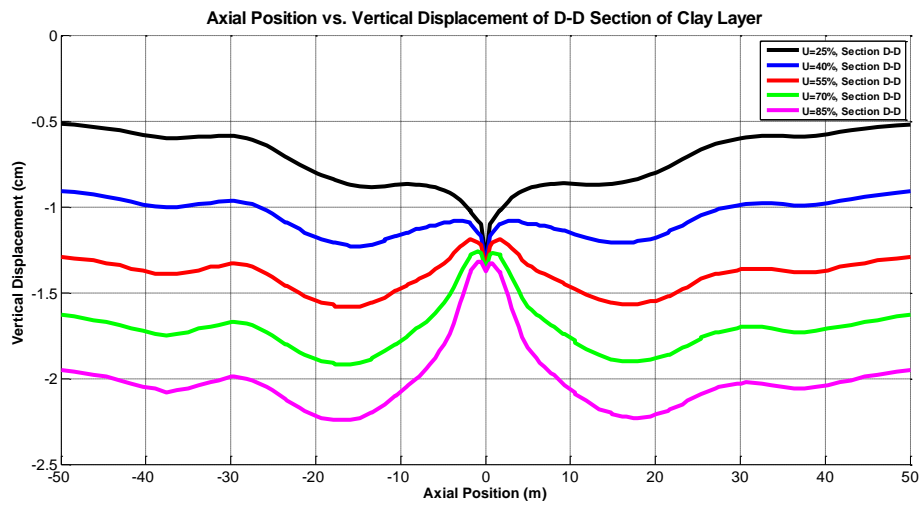


Figure 35: Vertical Displacement during 25 %, 40 %, 55 %, 70 % and 85 % of Consolidation Process at the Depth of 10 m

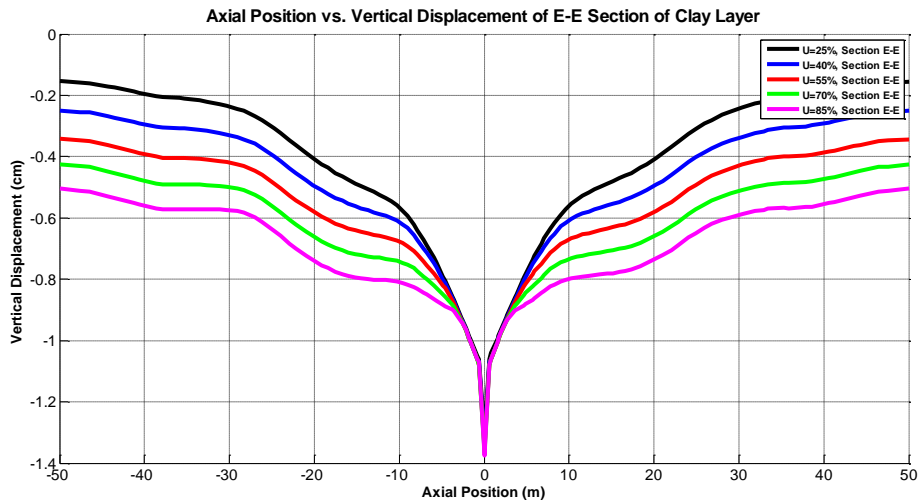


Figure 36: Vertical Displacement during 25 %, 40 %, 55 %, 70 % and 85 % of Consolidation Process at the Depth of 11 m

4.1.1.2. Relative Displacement vs. Vertical Position

Although the above illustrated figures are beneficial for analyzing the transient consolidation dynamics of the soil itself, it is essential to analyze the relative displacement between the mentioned soil section and the wall, in order to comment about the nature (i.e., direction) of the shear forces acting on the wall and thus the negative skin friction. The relative displacement of the wall and the soil is illustrated in Figure 37.

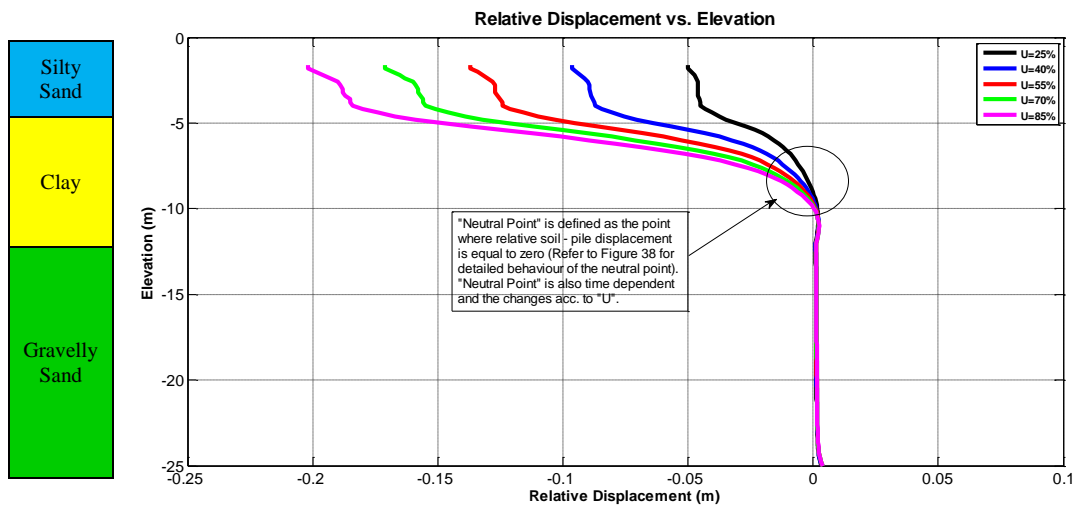


Figure 37: Relative Displacement of the Wall and the Soil

The exact position of the neutral point (i.e., the point where the relative displacement between the soil and the wall is zero) is clearly illustrated in Figure 38. As it can be observed from the figure, the position of the neutral point moves downward (and hence the magnitude of the total downdrag force increases) as the consolidation of the clay layer proceeds, as expected.

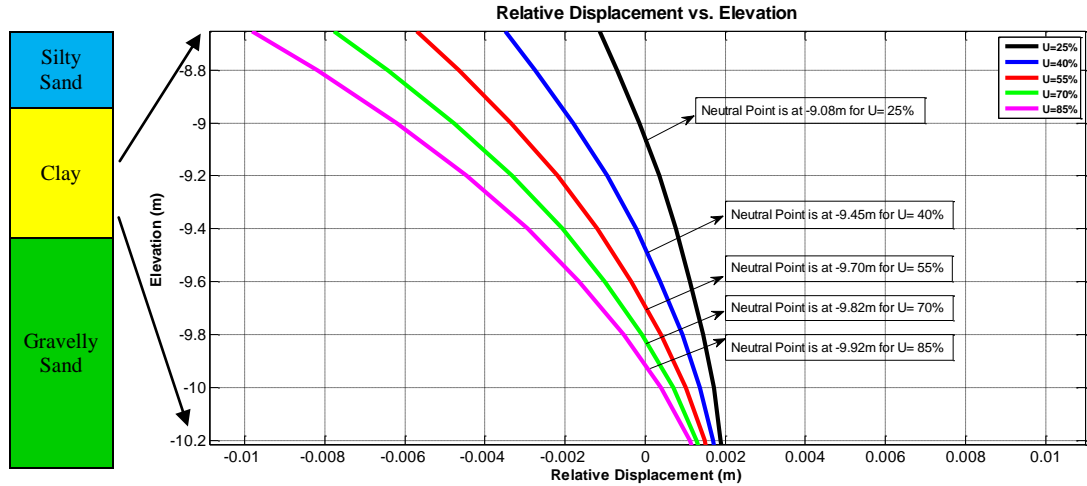


Figure 38: Relative Displacement of the Wall and the Soil Close to Neutral Point

4.1.1.3. Variation of Skin Friction Force Along the Pile Length

As a consequence of the relative displacement phenomena illustrated in the previous section, the skin friction force acting on the wall is illustrated as a function of vertical position of the wall in Figure 39.

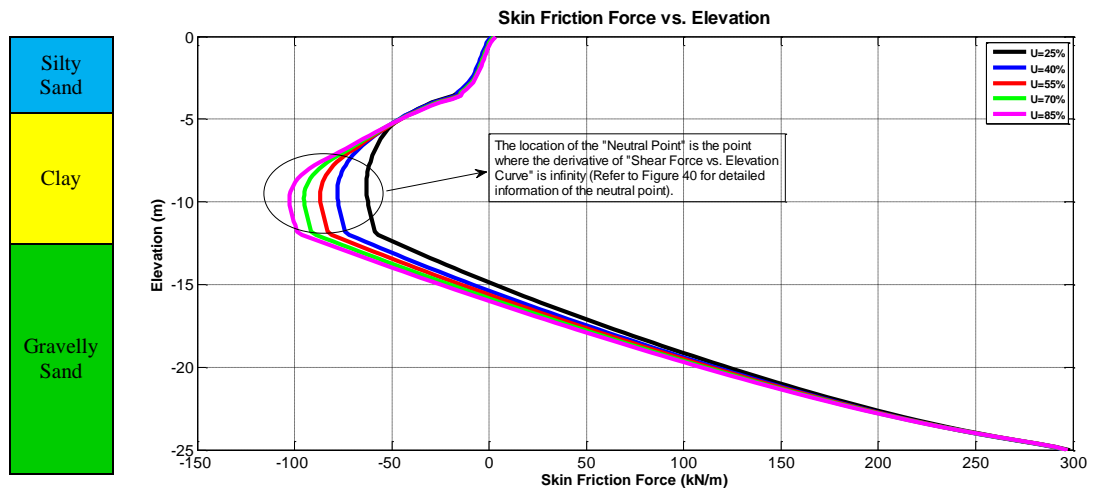


Figure 39: Skin Friction Force Acting on the Wall as a Function of Vertical Position of the Wall

The change of direction of the skin friction force acting on the wall around the neutral point, as a consequence of the relative displacement between the wall and the soil, is clearly illustrated in Figure 40.

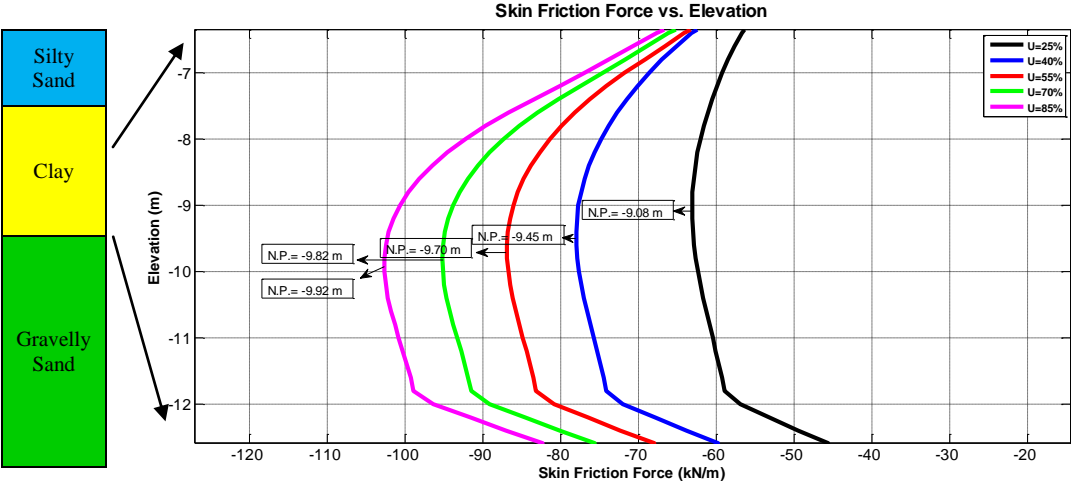


Figure 40: The Behavior of the Skin Friction Force Acting on the Wall around the Neutral Point

4.1.2. Case 2: Bitumen Coated Diaphragm Wall - Soil Interaction

4.1.2.1. Vertical Displacement vs. Axial Position

In order to analyze the vertical displacement of the analyzed soil section, axial slices of various depths represented in Figure 41 are provided through the clay layer. The settlement profile of axial slices taken from the sections (AA, BB, CC, DD and EE), during different average degrees of consolidation (U=25 %, U=40%, U=55 %, U=70 % and U=85 %) of the clay layer, for the cases where the wall is uncoated (solid line) and bitumen coated (dashed line), are illustrated in Figure 42 - Figure 46.

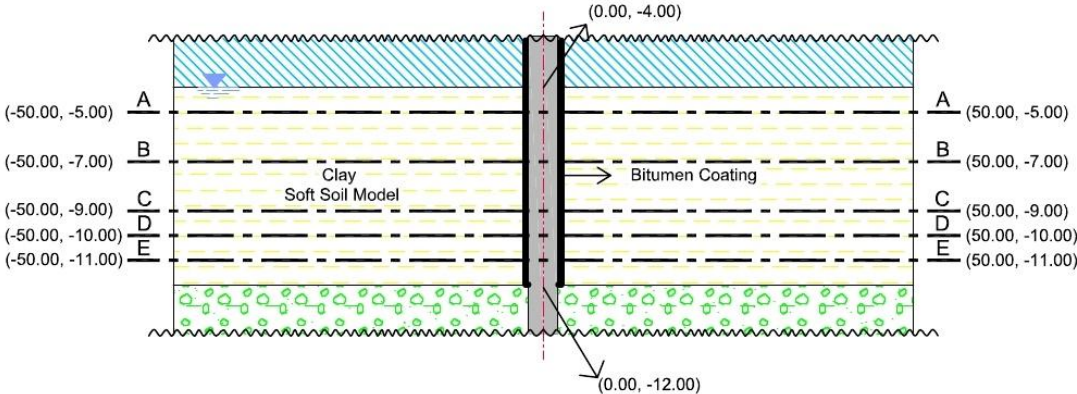


Figure 41: The Axial Sections of the Clay Layer

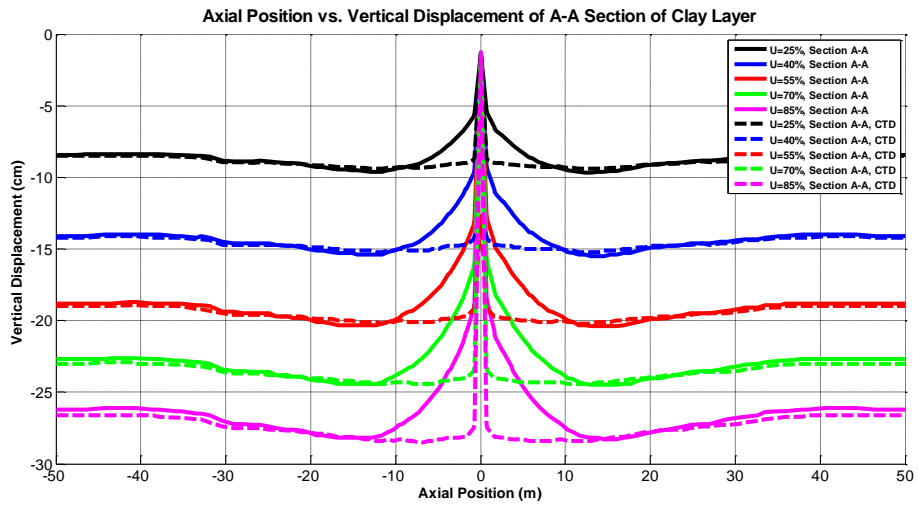


Figure 42: Vertical Displacement during 25 %, 40 %, 55 %, 70 % and 85 % of Consolidation Process at the Depth of 5 m

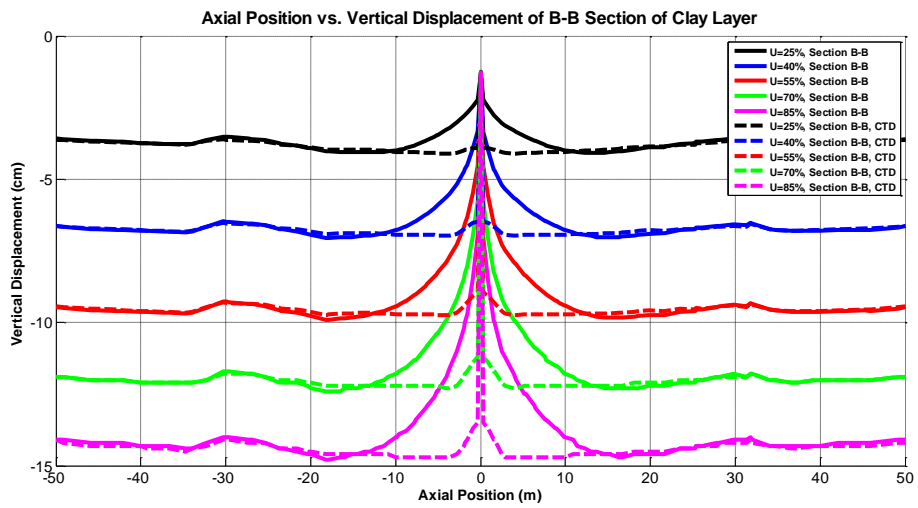


Figure 43: Vertical Displacement during 25 %, 40 %, 55 %, 70 % and 85 % of Consolidation Process at the Depth of 7 m

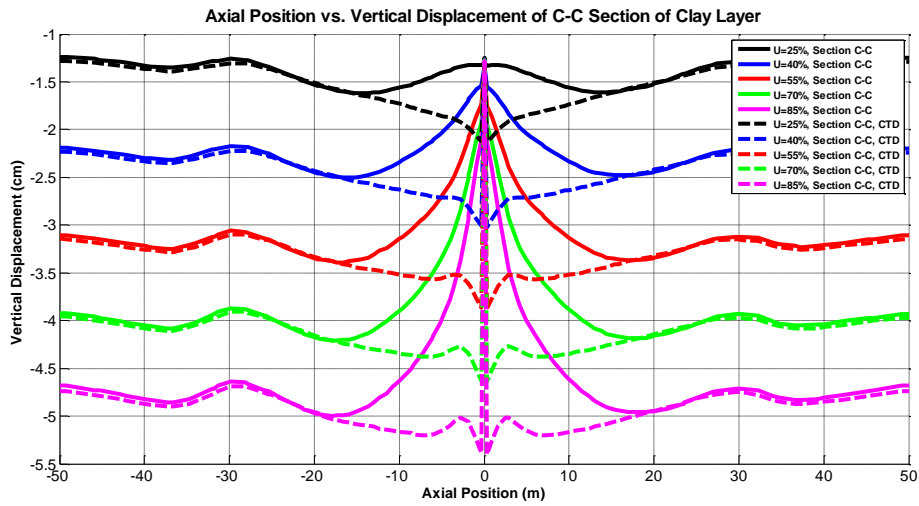


Figure 44: Vertical Displacement during 25 %, 40 %, 55 %, 70 % and 85 % of Consolidation Process at the Depth of 9 m

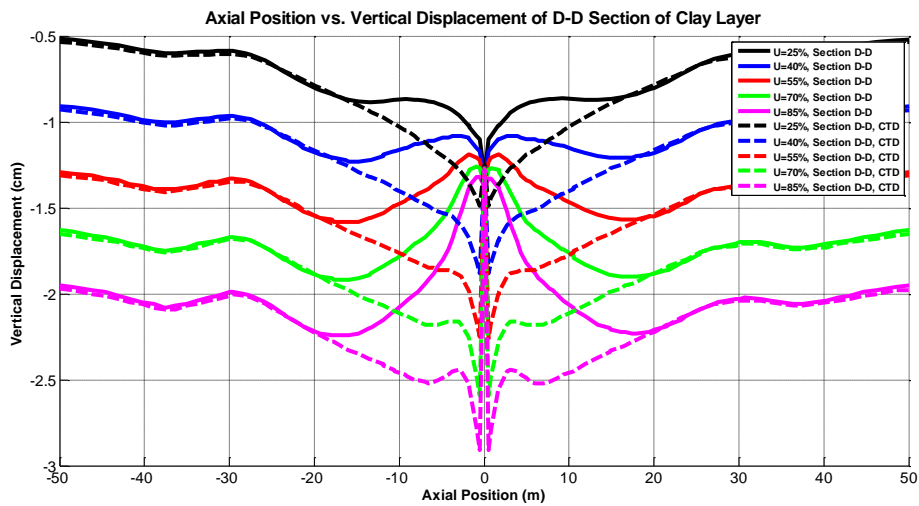


Figure 45: Vertical Displacement during 25 %, 40 %, 55 %, 70 % and 85 % of Consolidation Process at the Depth of 10 m

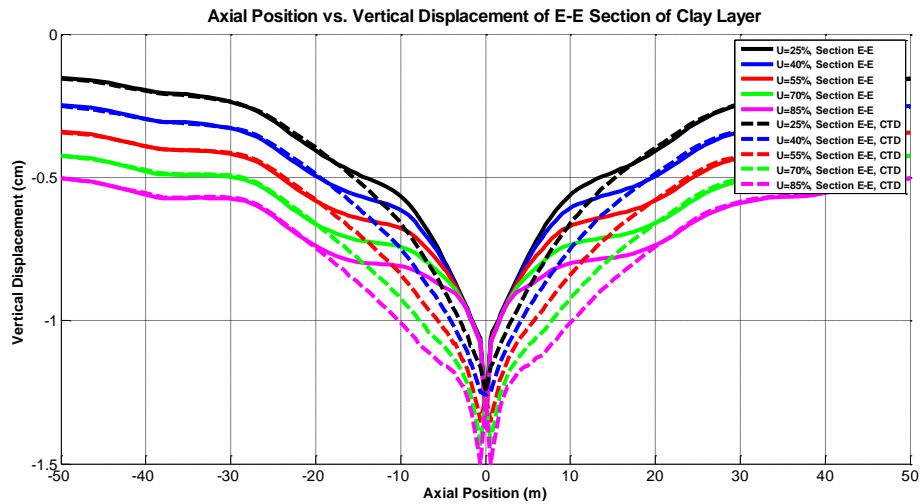


Figure 46: Vertical Displacement during 25 %, 40 %, 55 %, 70 % and 85 % of Consolidation Process at the Depth of 11 m

4.1.2.2. Relative Displacement vs. Vertical Position

The relative displacement of the wall and soil for the case where the wall is coated with bitumen is illustrated in Figure 47.

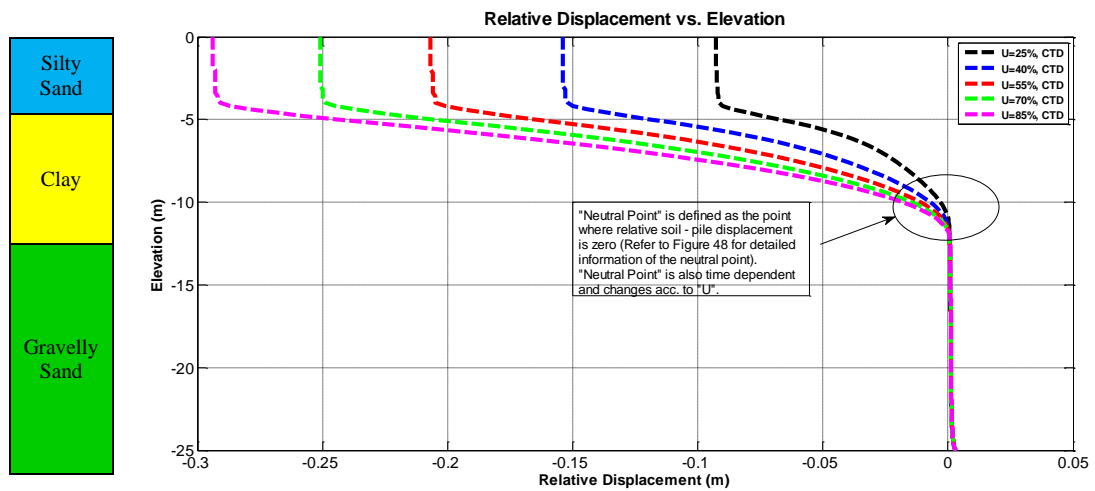


Figure 47: Relative Displacement of the Wall and the Soil

The exact position of the neutral point (i.e., the point where the relative displacement between the soil and the wall is zero) is clearly illustrated in Figure 48. In comparison to the previous case, the relative displacement between the soil and the wall is observed to be larger, since the stabilizing effect of the wall-soil interface is lower due to bitumen application.

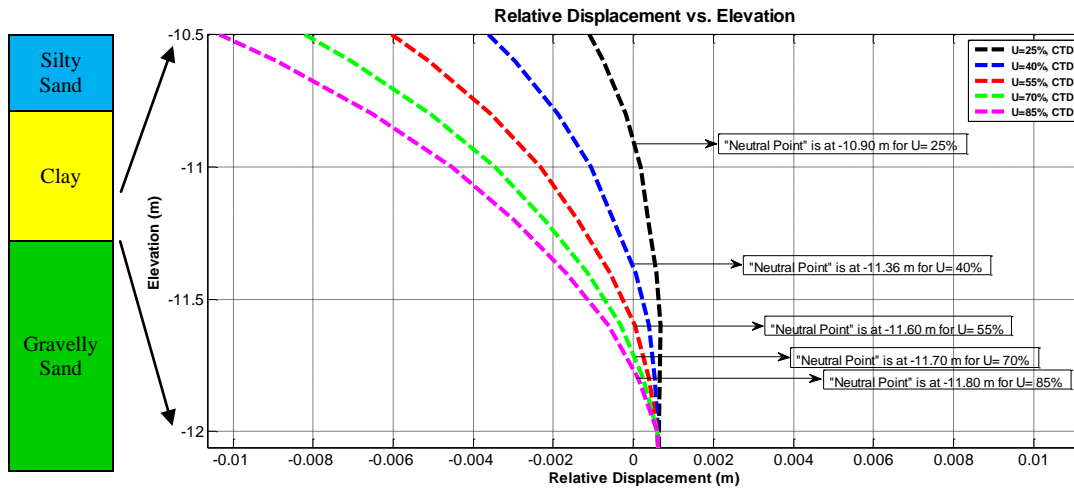


Figure 48: Relative Displacement of the Wall and the Soil Close to Neutral Point

4.1.2.3. Variation of Skin Friction Force Along the Pile Length

As a consequence of the relative displacement phenomena illustrated in the previous section, the skin friction force acting on the wall, for the cases where the wall is uncoated (solid line) and bitumen coated (dashed line), are illustrated as a function of vertical position of the wall in Figure 49.

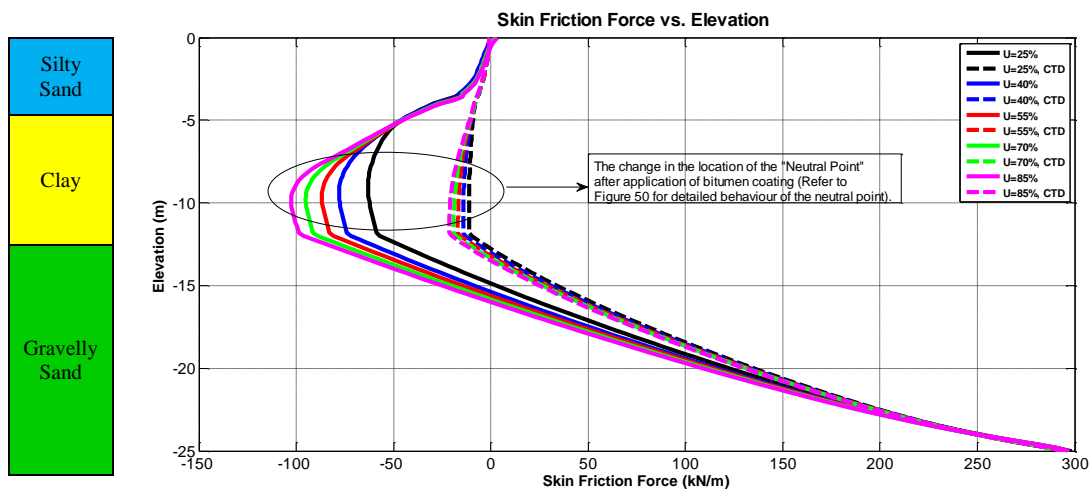


Figure 49: Skin Friction Force Acting on the Wall as a Function of Vertical Position of the Wall

The change of direction of the skin friction force acting on the wall around the neutral point for the cases where the wall is uncoated (solid line) and bitumen coated (dashed line), as a consequence of the relative displacement between the wall and the soil, is clearly illustrated in Figure 50. Although, as mentioned before, the relative displacement between the soil and the wall is observed to be larger and hence the position of the neutral plane is lower for this case, due to nonlinear viscous characteristics of the bitumen, the magnitude of the total skin friction force acting on the wall is observed to be smaller.

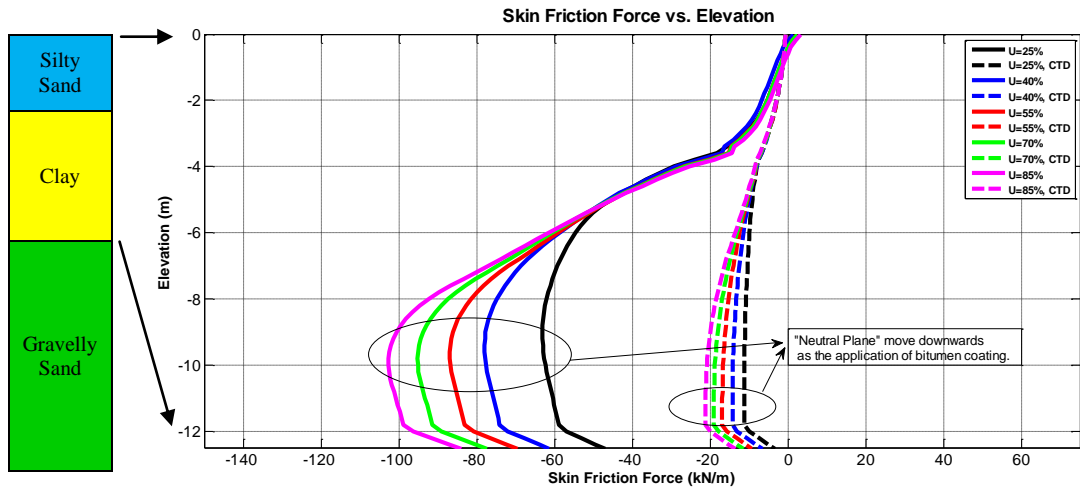


Figure 50: The Behavior of the Skin Friction Force Acting on the Wall around the Neutral Point

4.2. Scenario 2: Diaphragm Wall - Soil Interaction Model during Excavation

The second scenario illustrates the interaction of the diaphragm wall and the soil during the transient excavation process, with respect to the following considerations:

- The soil dynamics, as a consequence of which frictional forces are observed on the corresponding side of the retaining structure,
- The compression and bending characteristics of the retaining structure,
- The variation of frictional forces on corresponding sides of the retaining structure, due to displacement and their consequences on the bending moment acting on it.

4.2.1. Case 1: Diaphragm Wall - Soil Interaction during Excavation

4.2.1.1. Vertical Displacement vs. Axial Position

In order to analyze the vertical displacement of the analyzed soil section, axial slices of various depths represented in Figure 51 are provided through the clay layer. The settlement profile of axial slices taken from the sections (AA, BB, CC, DD and EE), during different degrees of consolidation ($U=25\%$, $U=40\%$, $U=55\%$, $U=70\%$ and $U=85\%$) of the clay layer, are illustrated in Figure 52 - Figure 55.

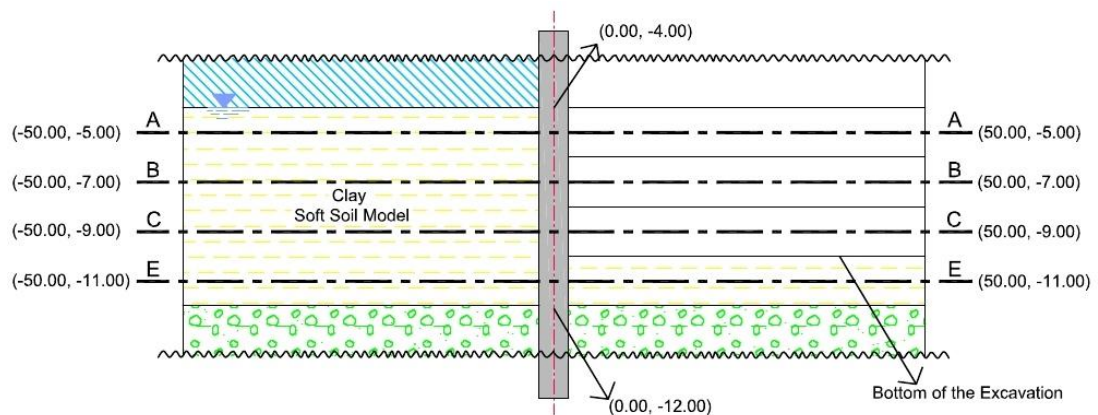


Figure 51: The Axial Sections of the Clay Layer

In comparison to Figure 31, instead of consolidation, uplift is observed in the soil section to the excavated (i.e., right) side of the wall. As a result, the mentioned displacement characteristics causes counter clockwise rotation in the wall section illustrated in Figure 28.

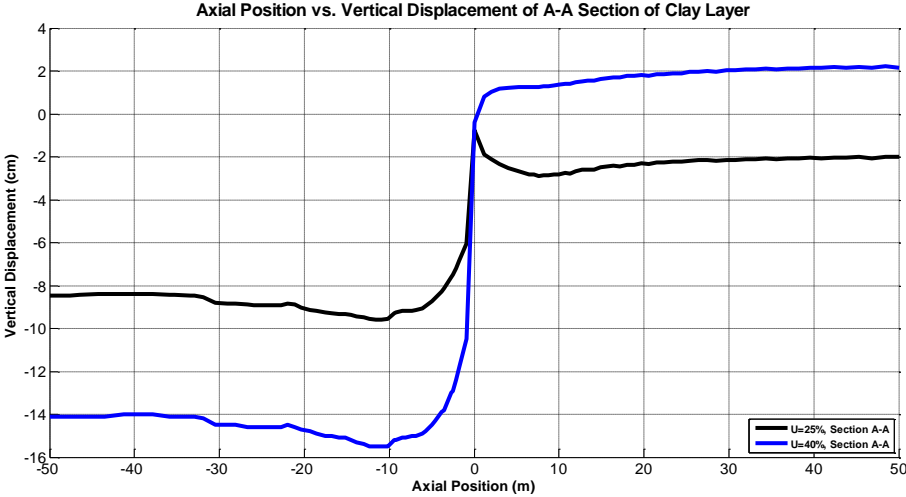


Figure 52: Vertical Displacement during 25 % and 40 % of Consolidation Process at the Depth of 5 m

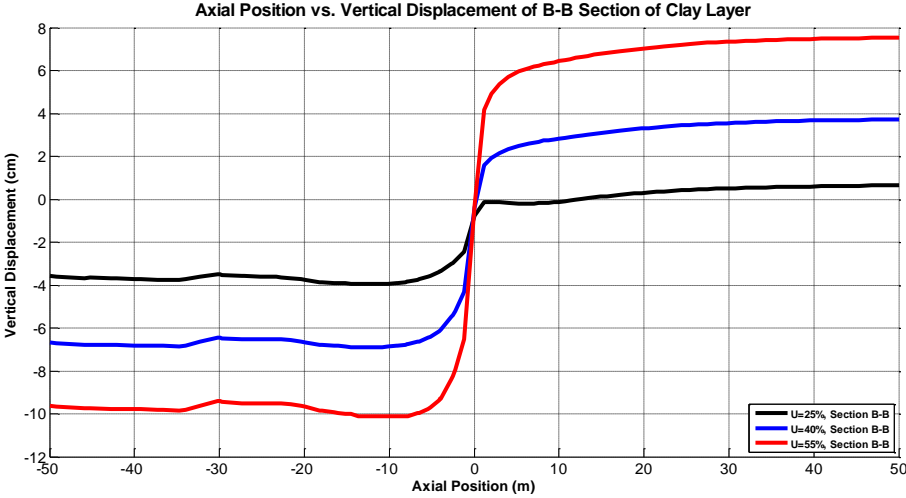


Figure 53: Vertical Displacement during 25 %, 40 % and 55 % of Consolidation Process at the Depth of 7 m

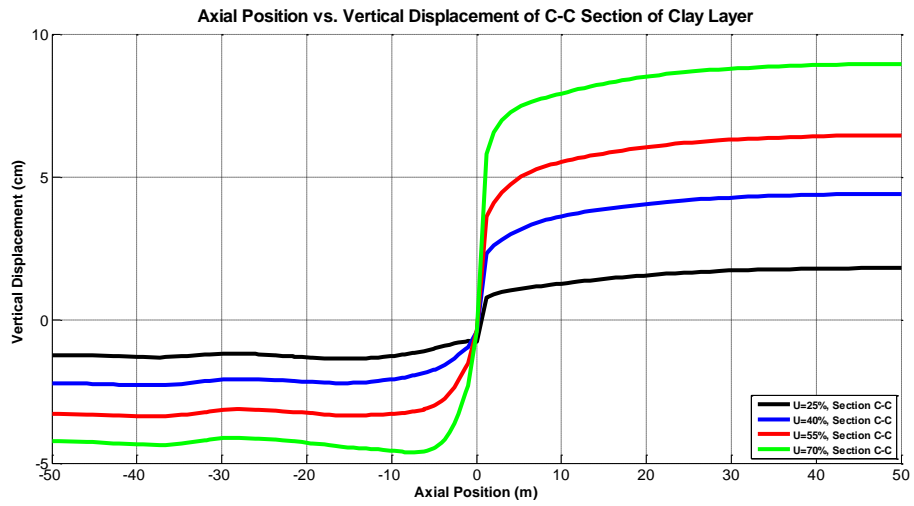


Figure 54: Vertical Displacement during 25 %, 40 %, 55 % and 70 % of Consolidation Process at the Depth of 9 m

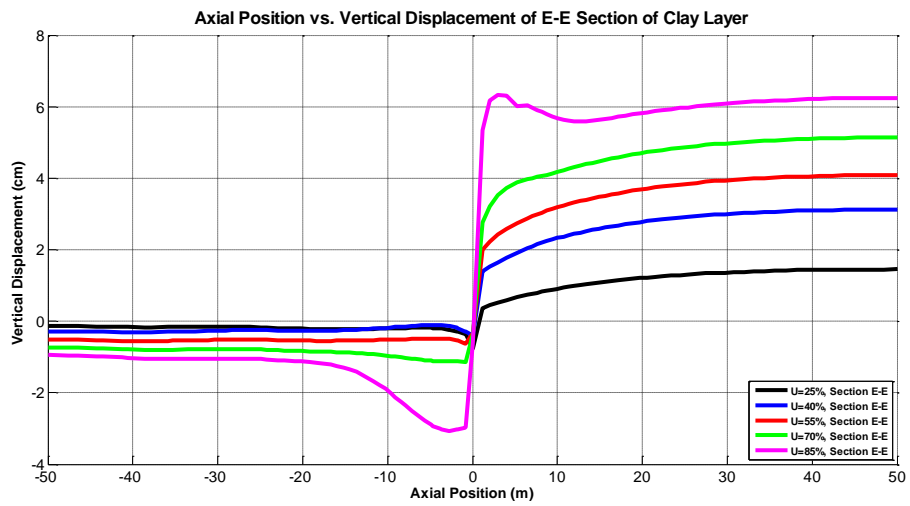


Figure 55: Vertical Displacement during 25 %, 40 %, 55 %, 70 % and 85 % of Consolidation Process at the Depth of 11 m

4.2.1.2. Relative Displacement vs. Vertical Position

The relative displacement of the wall and soil, corresponding to left and right sides of the diaphragm wall in Figure 28, are illustrated in Figure 56 and Figure 57, respectively.

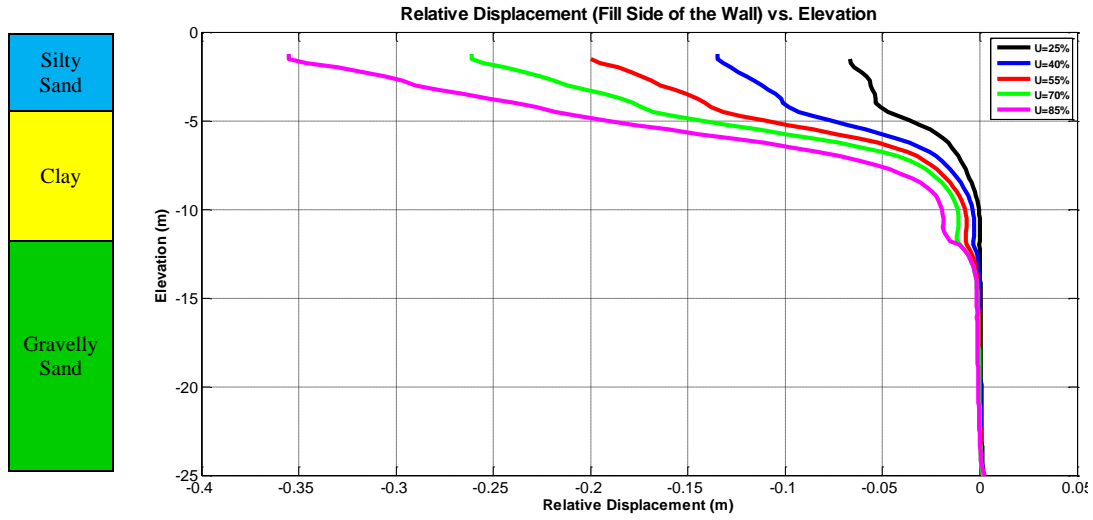


Figure 56: Relative Displacement of the Fill Side of the Wall and the Soil

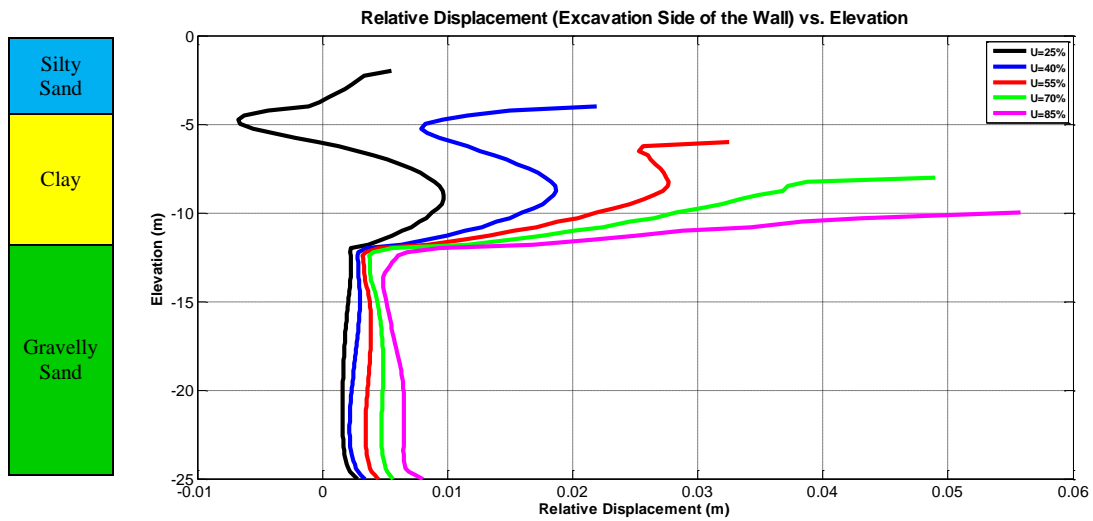


Figure 57: Relative Displacement of the Excavation Side of the Wall and the Soil

4.2.1.3. Variation of Skin Friction Force Along the Pile Length

As a consequence of the relative displacement phenomena illustrated in the previous section, the skin friction forces acting on the left and the right sides of the wall are illustrated as a function of vertical position of the wall in Figure 58 and Figure 59, respectively.

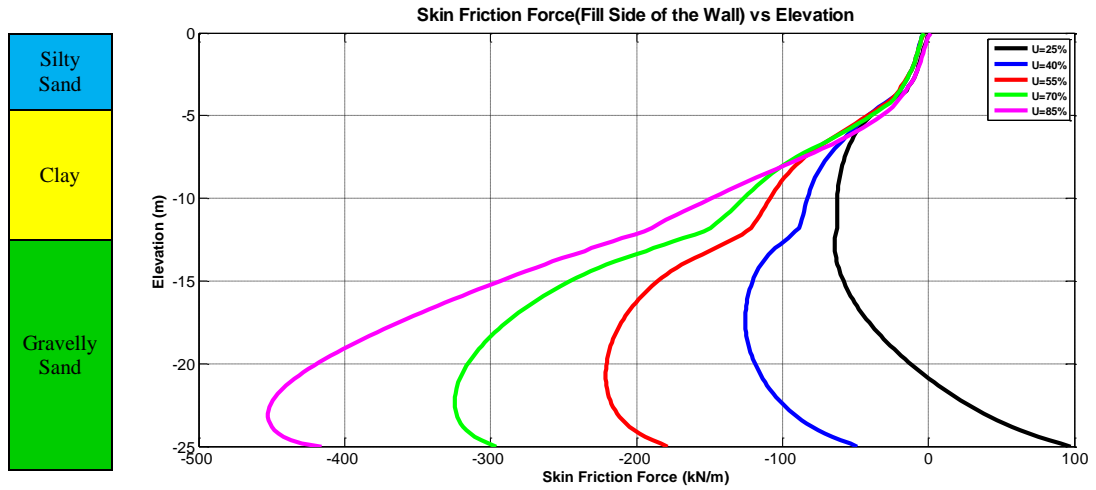


Figure 58: Skin Friction Force Acting on the Fill Side of the Wall as a Function of Vertical Position of the Wall

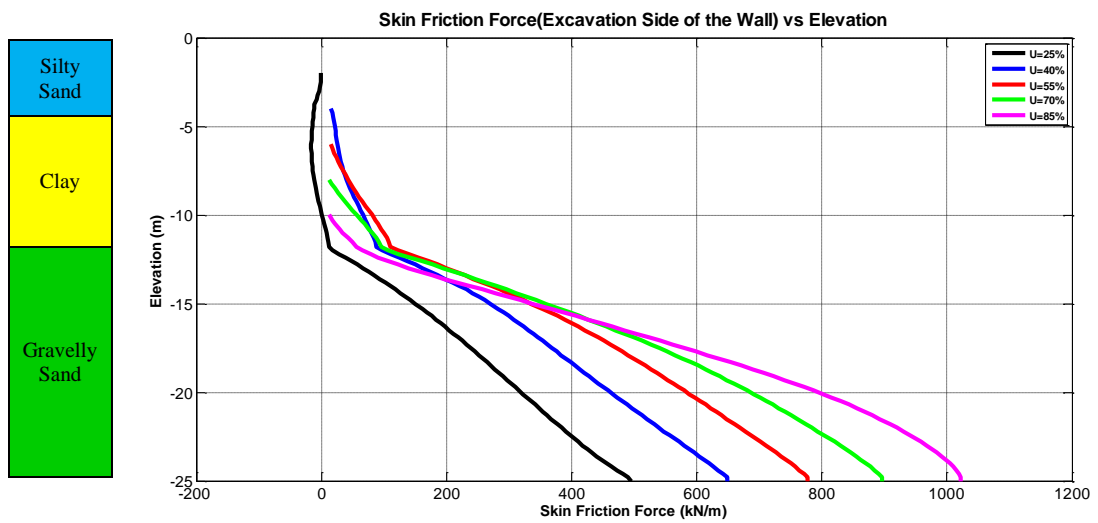


Figure 59: Skin Friction Force Acting on the Excavation Side of the Wall as a Function of Vertical Position of the Wall

4.2.2. Case 2: Bitumen Coated Diaphragm Wall - Soil Interaction during Excavation

4.2.2.1. Vertical Displacement vs. Axial Position

In order to analyze the vertical displacement of the analyzed soil section, axial slices of various depths represented in Figure 60 are provided through the clay layer. The settlement profile of axial slices taken from the sections (AA, BB, CC, DD and EE), during different degrees of consolidation (U=25 %, U=40%, U=55 %, U=70 % and U=85 %) of the clay layer, for the cases where the wall is uncoated (solid line) and bitumen coated (dashed line), are illustrated in Figure 61 - Figure 64.

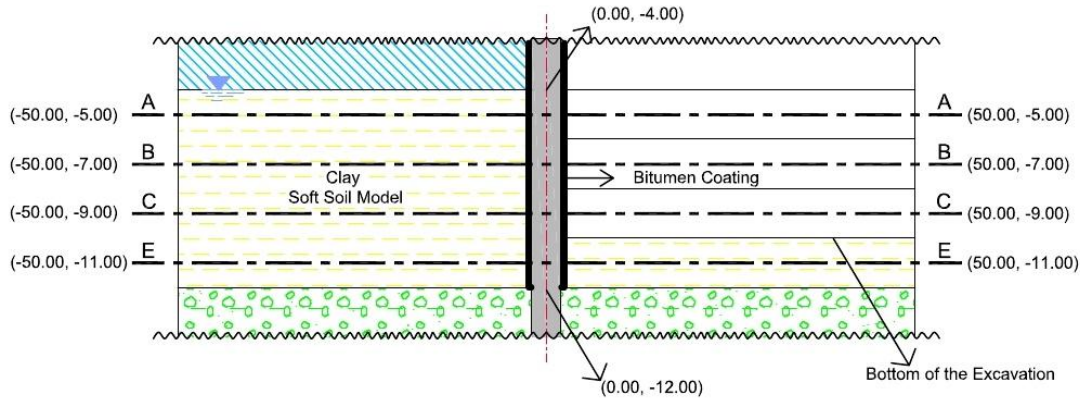


Figure 60: The Axial Sections of the Clay Layer

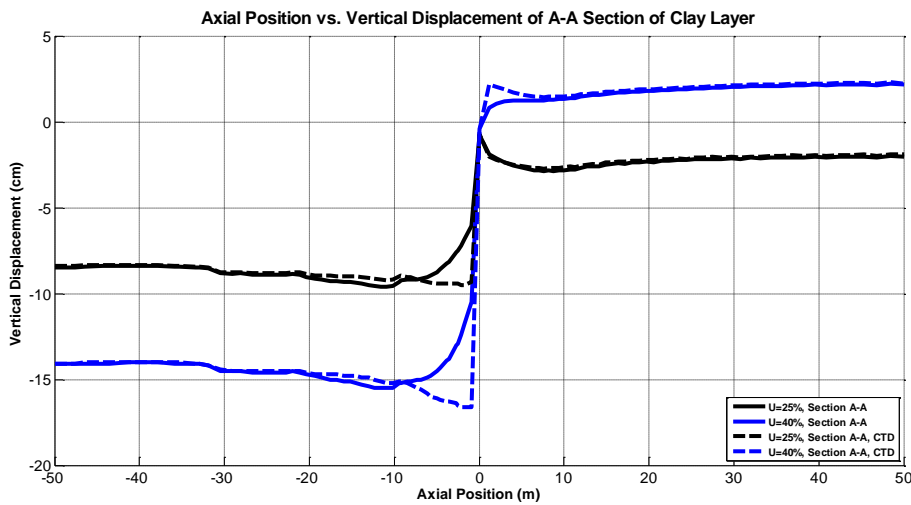


Figure 61: Vertical Displacement during 25 % and 40 % of Consolidation Process at the Depth of 5 m

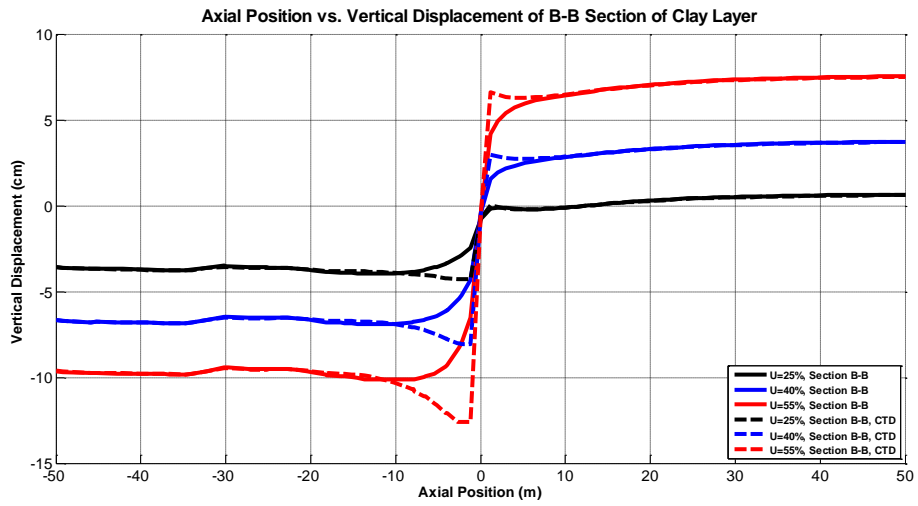


Figure 62: Vertical Displacement during 25 %, 40 % and 55 % of Consolidation Process at the Depth of 7 m

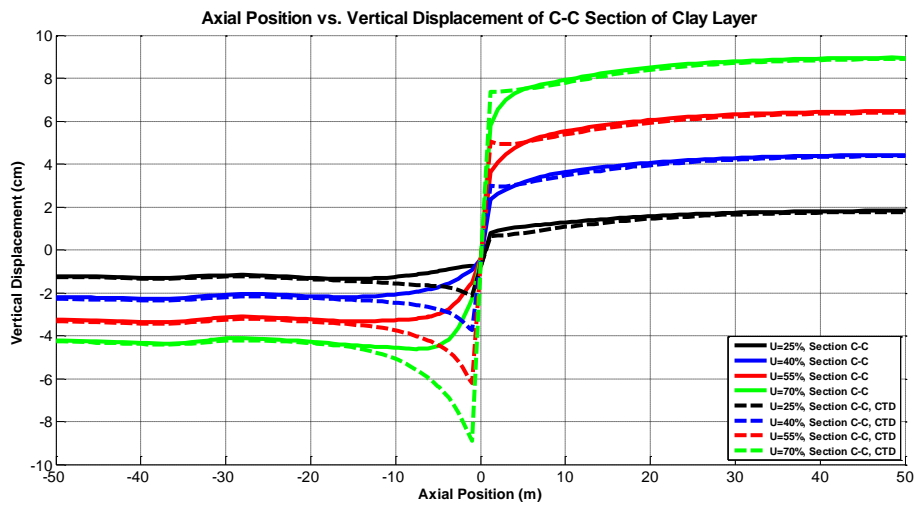


Figure 63: Vertical Displacement during 25 %, 40 %, 55 % and 70 % of Consolidation Process at the Depth of 9 m

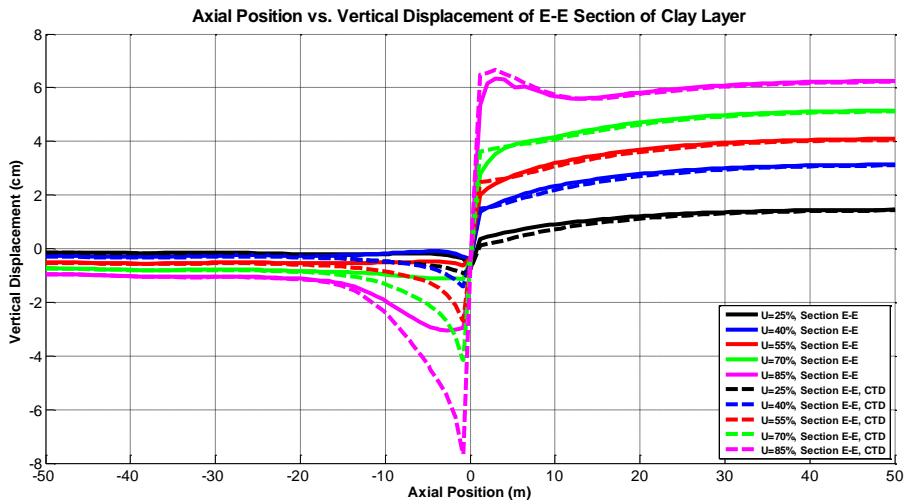


Figure 64: Vertical Displacement during 25 %, 40 %, 55 %, 70 % and 85 % of Consolidation Process at the Depth of 11 m

4.2.2.2. Relative Displacement vs. Vertical Position

The relative displacement of the wall and soil, corresponding to left and right sides of the diaphragm wall in Figure 28, are illustrated in Figure 65 and Figure 66, respectively.

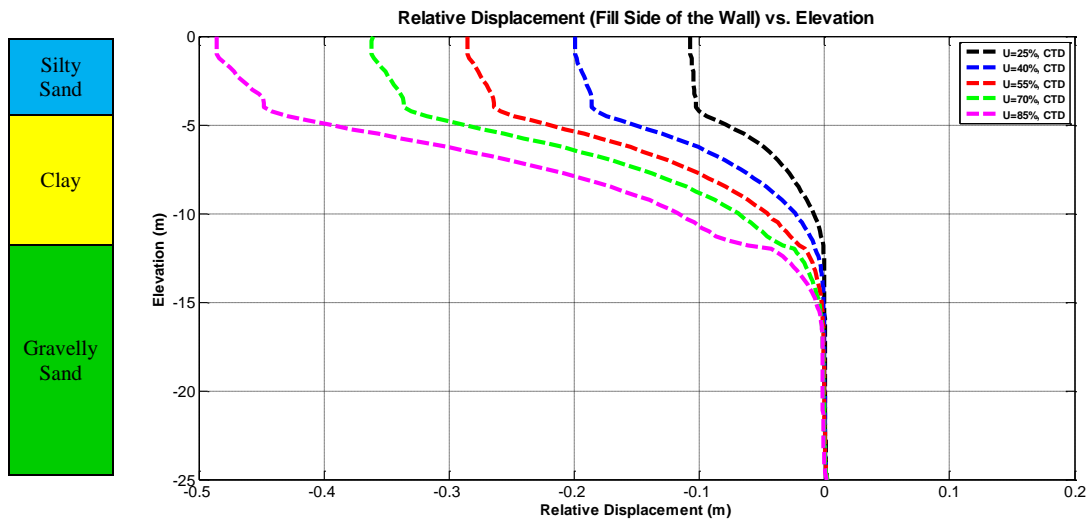


Figure 65: Relative Displacement of the Fill Side of the Wall and the Soil

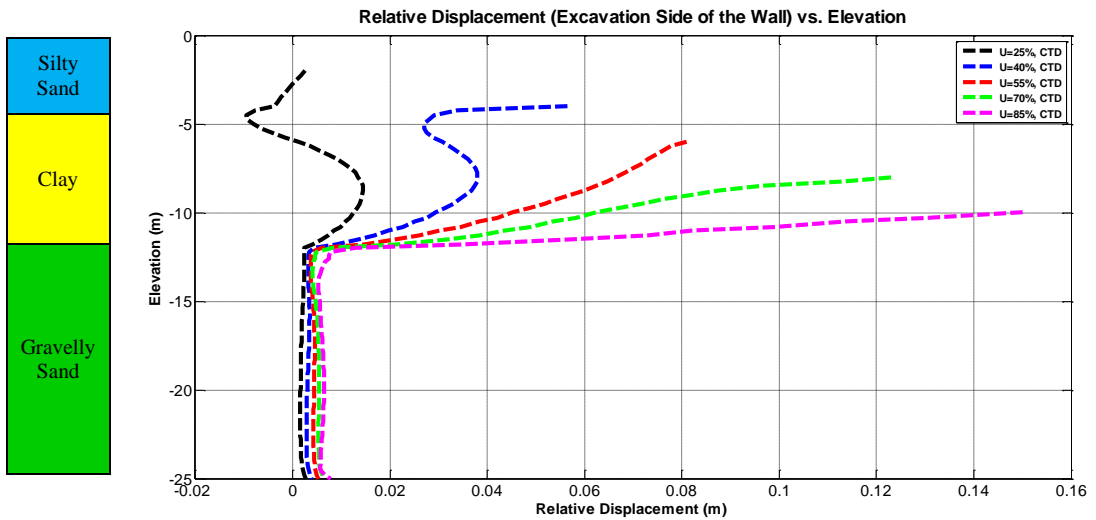


Figure 66: Relative Displacement of the Excavation Side of the Wall and the Soil

4.2.2.3. Variation of Skin Friction Force Along the Pile Length

As a consequence of the relative displacement phenomena illustrated in the previous section, the skin friction forces acting on the left and the right sides of the wall, for the cases where the wall is uncoated (solid line) and bitumen coated (dashed line), are illustrated as a function of vertical position of the wall in Figure 67 and Figure 68, respectively.

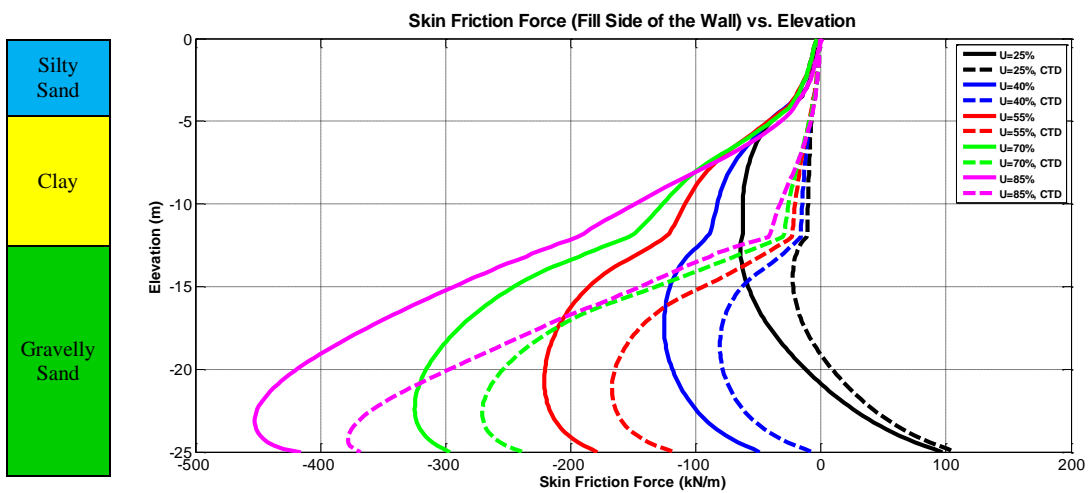


Figure 67: Skin Friction Force Acting on the Fill Side of the Wall as a Function of Vertical Position of the Wall

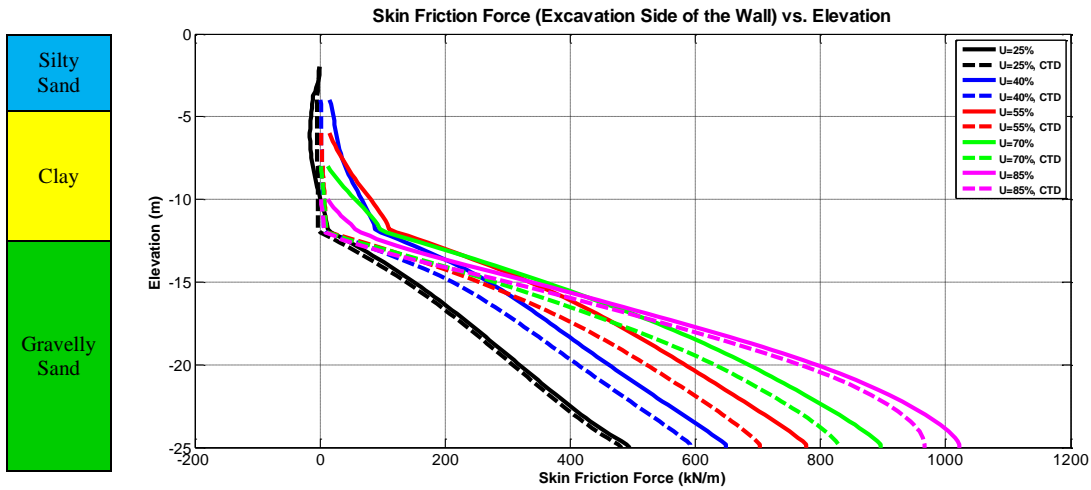


Figure 68: Skin Friction Force Acting on the Excavation Side of the Wall as a Function of Vertical Position of the Wall

4.2.2.4. Bending Moment vs. Axial Force

The bending moment vs. axial force characteristics of the wall section during different degrees of consolidation ($U=25\%$, $U=40\%$, $U=55\%$, $U=70\%$ and $U=85\%$) of the clay layer, for the cases where the wall is uncoated (solid line) and bitumen coated (dashed line), are illustrated in Figure 69-Figure 73. As can be observed from the figures, the bending moment characteristics becomes more critical for the coated case, whereas the axial force characteristics become more critical for the uncoated case, considering the ultimate bending moment-axial force interaction characteristics.

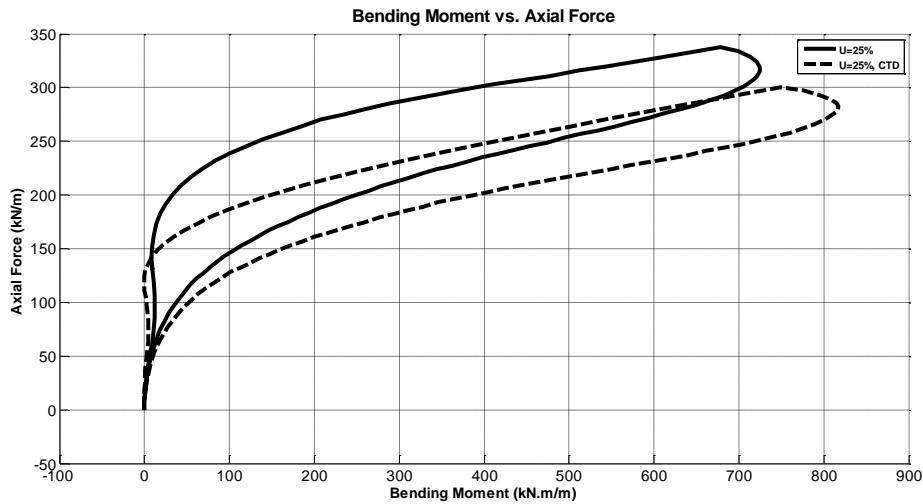


Figure 69: Bending Moment vs. Axial Force Characteristics for Simulation Step 3

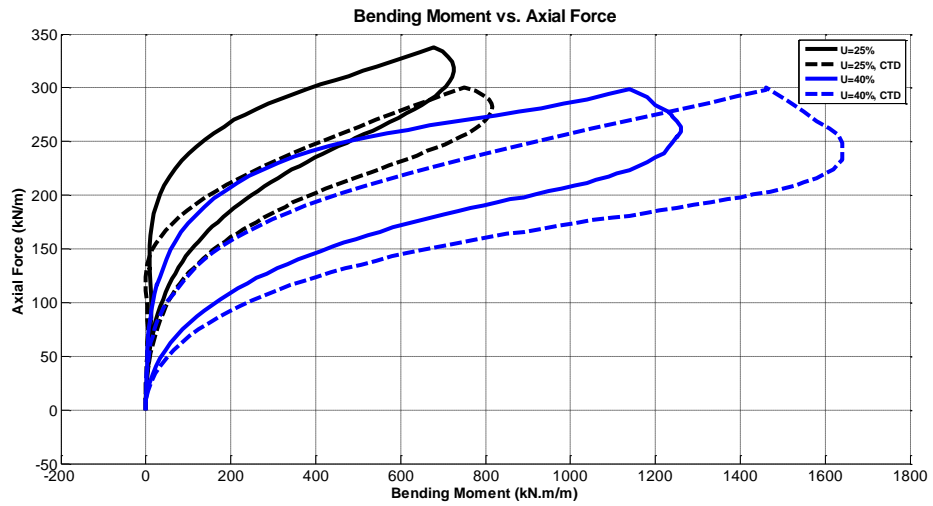


Figure 70: Bending Moment vs. Axial Force Characteristics for Simulation Steps 3 and 4

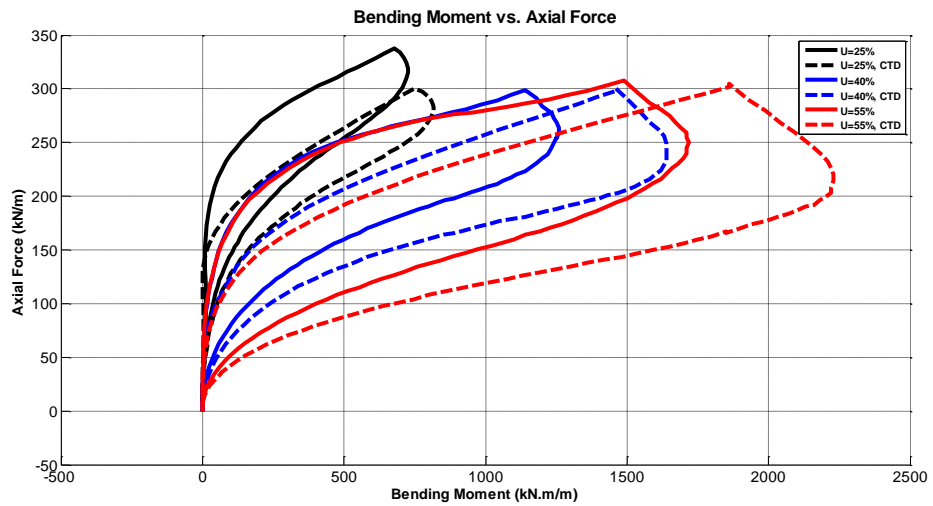


Figure 71: Bending Moment vs. Axial Force Characteristics for Simulation Steps 3, 4 and 5

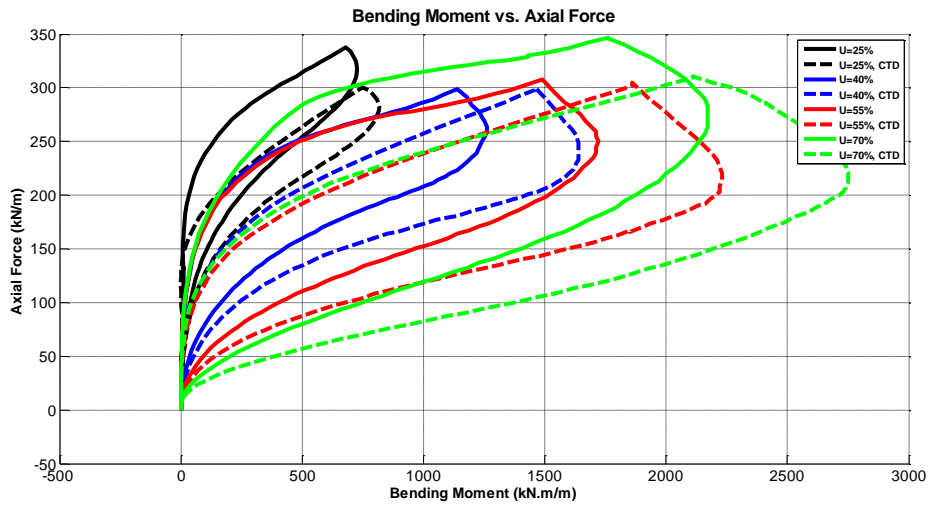


Figure 72: Bending Moment vs. Axial Force Characteristics for Simulation Steps 3, 4, 5 and 6

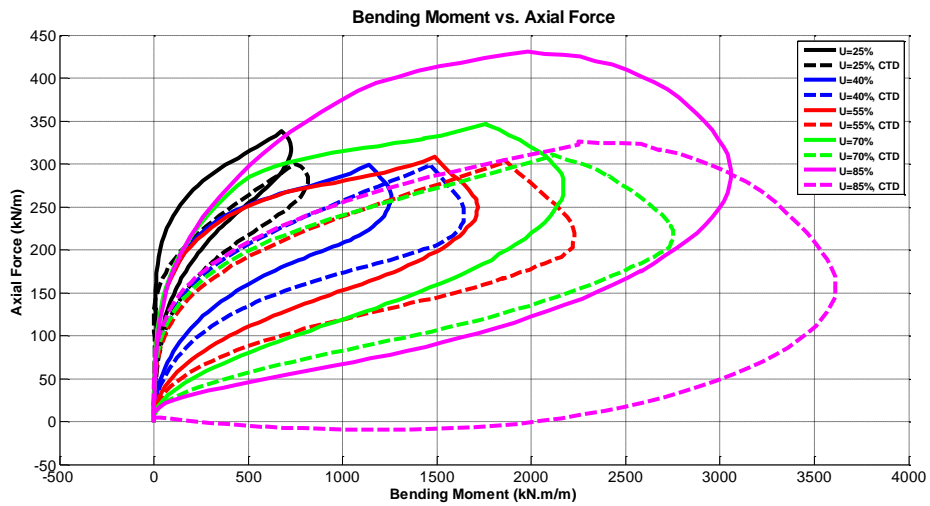


Figure 73: Bending Moment vs. Axial Force Characteristics for Simulation Steps 3, 4, 5, 6 and 7

4.3. Calculation of Negative Skin Friction by Analytical Methods

In order to verify the digital simulation results by the conventional methods explained in "Analytical Methods to Assess a Pile Subjected to Negative Skin Friction", the algorithm for analytical calculation of negative skin friction is illustrated in Figure 74.

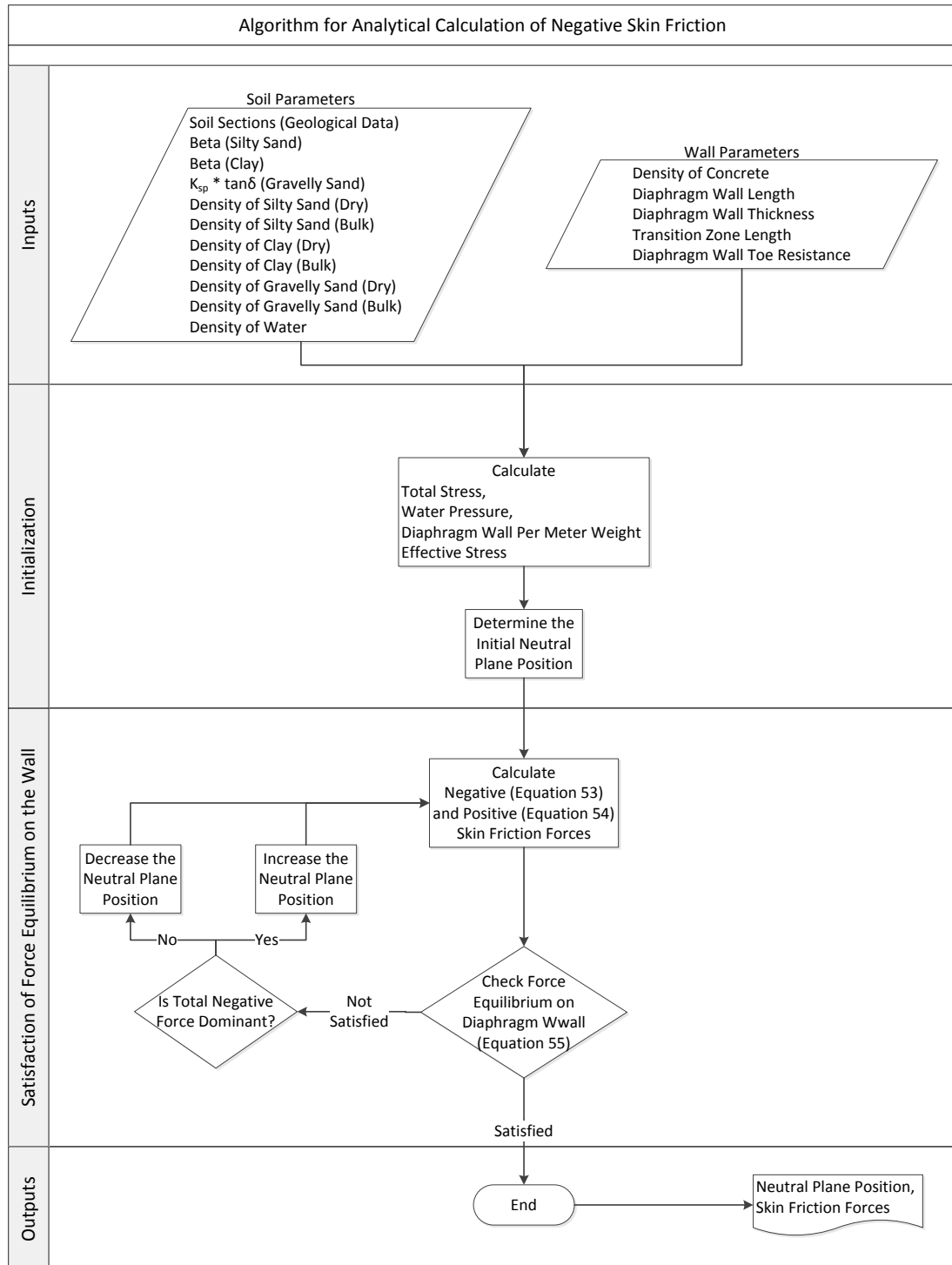


Figure 74: Flowchart for Analytical Negative Skin Friction Calculation Algorithm

The utilized equations for analytical calculation are given in (53) - (54). The parameters and corresponding values for the analytical calculations as per the methods explained in section "Analytical Methods to Assess a Pile Subjected to Negative Skin Friction" are given in Table 10.

$$Q_n = \int_{-Z_{NP}}^0 A_s \beta \sigma'_z dz \quad (53)$$

$$Q_p = \int_{-L}^{-Z_{NP}} A_s K \sigma'_z \tan \delta dz \quad (54)$$

$$W_p + \int_{-Z_{NP}}^0 A_s \beta \sigma'_z dz = R_t + \int_{-L}^{-Z_{NP}} A_s K \sigma'_z \tan \delta dz \quad (55)$$

Table 10: The Parameters and Corresponding Values Used in Analytical Calculations

Parameter	Explanation	Value	Unit
L	Wall Penetration Length	25,00	m
β_1	Beta (Silty Sand)	0,50	-
β_2	Beta (Clay)	0,50	-
β_3	$K_{sp} * \tan \delta$ (Gravelly Sand)	0,30	-
At	Cross Section Area	1,20	m ²
γ_{SSD}	Density of Silty Sand (Dry)	18,0	kN/m ³
γ_{SSB}	Density of Silty Sand (Bulk)	19,0	kN/m ³
γ_{CD}	Density of Clay (Dry)	18,0	kN/m ³
γ_{CB}	Density of Clay (Bulk)	19,0	kN/m ³
γ_{GSD}	Density of Gravelly Sand (Dry)	20,0	kN/m ³
γ_{GSB}	Density of Gravelly Sand (Bulk)	21,0	kN/m ³
γ_w	Density of Water	10,0	kN/m ³
γ_p	Density of Concrete	24,0	kN/m ³
W_p	Pile Weight	720,0	kN
R_t	Pile Toe Resistance	120,0	kN

The comparison of total stress, water pressure, and effective stress as a function of depth, obtained by the analytical calculations and digital simulations (obtained when the average degree of consolidation (U) is 85 %) are illustrated in Figure 75, Figure 76 and Figure 77, respectively. As can be assessed from the corresponding figures, both methods end up with similar results. This crosscheck verifies the initialization phase of the analytical negative skin friction algorithm illustrated in Figure 74.

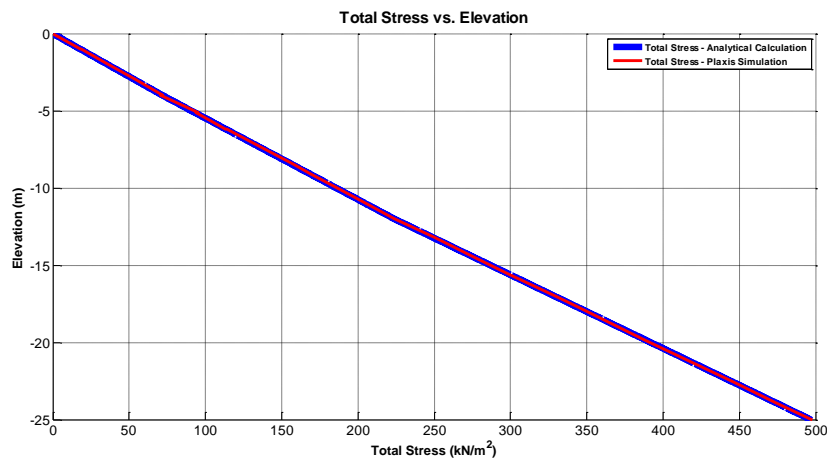


Figure 75: Comparison of Total Stress Calculation of PLAXIS™ Simulation and the Analytical Method Utilized

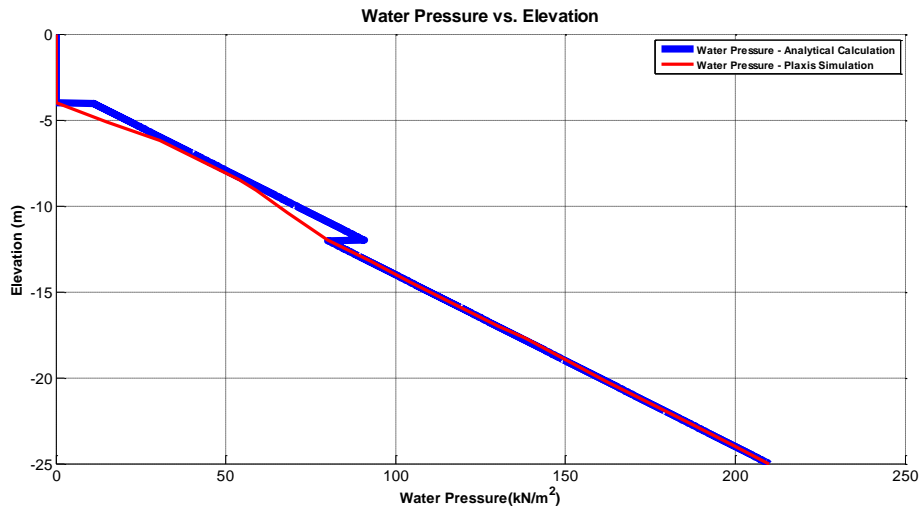


Figure 76: Comparison of Water Pressure Calculation of PLAXIS™ Simulation and the Analytical Method Utilized

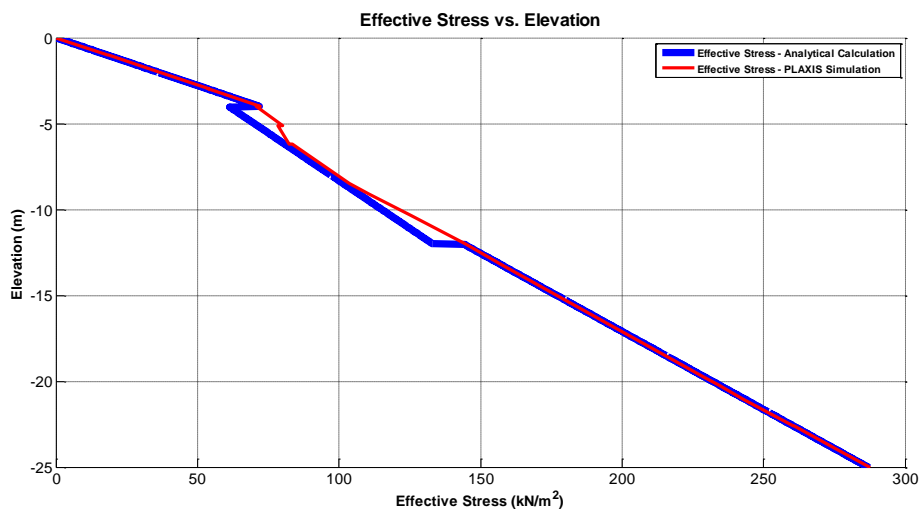


Figure 77: Comparison of Effective Stress Calculation of PLAXIS™ Simulation and the Analytical Method Utilized

4.3.1. Rigid - Plastic Model: Diaphragm Wall - Soil Interaction

The parameters and corresponding values for the analytical calculation with "Rigid Plastic Model" as per the methods explained in section "Analytical Methods to Assess a Pile Subjected to Negative Skin Friction" are given in Table 10.

The comparison of skin friction force as a function of elevation calculated according to "Rigid Plastic Model" and the digital simulation (obtained when the average degree of consolidation (U) is 85 %) are illustrated in Figure 78. As can be assessed from the corresponding figure, the position of the neutral point appears to be at 10,24 m, whereas the location of the neutral point obtained from the digital simulation was 9,92 m.

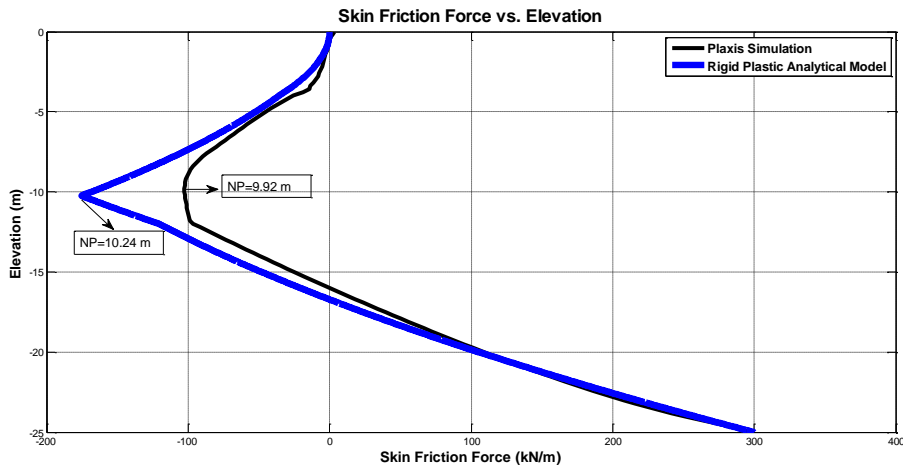


Figure 78: Comparison of Skin Friction Force Calculation of PLAXIS™ Simulation and the Analytical Method Utilized (Simplified)

4.3.2. Elastic - Plastic Model: Diaphragm Wall - Soil Interaction

The parameters and corresponding values for the analytical calculation with "Elastic Plastic Model" as per the methods explained in section "Analytical Methods to Assess a Pile Subjected to Negative Skin Friction" are given in Table 10. In addition to those parameters, the set of points, where the settlement profile of the digital simulation gets saturated (i.e., the points where the derivative of the Skin Friction Force vs. Elevation characteristics approach infinity) are assumed to be in the transition zone.

The comparison of skin friction force as a function of elevation calculated according to "Elastic Plastic Model" and the digital simulation (obtained when the average degree of consolidation (U) is 85 %) are illustrated in Figure 79. As can be assessed from the corresponding figure, the position of the neutral point appears to be at 10,14 m, whereas the location of the neutral point obtained from the digital simulation was 9,92 m.

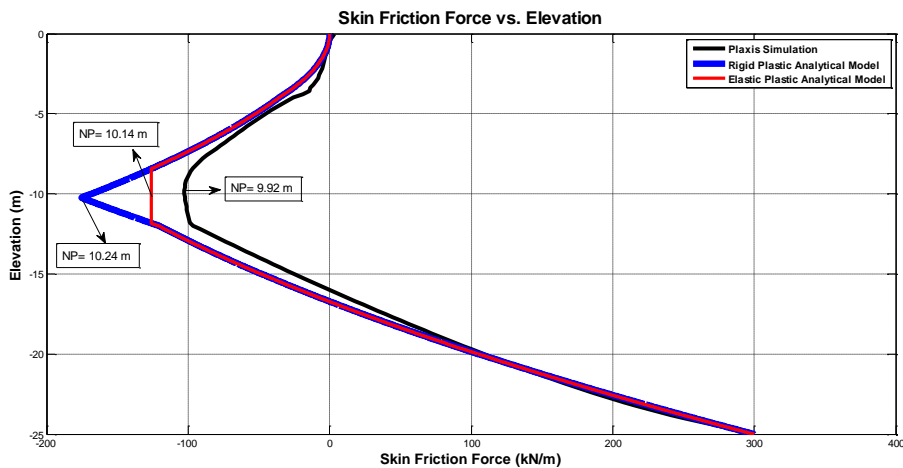


Figure 79: Comparison of Skin Friction Force Calculation of PLAXIS™ Simulation and the Analytical Method Utilized

CHAPTER 5

SUMMARY AND CONCLUSIONS

5.1. Summary

In the literature, there exist principally two design approaches utilized for the design of pile foundations subjected to negative shaft resistance. These approaches significantly differ in assessing the pile length subjected to downdrag forces, which in turn leads to different pile capacities.

The traditional method is rather conservative, and assumes that negative shaft resistance occurs along the pile shaft at soil layers with settlement greater than 10 mm. As part of the method, the magnitude of negative shaft resistance is considered as an additional load acting on the pile system.

However, the alternative method assesses the negative shaft resistance as a function of relative pile - soil movement, as explained in Briaud & Tucker (1996). Hence, design of piles subjected to downdrag requires the estimation of settlement response of the pile and the surrounding soil. Briaud & Tucker (1996) emphasized that transient live loads should not be considered at the neutral point because they only reverse the negative skin friction caused by induced-temporary downdrag forces.

Fellenius (1984) stated that, negative skin friction phenomenon is a settlement induced problem and is not directly related to the bearing capacity of the pile system. Moreover, it is mentioned that the dragload should be considered as a beneficial force prestressing the pile and reducing the deformation that occurs from live loads. Fellenius (1984) proposed that dragload must not be subtracted from the pile capacity when determining the allowable load, as long as the pile structural strength was not exceeded.

Although these approaches are observed to be fundamentally different and mostly contradicting, both approaches are widely used and referred to in the state of the art pile design procedures. Within the scope of this study, it is intended to discuss, in-detail, these contradictory design approaches, and compare their predictions through assessment of generic cases selected for the purpose. Additionally, the effects of downdrag forces will be assessed for not only vertically loaded systems but also for laterally loaded diaphragm walls, through finite element-based numerical analyses.

Numerical simulations of time dependent variation of downdrag forces on the diaphragm walls are analyzed for a soil site, where consolidation is not completed, for two generic scenarios:

As part of the first scenario, consolidation of a clayey site due to the application of the embankment is assessed. Then two sets of diaphragm walls, with and without bitumen coating, are installed. For comparison purposes, conventional analytical calculation methods (i.e., rigid - plastic and elastic - plastic soil models) are also used, the results of which, establish a good basis of comparison with PLAXIS™ simulation results.

Within the scope of the second scenario, when consolidation process is still continuing, excavation behind the diaphragm wall is simulated, still for two sub-scenarios (i.e., diaphragm wall with and without bitumen coating).

As a result of these simulations, time dependent stress and displacement responses of bitumen coated and uncoated diaphragm walls are assessed.

5.2. Conclusions

On the basis of finite element-based and analytical simulations and available literature, following conclusions are listed:

- In the literature, there exist fundamentally different and mostly contradicting methods for the assessment of downdrag forces acting on pile or diaphragm wall systems.
- The conservative approach (Hannigan, Goble, Thendon, Likins and Rausche (1998)) assumes that, downdrag forces act along the length of the pile or the diaphragm wall where soil layer settlement is greater than 10 mm. The downdrag forces are subtracted from the estimated ultimate pile or diaphragm capacity.
- The alternative approach (Briaud & Tucker (1996)), assumes that downdrag forces can develop, if and only if pile settlement is less than surrounding soil movement. Hence neutral point, defined as the point where both pile and soil settlements are identical, needs to be estimated. At the pile cap both temporary and permanent loads are assessed for pile capacity estimations. However, at the neutral point deadloads, permanent loads and downdrag forces are considered. Temporary loads are never considered for downdrag since they only reverse the mobilized negative skin friction.
- Numerical simulations have proven that:
 - Downdrag forces develop as part of an interaction among the soil, pile and the applied load.
 - For soils where consolidation is not completed, the amount of downdrag forces as well as the location of the neutral point changes. Hence an effective stress based as opposed to total stress assessment can provide realistic results.
 - Meanwhile, if the pile of the diaphragm wall system is laterally loaded, this interaction becomes more complex, and requires a complete assessment of soil-pile-load interaction.
 - For diaphragm wall installed in soils where consolidation is not completed, if bitumen coating is applied and excavation is performed before the completion of consolidation, the downdrag forces acting on the system decreases.
 - However, this decrease negatively affects the structural response of the system.
 - Reduced downdrag forces, either due to excavation or the application of bitumen coating decreases axial forces, and increases moments acting on the pile or diaphragm wall. This may lead to larger structural dimensions or increased reinforcement.
 - More specifically, for the generic cases studies, after excavation, moments acting on bitumen coated diaphragm wall are observed to be 15-30 % higher than the non-bitumen coated system. Hence beneficial effects of bitumen coating under axial loading may become disadvantageous under flexural response.

As the concluding remark, downdrag phenomenon is defined by the complex interaction of the pile, soil and the load system, hence for realistic assessment of it the interaction needs to be properly modeled. Current methods can overestimate frictional forces and underestimate moments due to excavations in soils where consolidation is not completed.

REFERENCES

- American Association of State Highway and Transportation Officials (2007). AASHTO LRFD Bridge Design Specification
- Briaud, J.B. and Tucker, L.M. (1996). Design and Construction Guidelines for Downdrag on Uncoated and Bitumen-Coated Piles Texas Transportation Institute, USA, January
- Bolton, M.D. (1986). The Strength and Dilatancy of Sands, *Géotechnique* 36, No.1, 65-78
- Bowles, J.E. (1997). *Foundation Analysis and Design*, The McGraw-Hill Companies, The United States
- Carter M. and Bentley S.P. (1991). *Correlations of Soil Properties*, London, Pentech Press
- Dan A. Brown, Ph.D, P.E., John P. Turner, Ph.D, P.E., and Raymond J. Castelli, P.E. (2010). *Drilled Shafts: Construction Procedures and LRFD Design Methods*, National Highway Institute
- Eurocode 7: Geotechnical Design - Part 1: General Rules (2004)
- Fellenius, B. H. (1984). Negative skin friction and settlement of piles. Second International Seminar, Pile Foundations, Nanyang Technological Institute, Singapore, November
- Hannigan, P.J., Goble, G.G., Thendon, G., Likins, G.E., and Rausche, F. (1998). *Design and Construction of Driven Pile Foundations*, Federal Highway Administration
- PLAXIS 2D 2010 Material Models Manual (2010). Delft University of Technology & PLAXIS B.V.
- PLAXIS 2D 2010 Reference Manual (2010). Delft University of Technology & PLAXIS B.V.
- Shong L. S. (2002). Pile Design with Negative Skin Friction, Tripartite Meeting and Technical Courses - Geotechnical Engineering, Johore
- Tomlinson, M. and Woodward, J. (2008). *Pile Design and Construction Practice* 5th Edition, USA and Canada
- TS 500, Requirements for Design and Construction of Reinforced Concrete Structures (2000)

APPENDIX A

NUMERICAL SIMULATION OUTPUTS OF ANALYSIS SCENARIO 1

Case 1: Diaphragm Wall - Soil Interaction Model

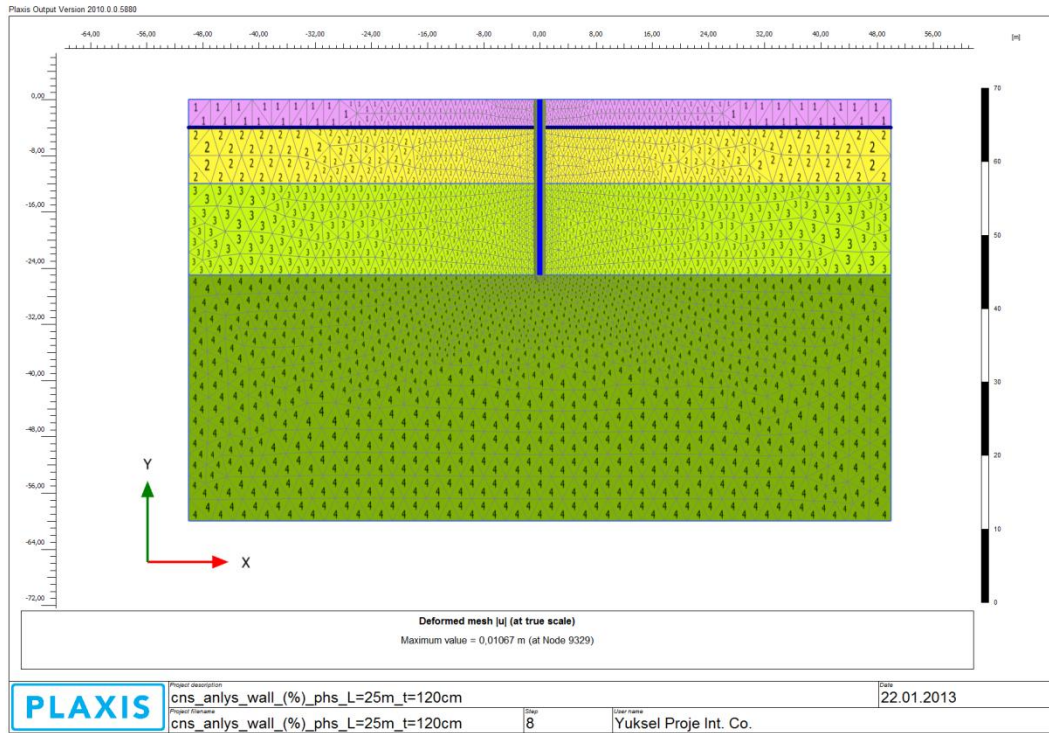


**Figure A 1: Diaphragm Wall - Soil Interaction Model
(Case 1)**

	Soil General			
Identification	Silty Sand	Clay	Sand	Sand (Rigid)
Material model	Mohr-Coulomb	Soft soil	Hardening soil	Hardening soil
Identification number	1	2	3	4

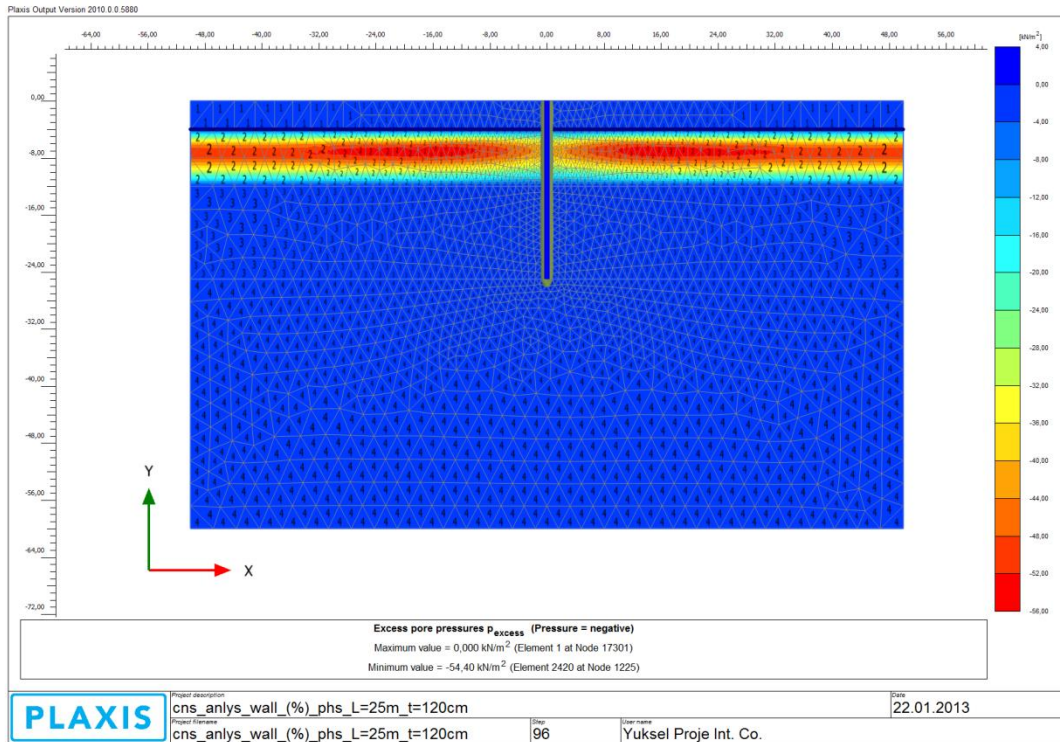


Figure A 2: Average Degree of Consolidation (U) = 25 % (Step 3)

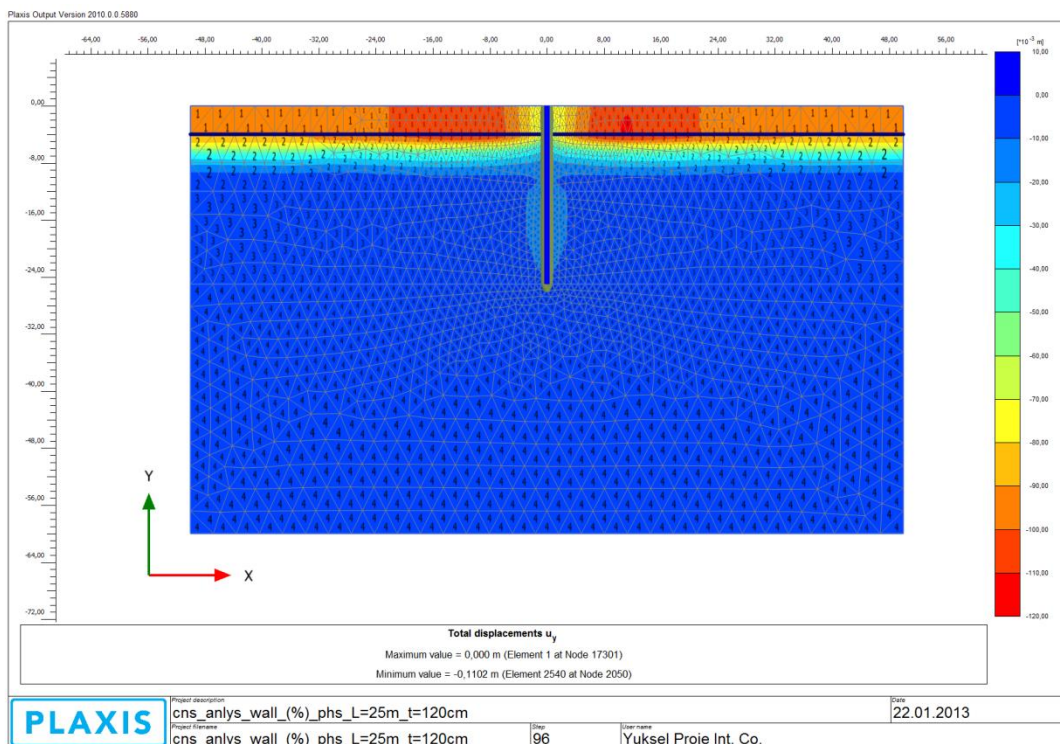


Figure A 3: Total Displacements (u_y) (Step 3)

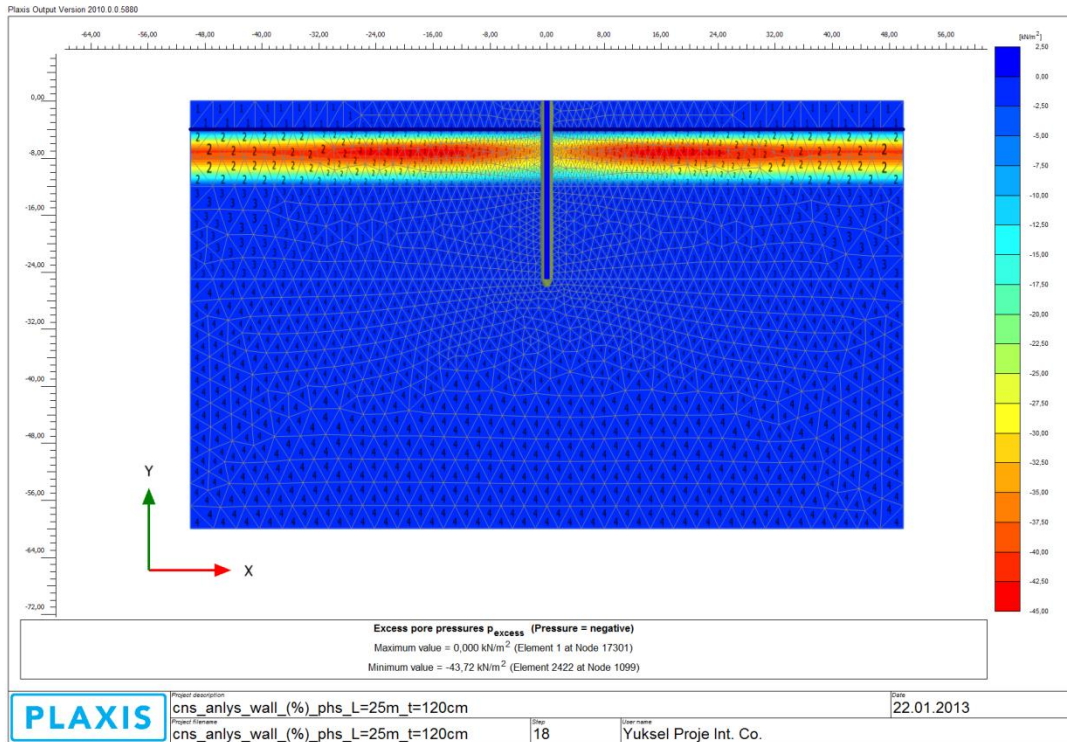


Figure A 4: Average Degree of Consolidation (U) = 40 % (Step 4)

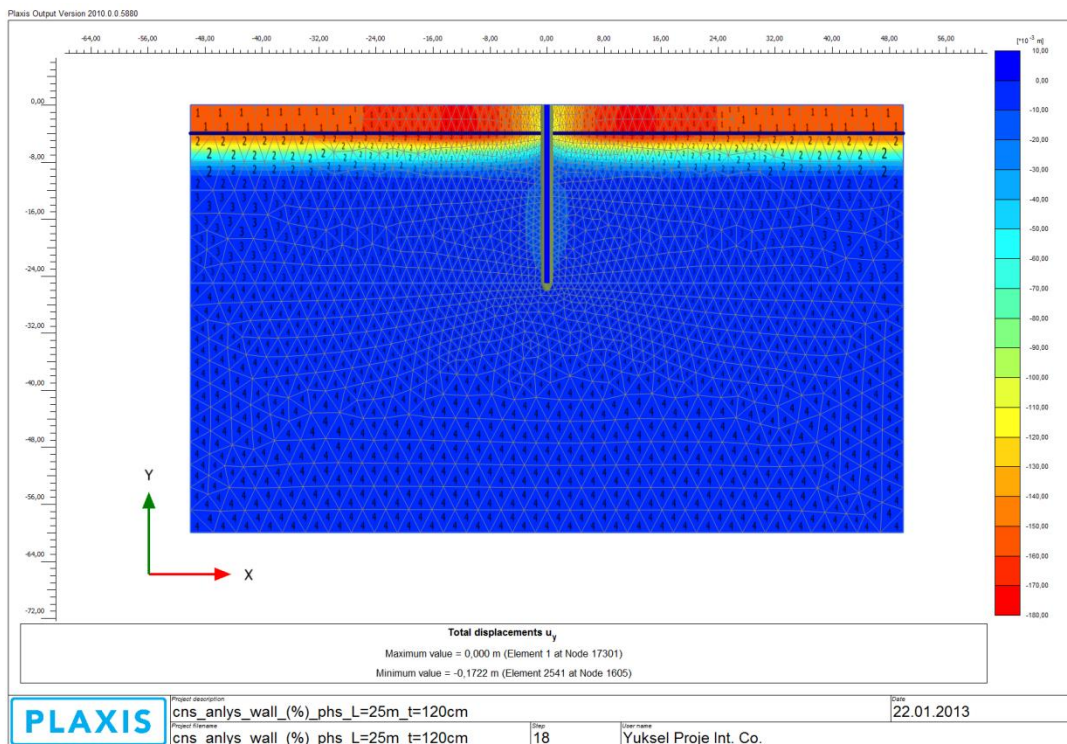


Figure A 5: Total Displacements (u_y) (Step 4)

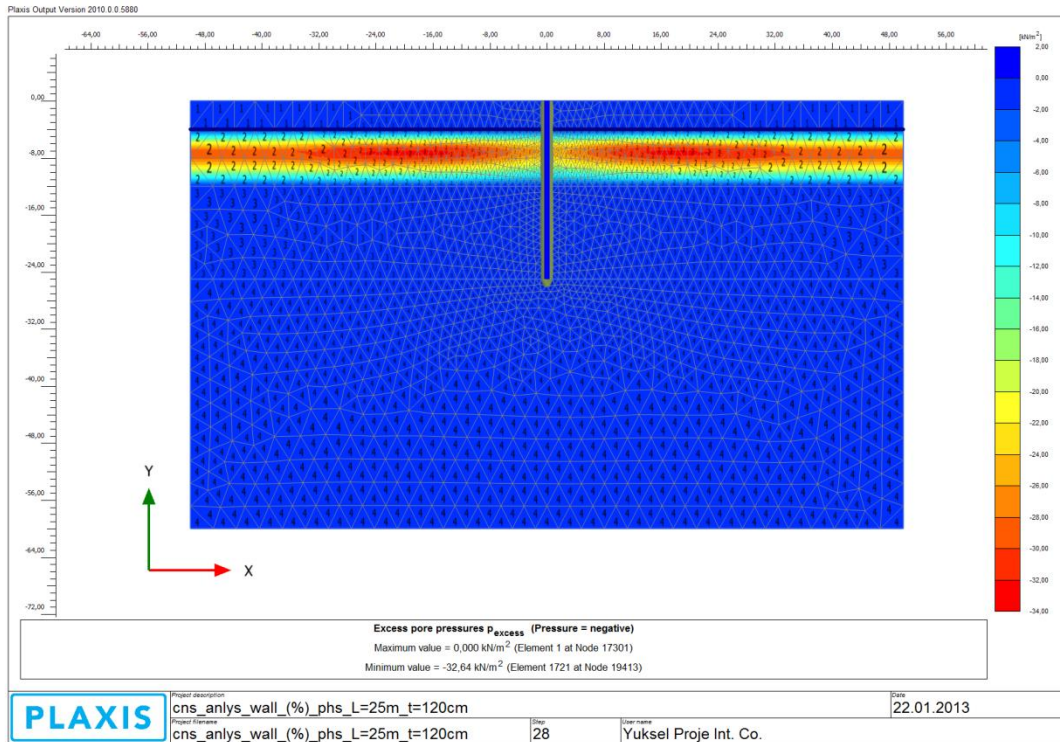


Figure A 6: Average Degree of Consolidation (U) = 55 % (Step 5)

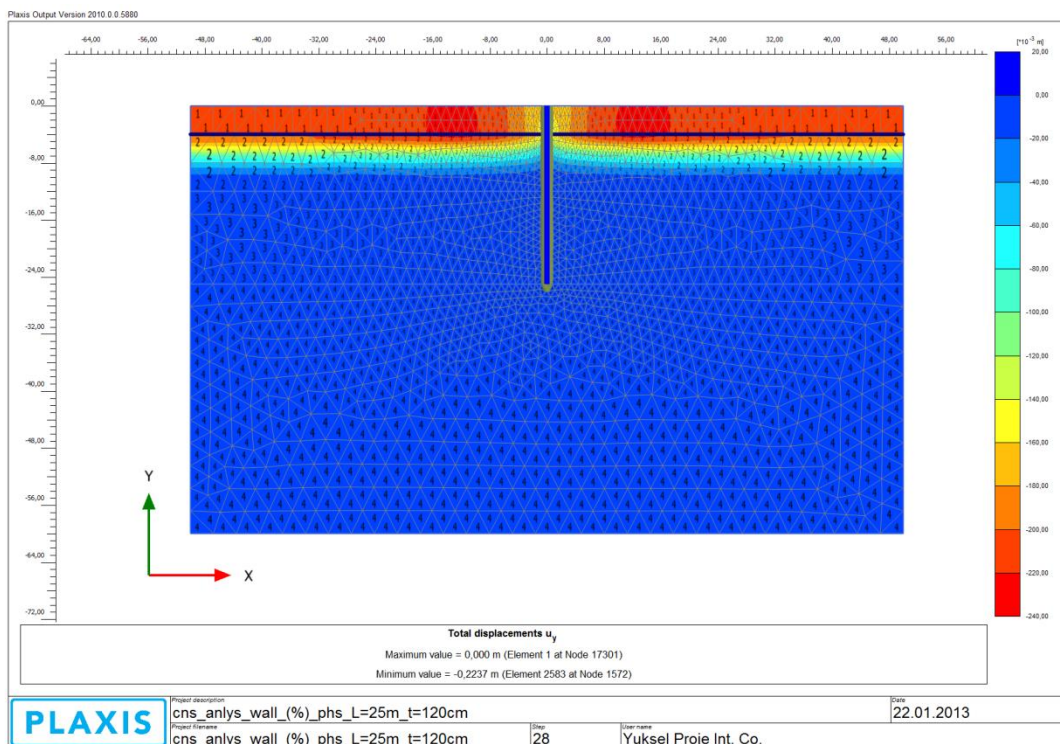


Figure A 7: Total Displacements (u_y) (Step 5)

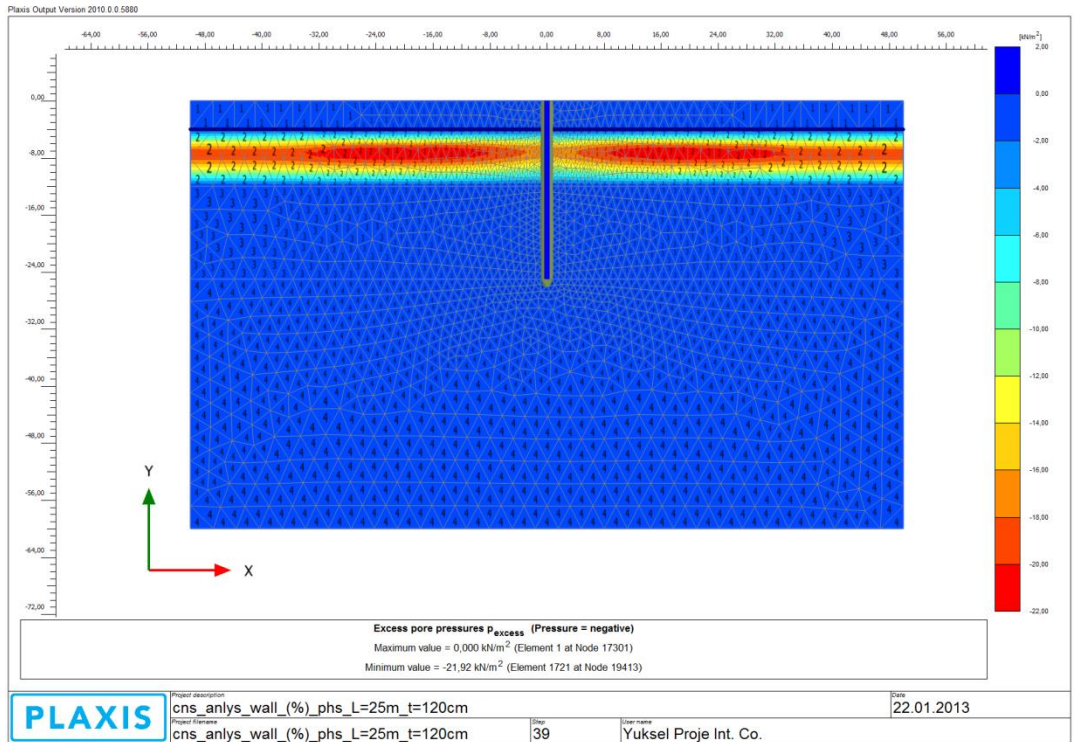


Figure A 8: Average Degree of Consolidation (U) = 70 % (Step 6)

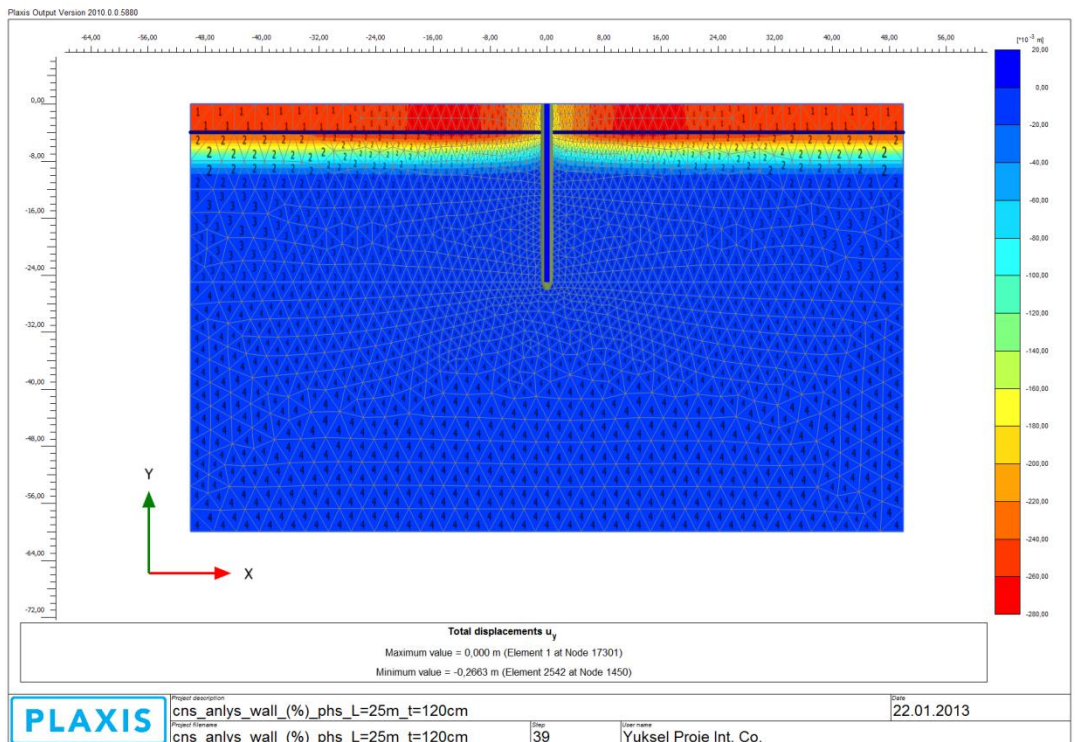


Figure A 9: Total Displacements (u_y) (Step 6)

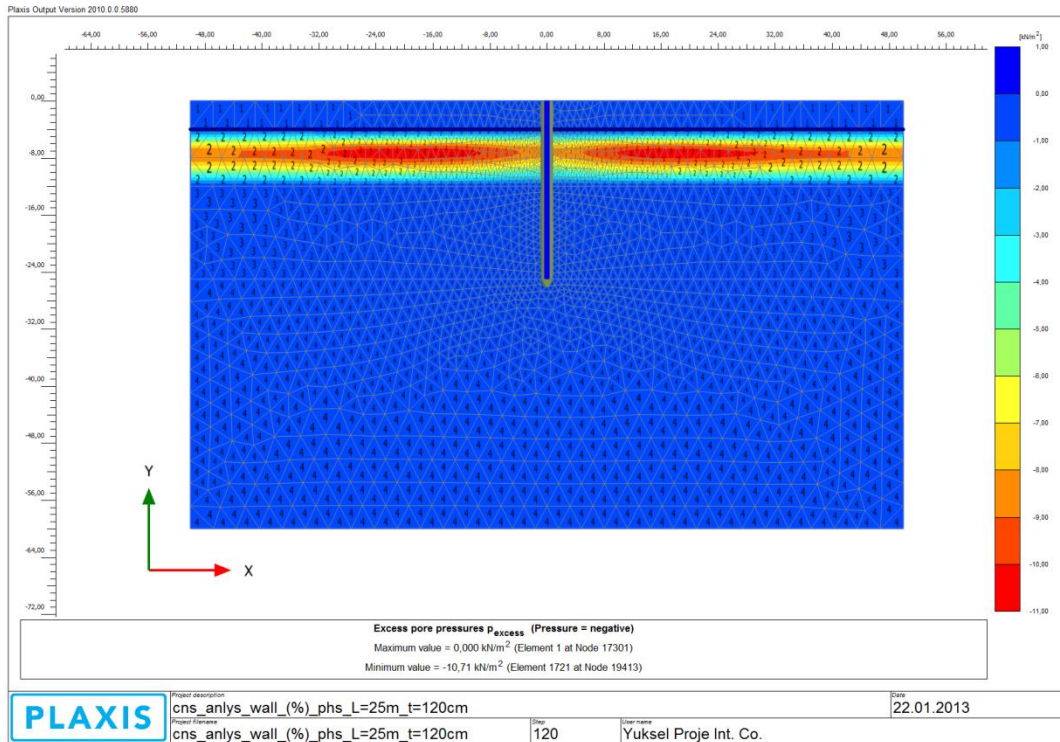


Figure A 10: Average Degree of Consolidation (U) = 85 % (Step 7)

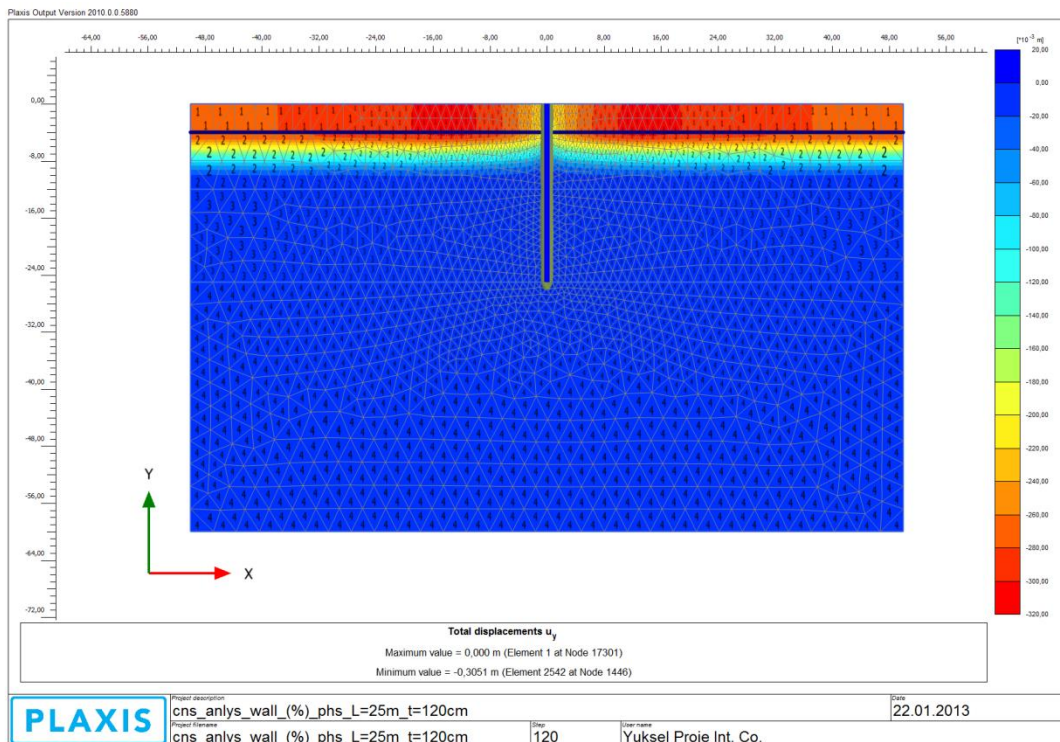


Figure A 11: Total Displacements (u_y) (Step 7)

Case 2: Bitumen Coated Diaphragm Wall - Soil Interaction Model

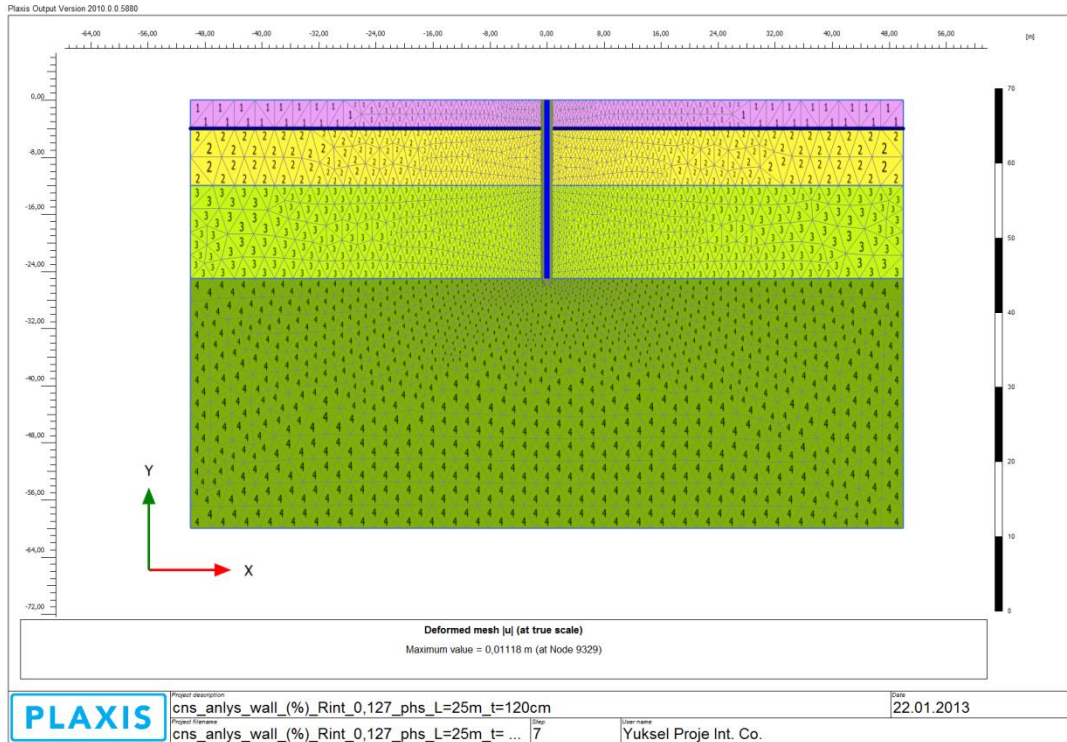


Figure A 12: Bitumen Coated Diaphragm Wall - Soil Interaction Model (Case 2)

Identification	Soil General			
	Silty Sand	Clay	Sand	Sand (Rigid)
Material model	Mohr-Coulomb	Soft soil	Hardening soil	Hardening soil
Identification number	1	2	3	4

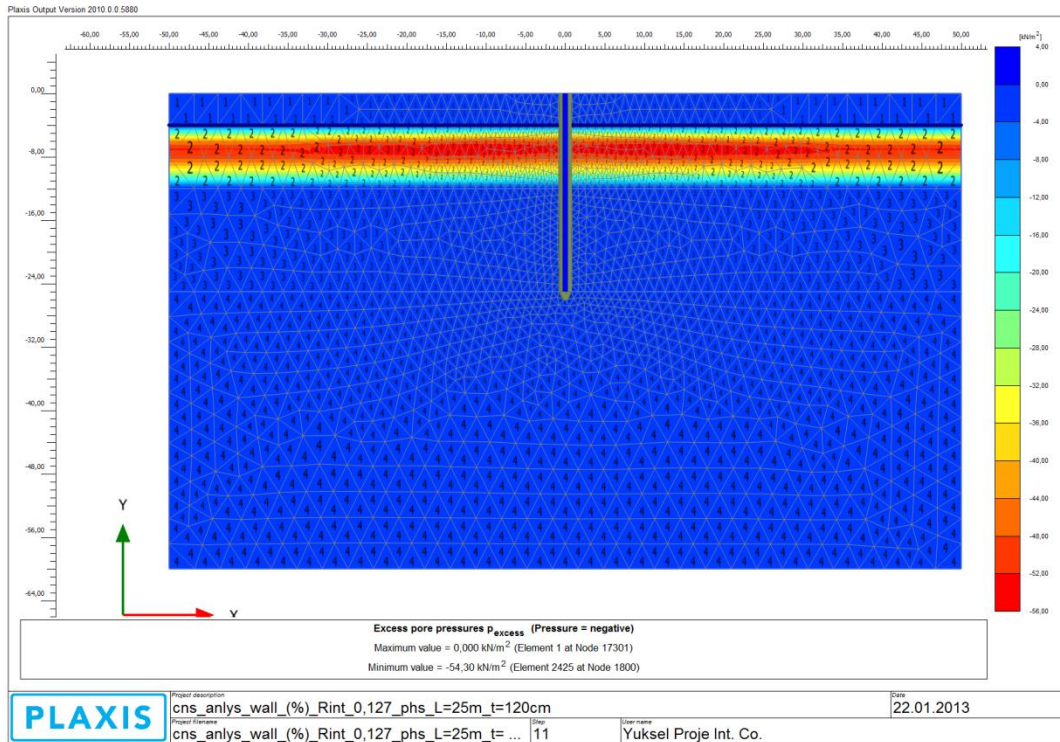


Figure A 13: Average Degree of Consolidation (U) = 25 % (Step 3)

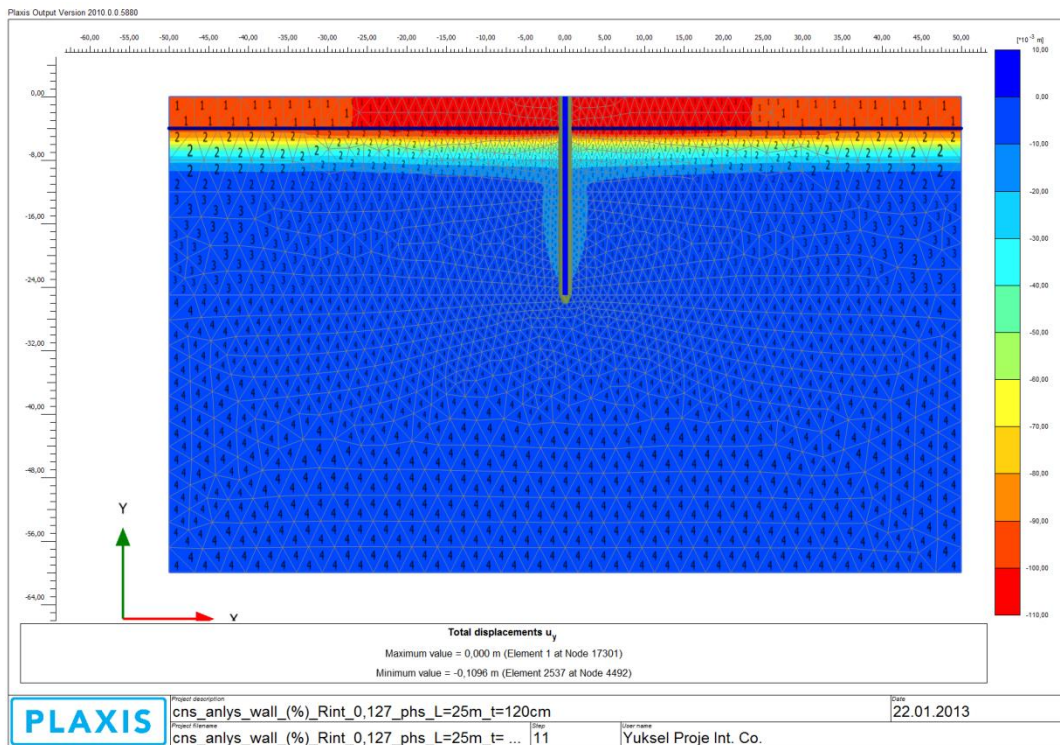


Figure A 14: Total Displacements (u_y) (Step 3)

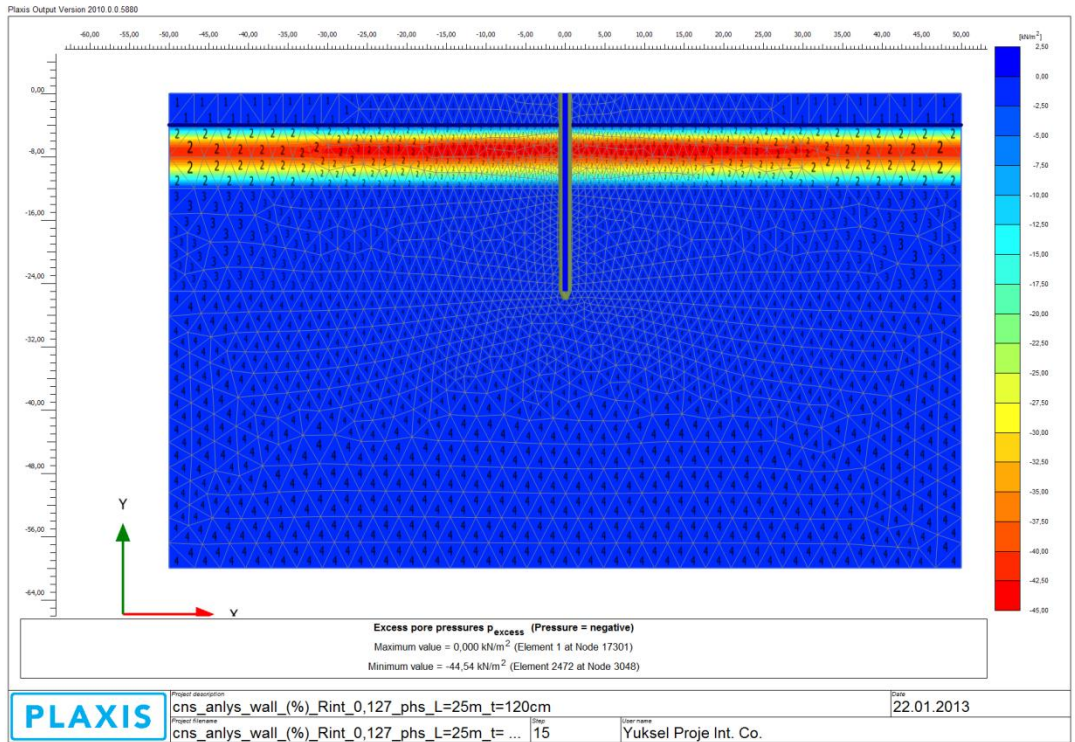


Figure A 15: Average Degree of Consolidation (U) = 40 % (Step 4)

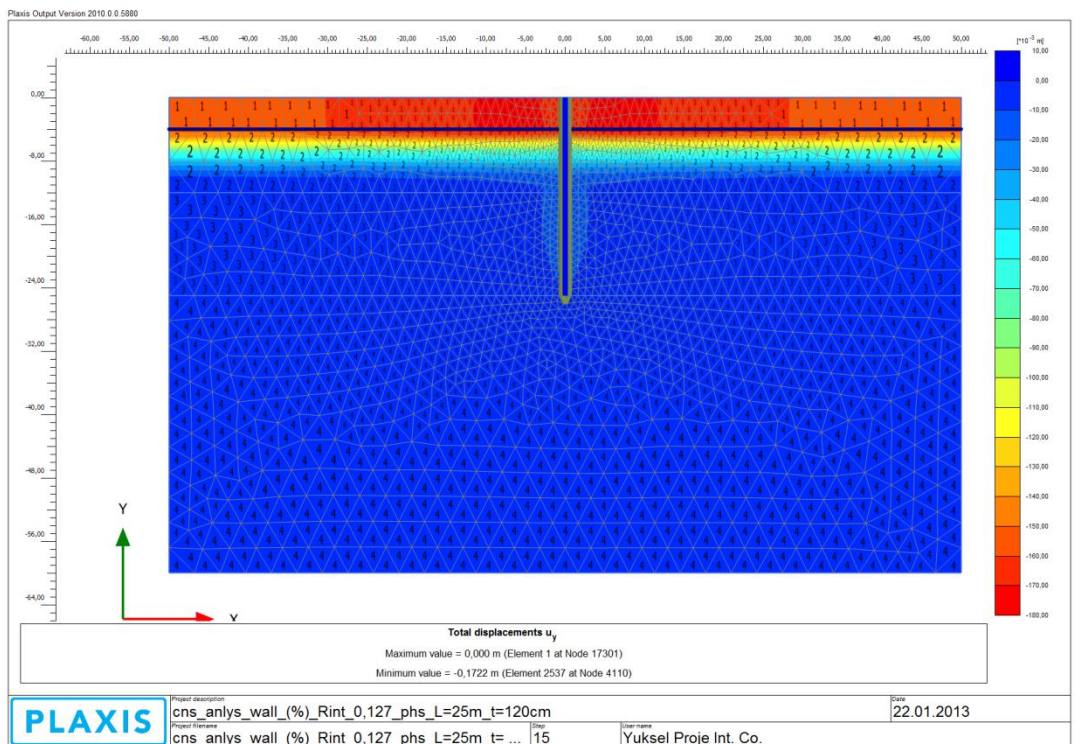


Figure A 16: Total Displacements (u_y) (Step 4)

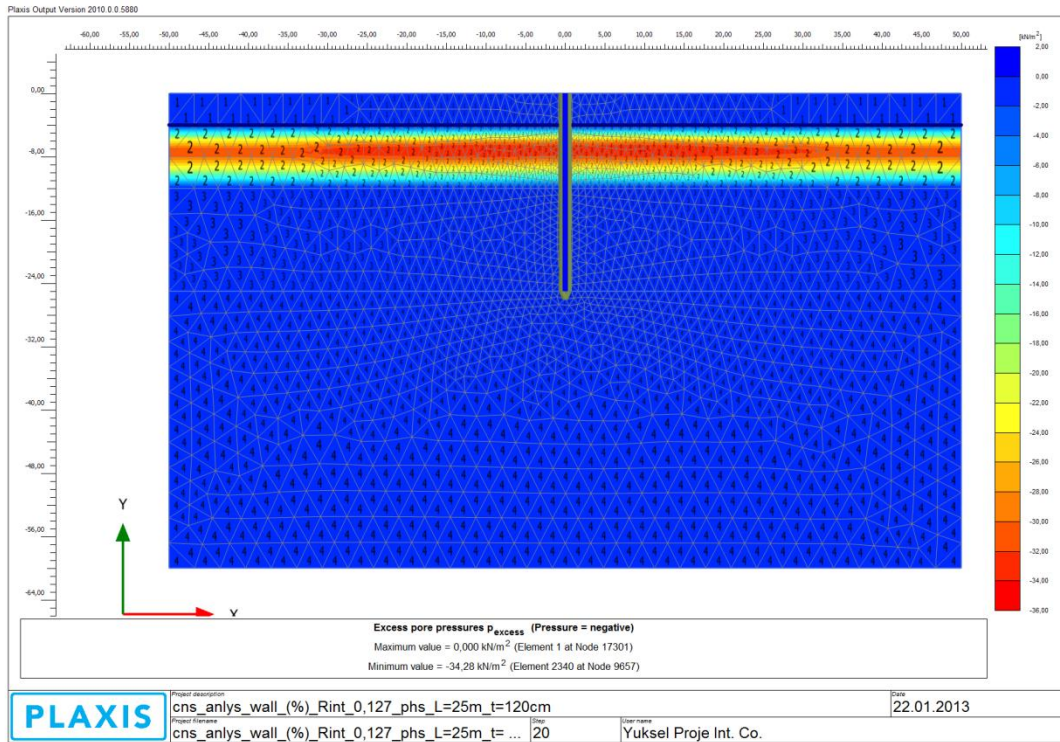


Figure A 17: Average Degree of Consolidation (U) = 55 % (Step 5)

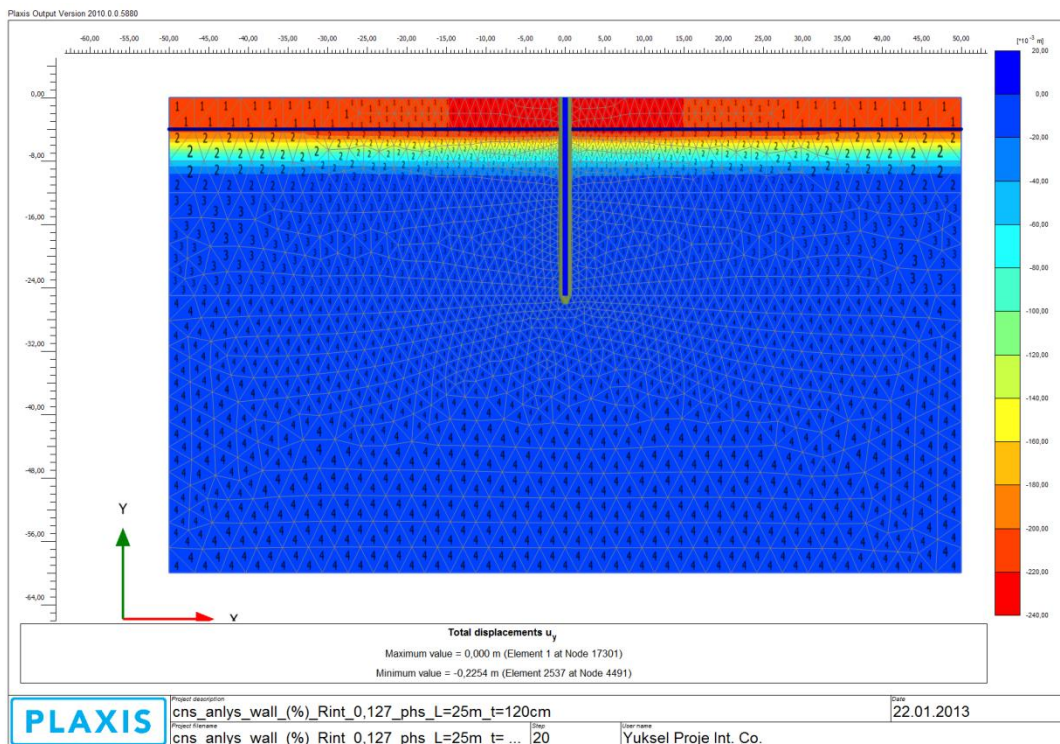


Figure A 18: Total Displacements (u_y) (Step 5)

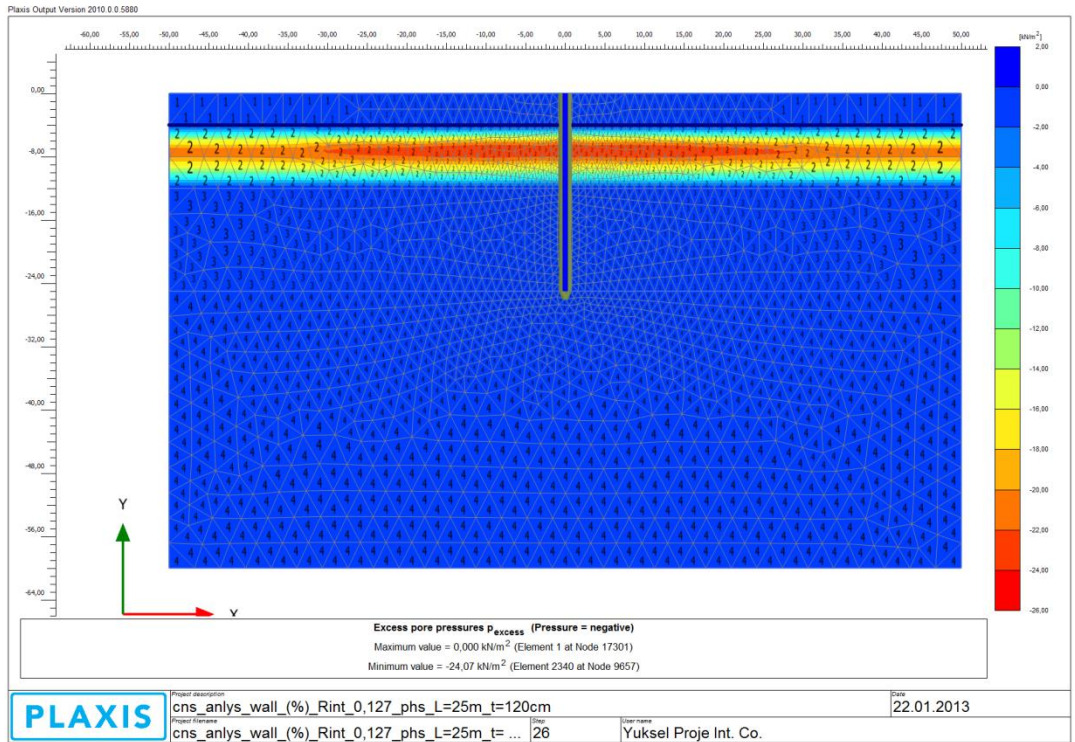


Figure A 19: Average Degree of Consolidation (U) = 70 % (Step 6)

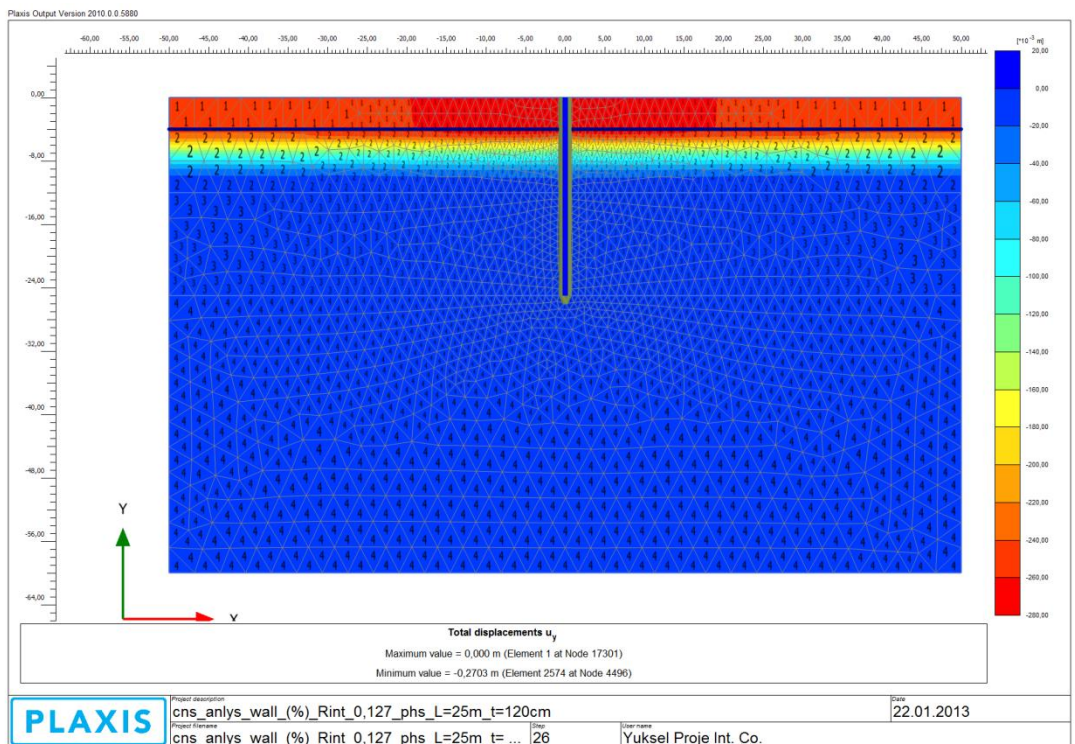


Figure A 20: Total Displacements (u_y) (Step 6)

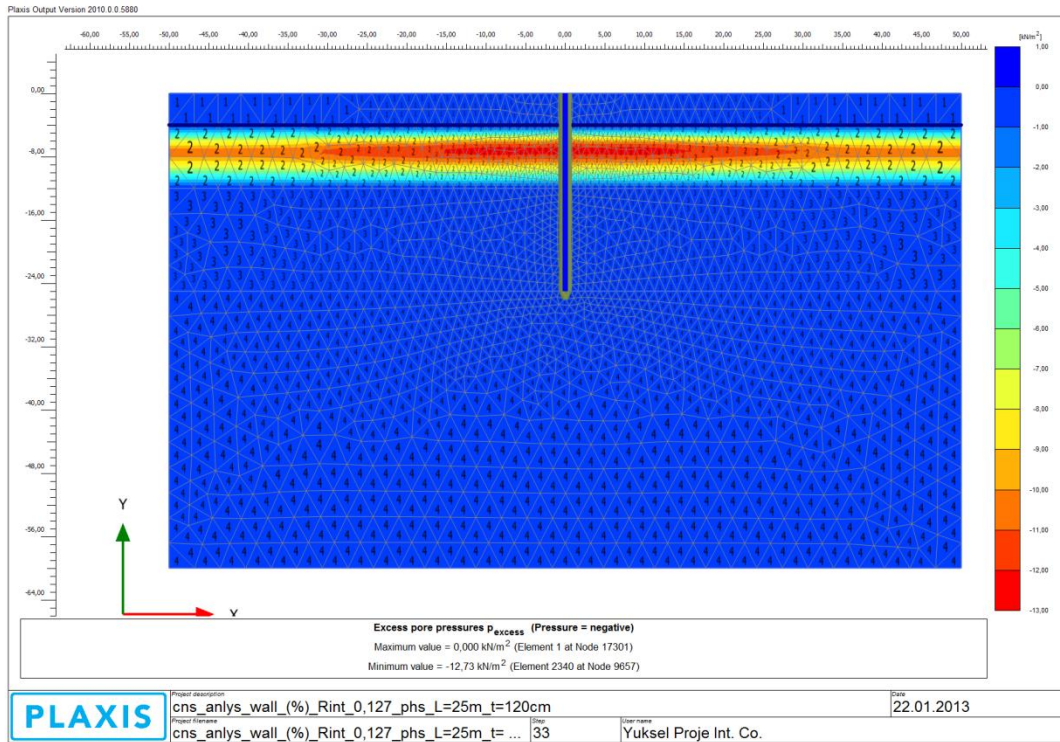


Figure A 21: Average Degree of Consolidation (U) = 85 % (Step 7)

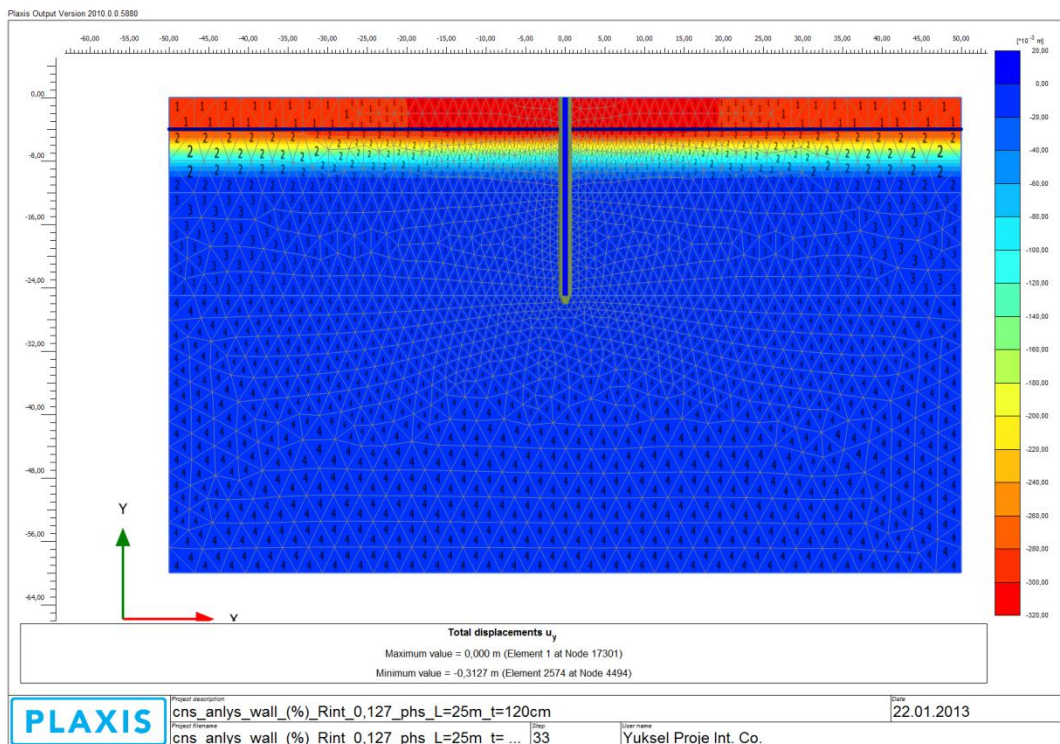


Figure A 22: Total Displacements (u_y) (Step 7)

APPENDIX B

NUMERICAL SIMULATION OUTPUTS OF ANALYSIS SCENARIO 2

Case 1: Diaphragm Wall - Soil Interaction Model during Excavation

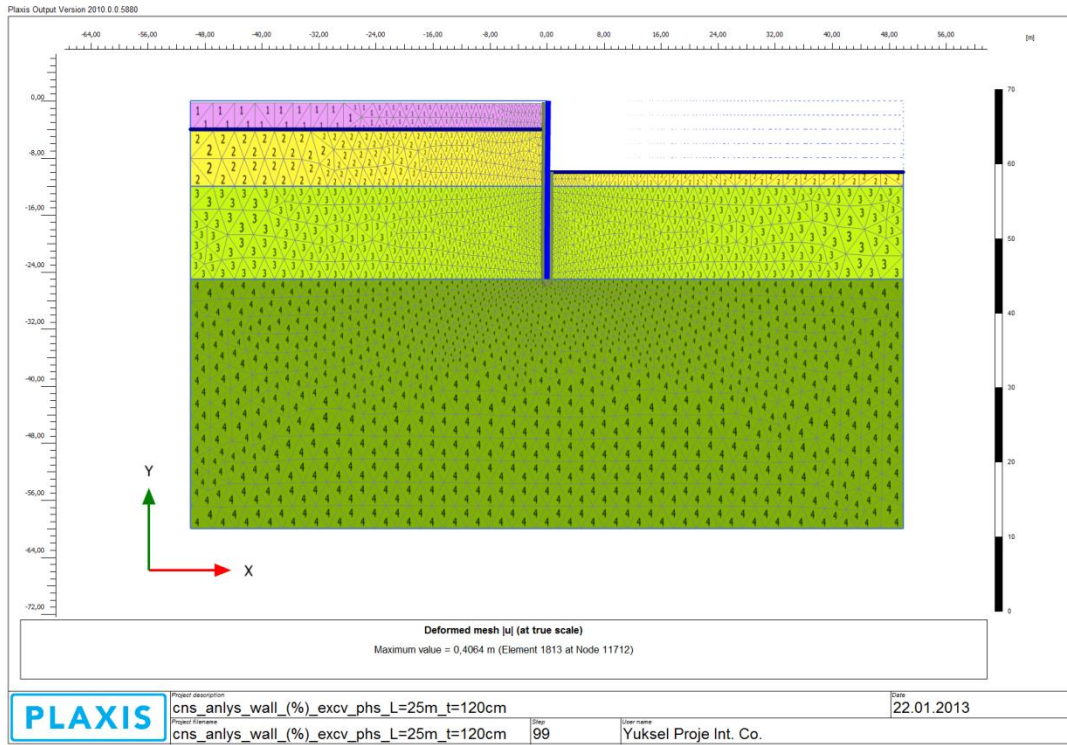


Figure B 1: Diaphragm Wall - Soil Interaction Model during Excavation (Case 1)

	Soil General			
Identification	Silty Sand	Clay	Sand	Sand (Rigid)
Material model	Mohr-Coulomb	Soft soil	Hardening soil	Hardening soil
Identification number	1	2	3	4

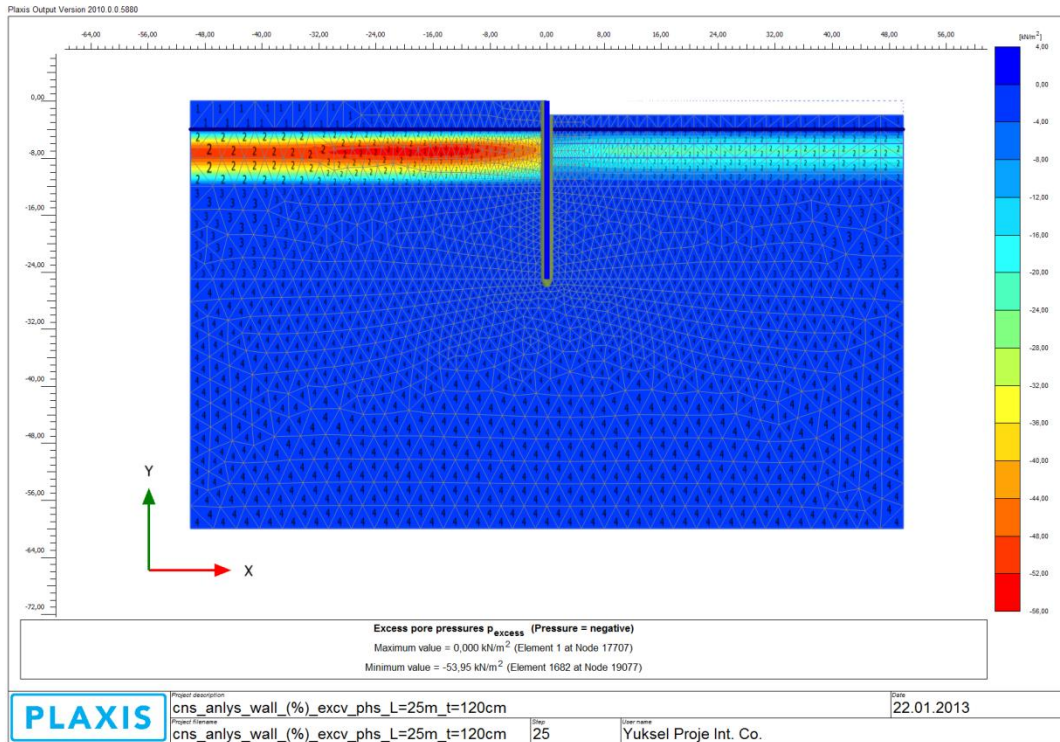


Figure B 2: Average Degree of Consolidation (U) = 25 % (Step 3)

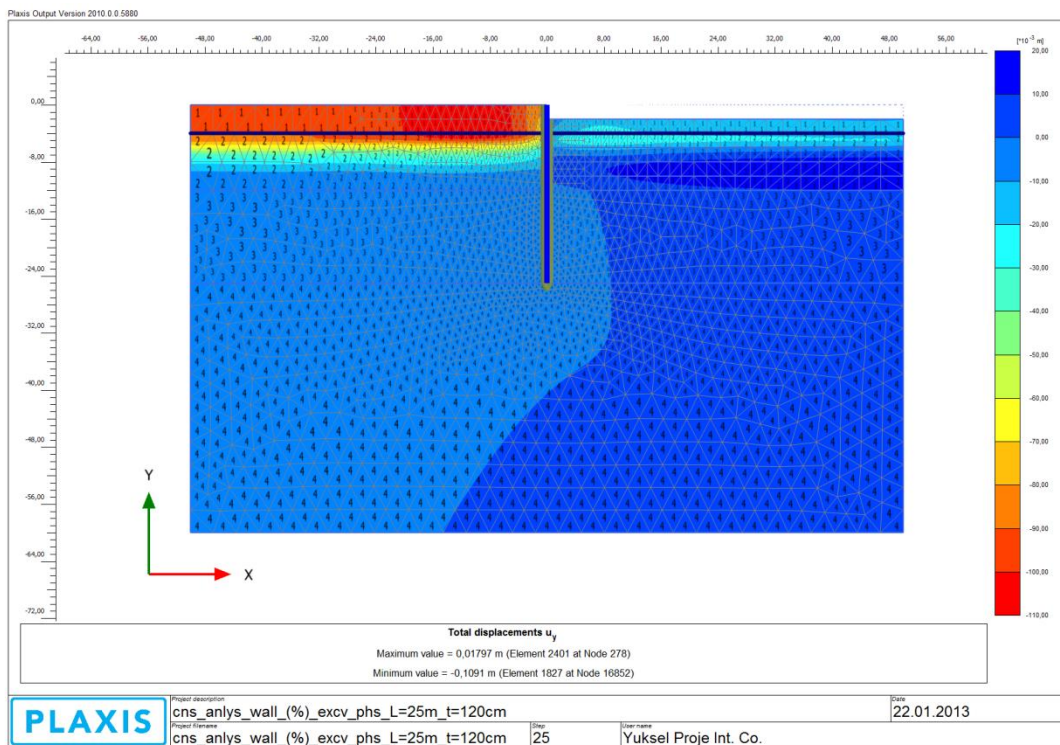


Figure B 3: Total Displacements (u_y) (Step 3)

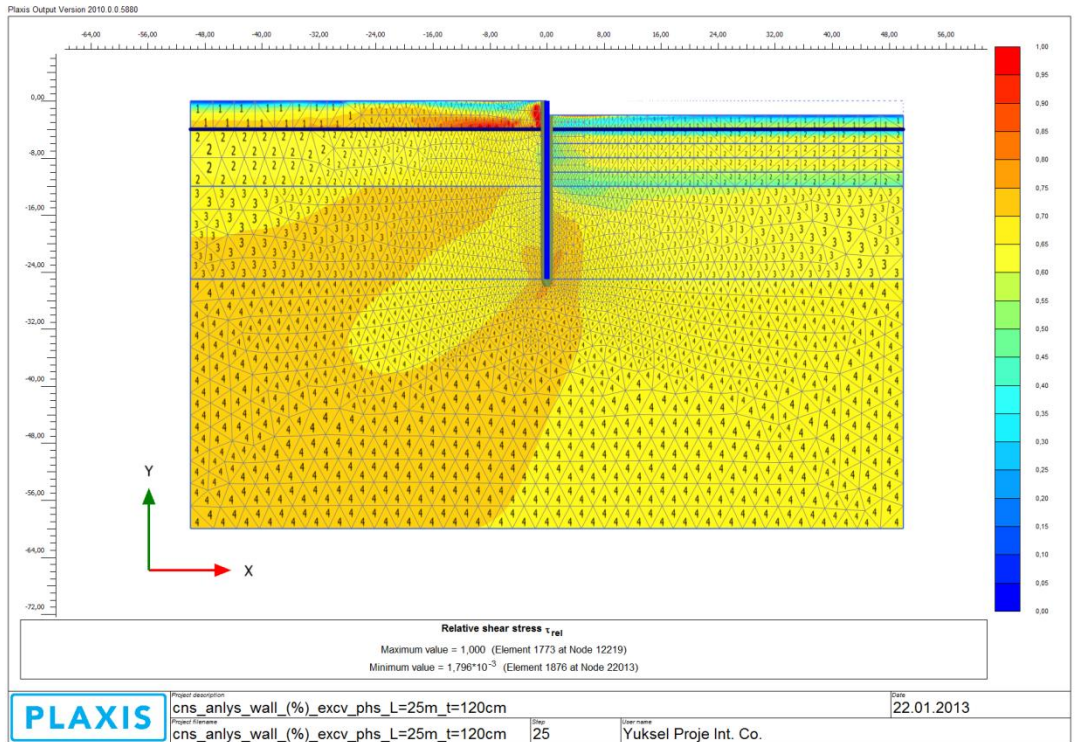


Figure B 4: Relative Shear Stress (τ_{rel}) (Step 3)

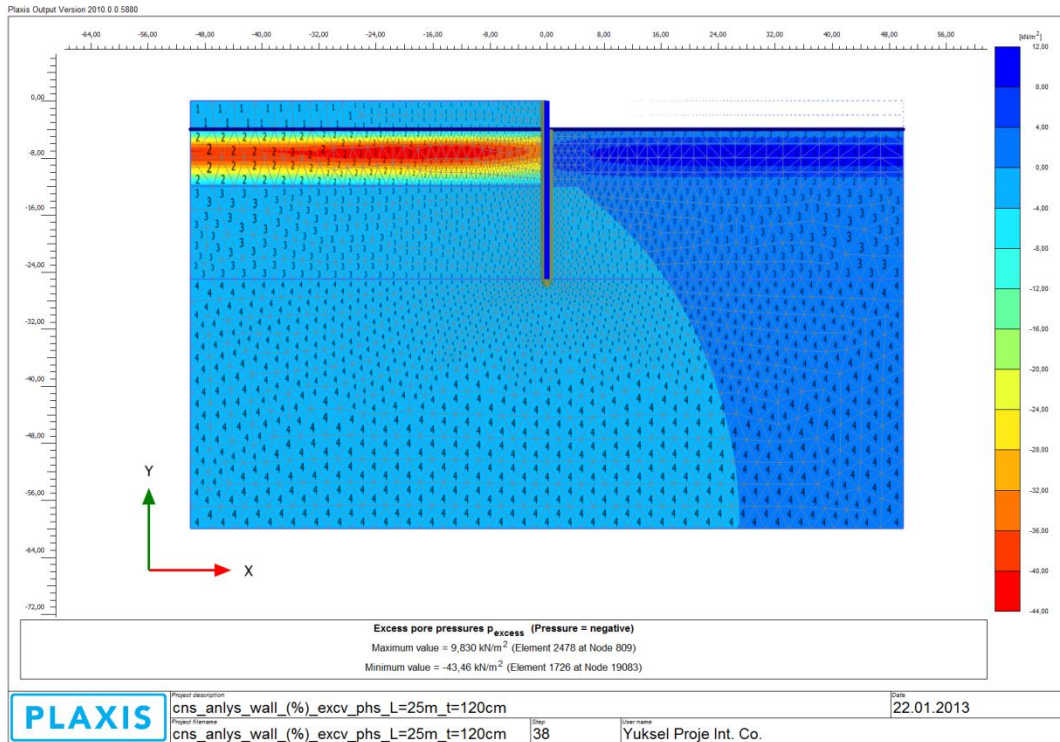


Figure B 5: Average Degree of Consolidation (U) = 40 % (Step 4)

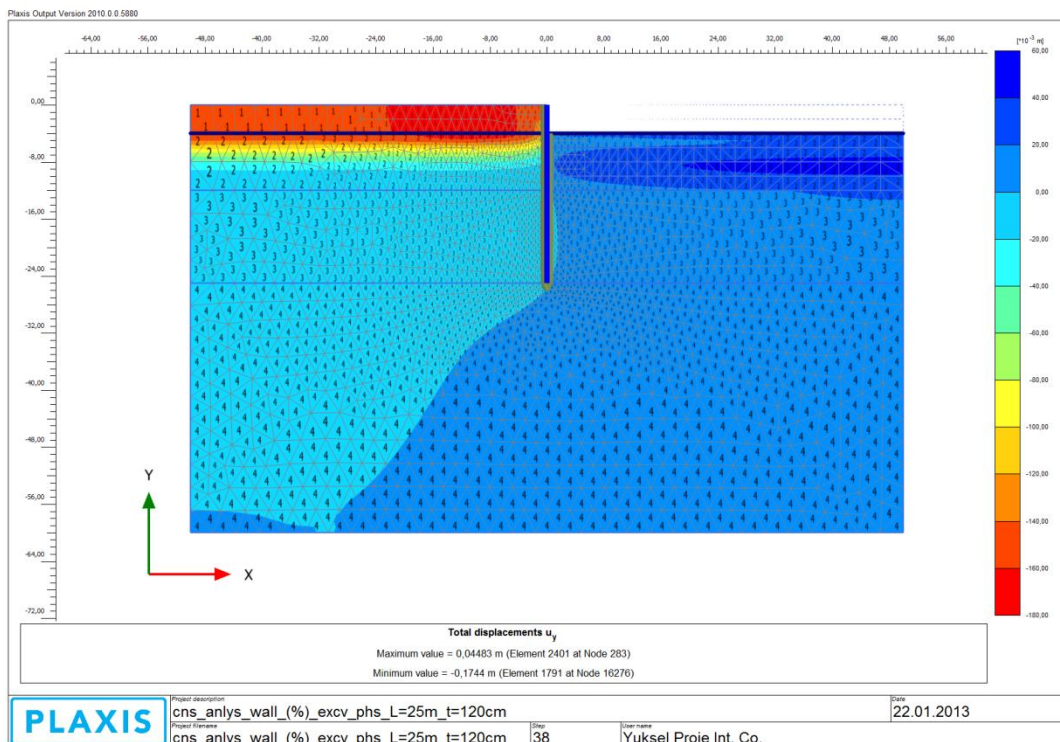


Figure B 6: Total Displacements (u_y) (Step 4)

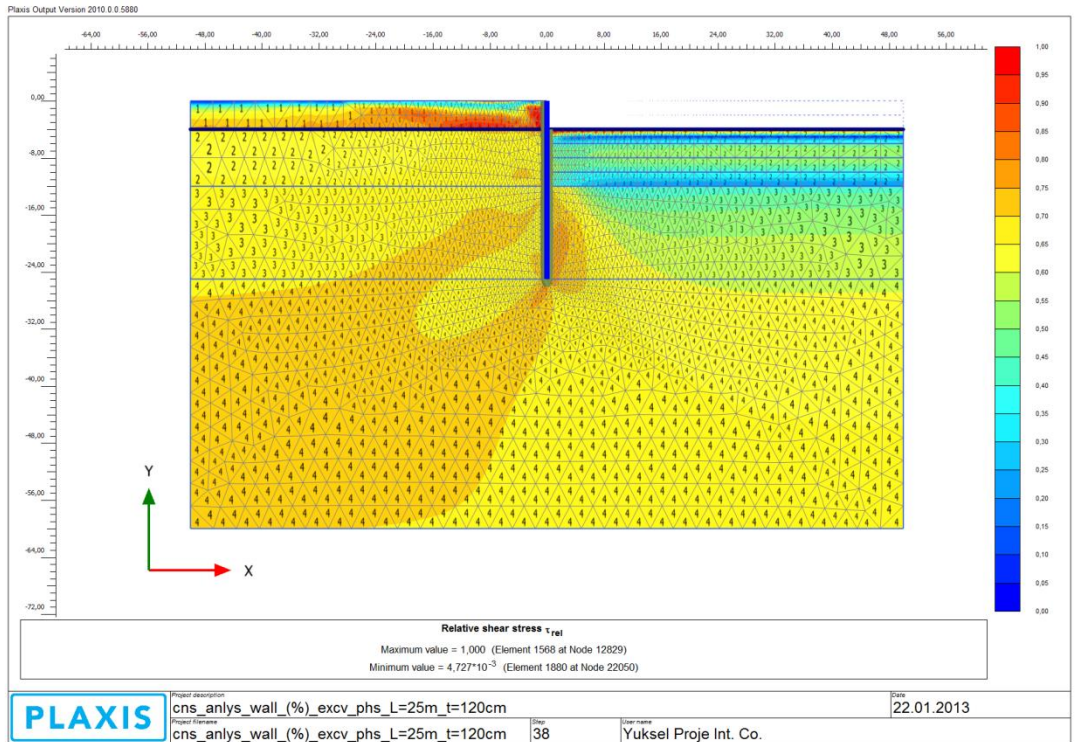


Figure B 7: Relative Shear Stress (τ_{rel}) (Step 4)

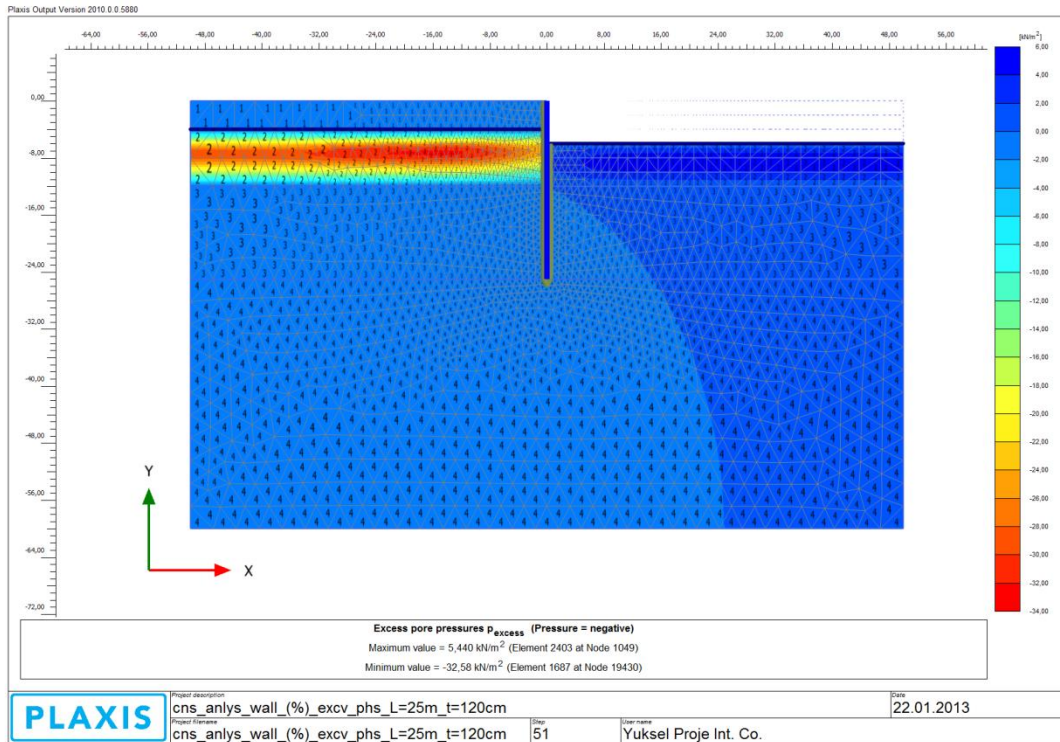


Figure B 8: Average Degree of Consolidation (U) = 55 % (Step 5)

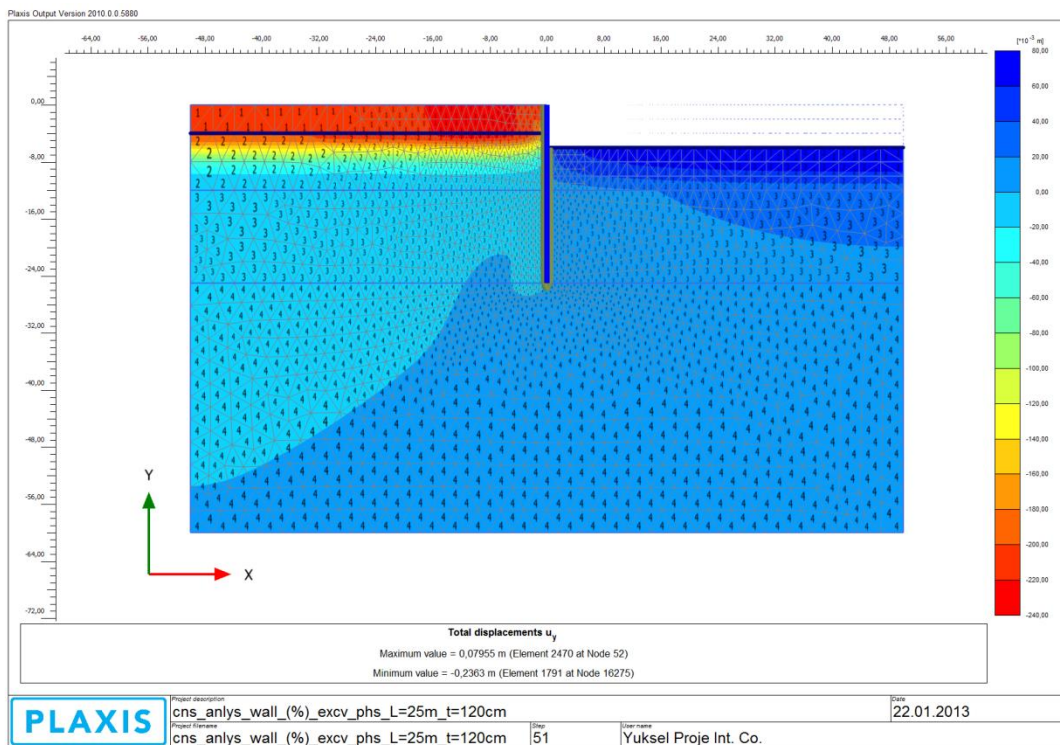


Figure B 9: Total Displacements (u_y) (Step 5)

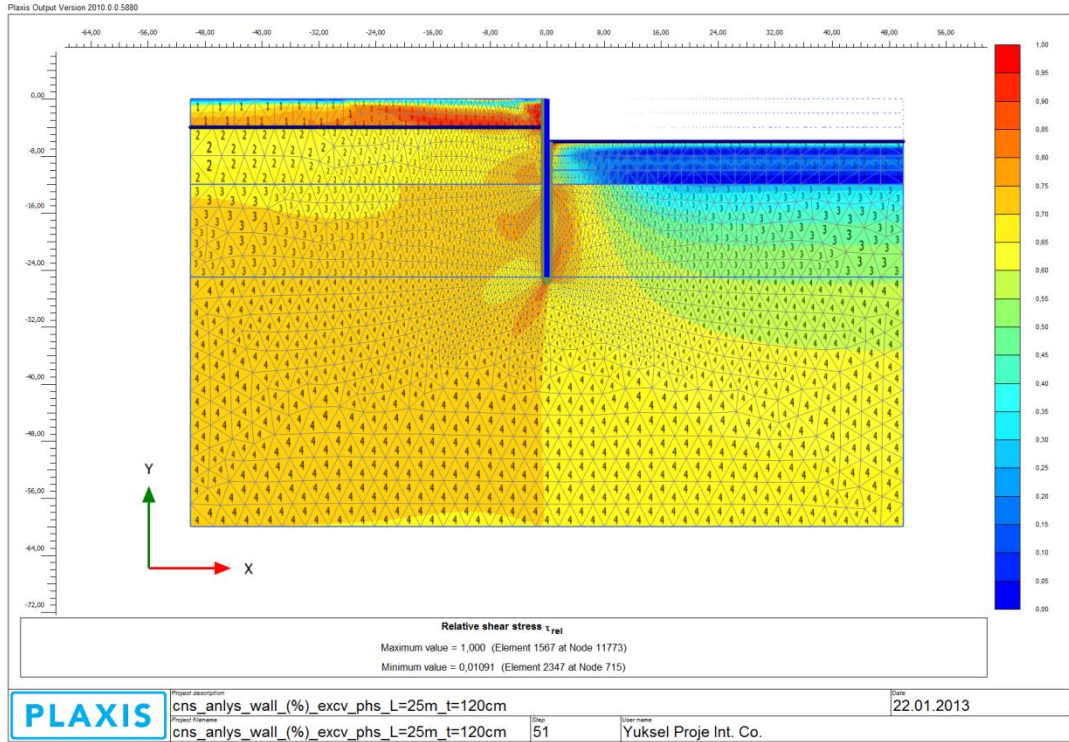


Figure B 10: Relative Shear Stress (τ_{rel}) (Step 5)

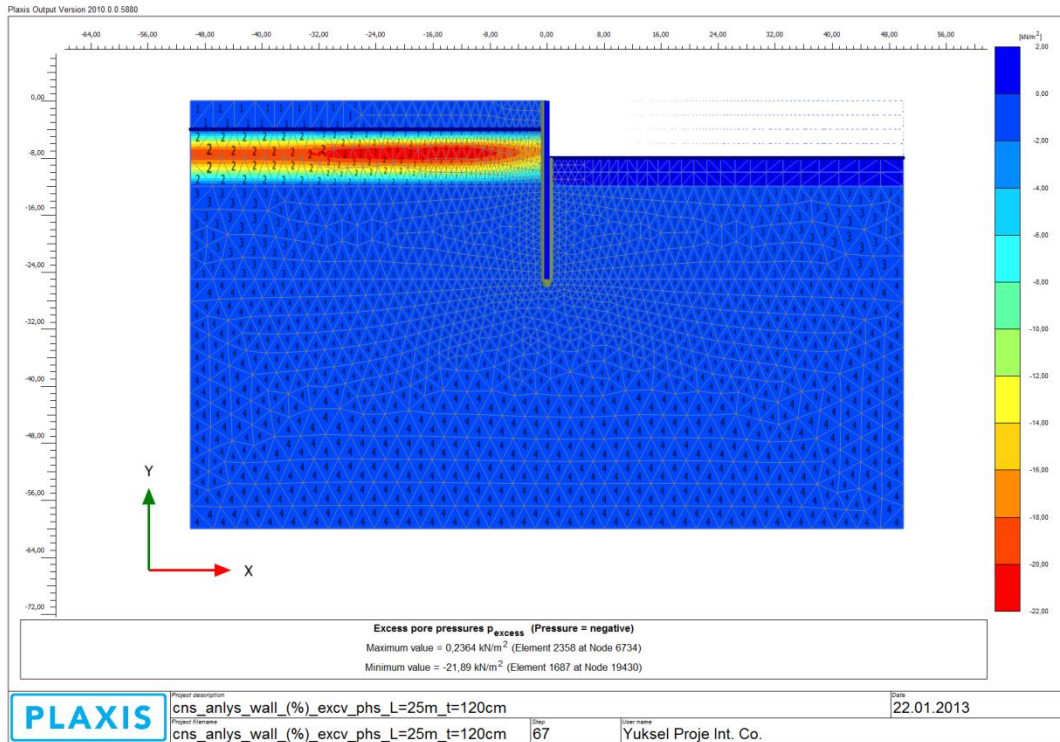


Figure B 11: Average Degree of Consolidation (U) = 70 % (Step 6)

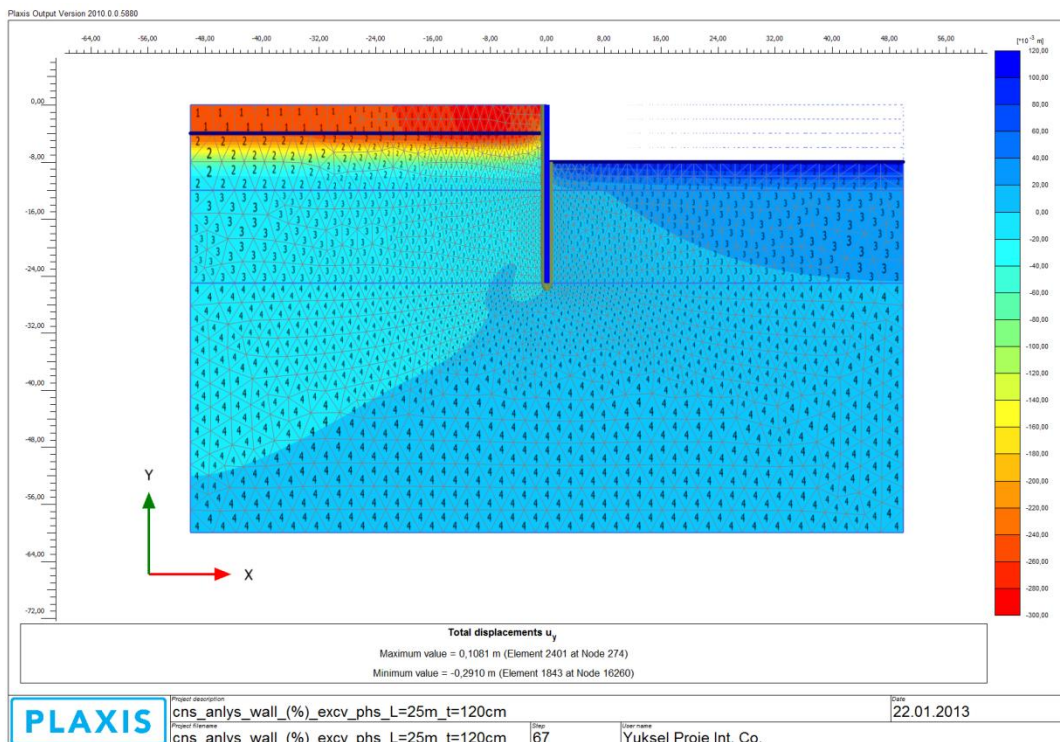


Figure B 12: Total Displacements (u_y) (Step 6)

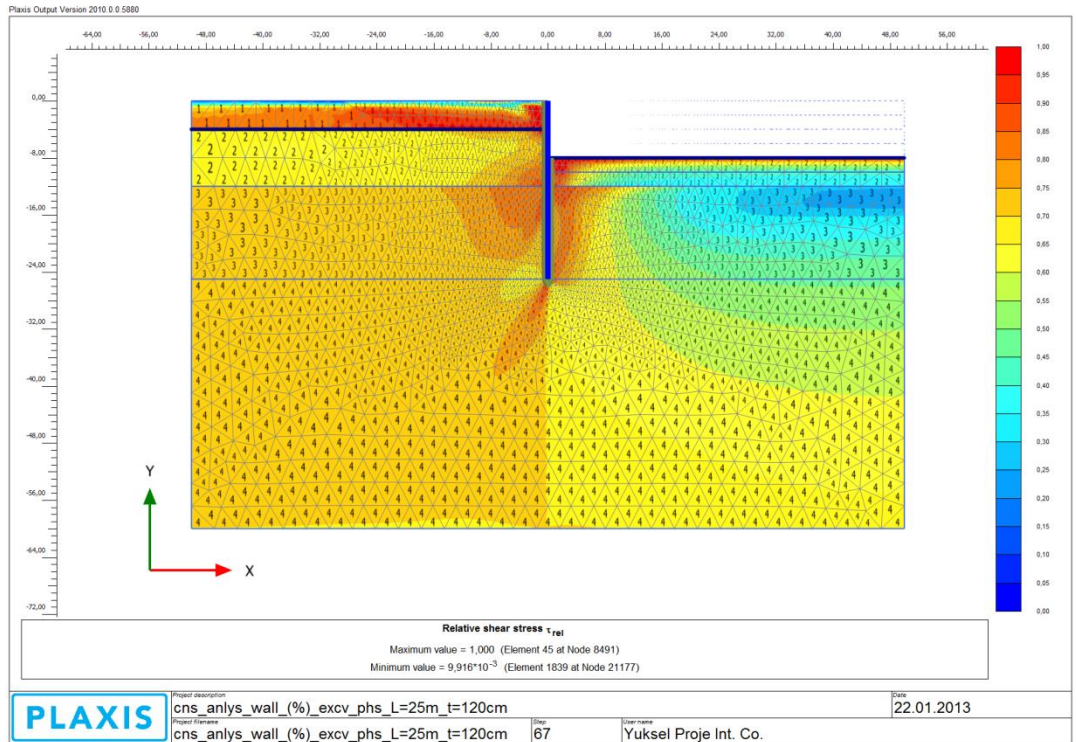


Figure B 13: Relative Shear Stress (τ_{rel}) (Step 6)

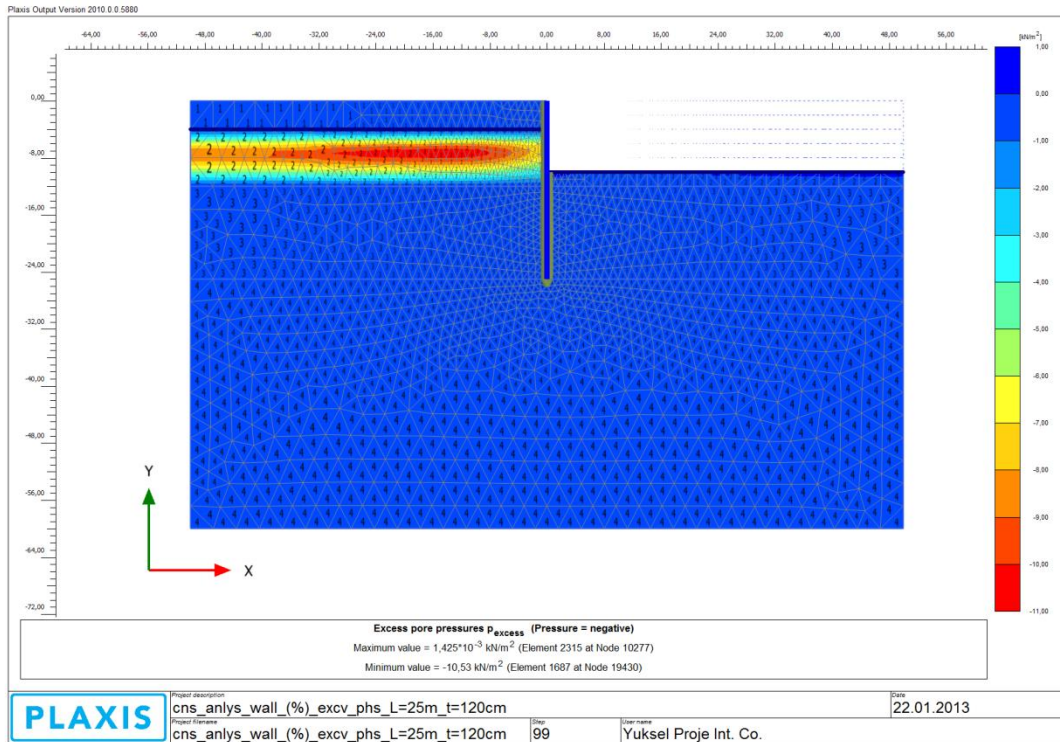


Figure B 14: Average Degree of Consolidation (U) = 85 % (Step 7)

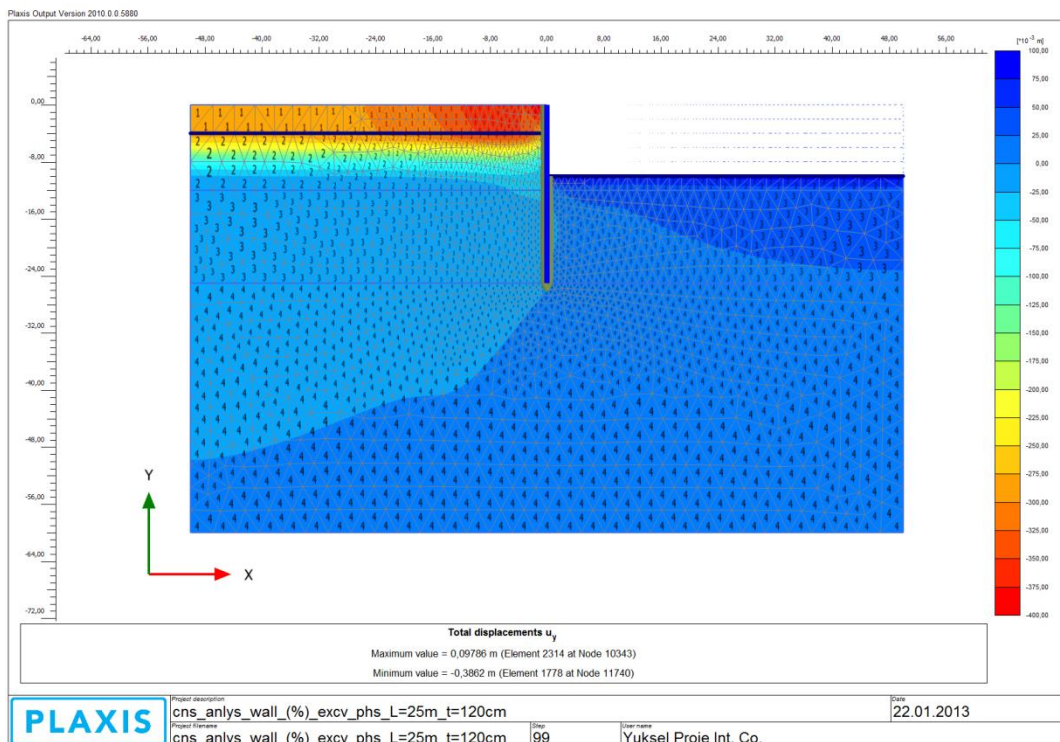


Figure B 15: Total Displacements (u_y) (Step 7)

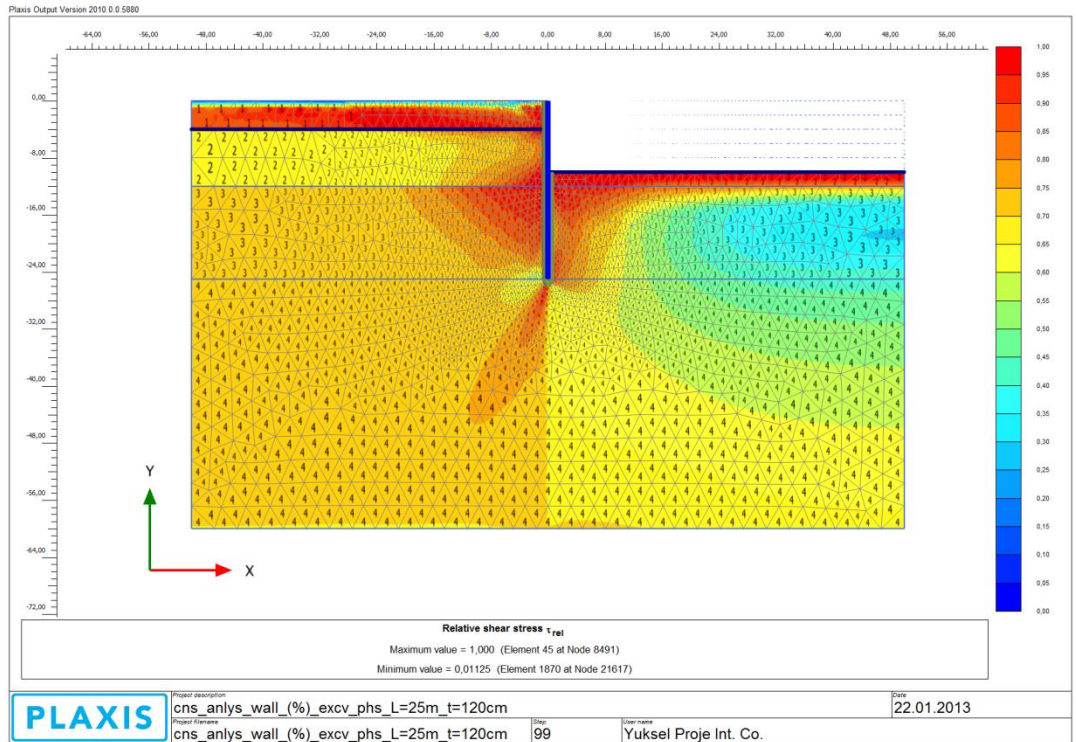


Figure B 16: Relative Shear Stress (τ_{rel}) (Step 7)

Case 2: Bitumen Coated Diaphragm Wall - Soil Interaction Model during Excavation

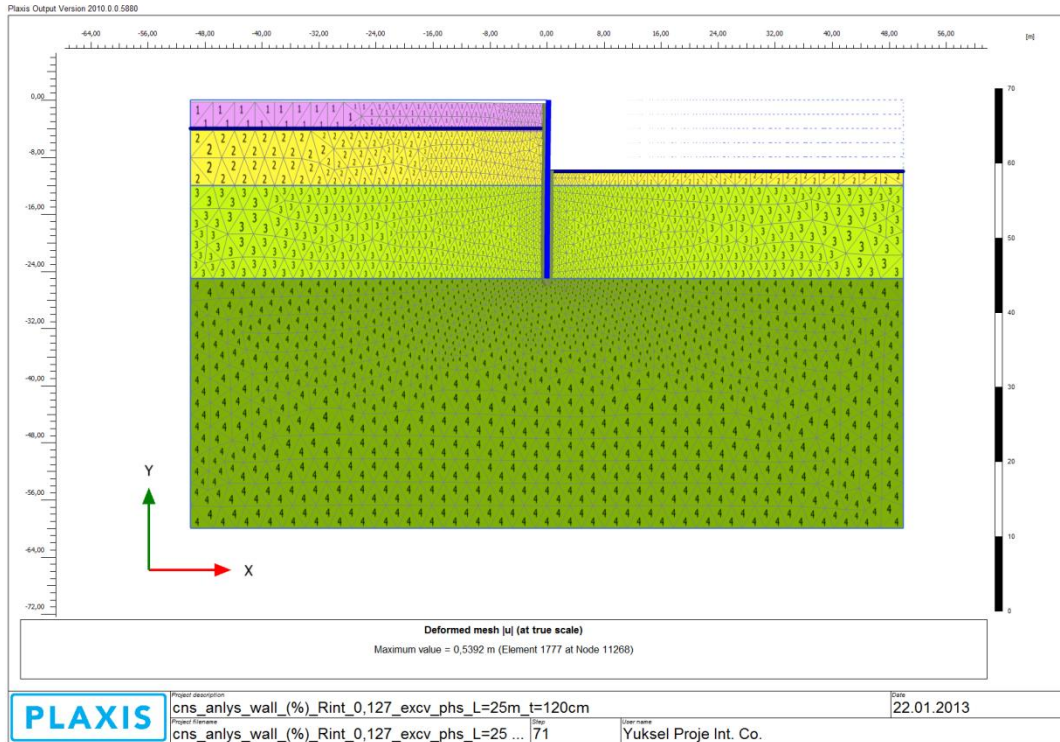


Figure B 17: Bitumen Coated Diaphragm Wall - Soil Interaction Model during Excavation (Case 2)

Identification	Soil General			
	Silty Sand	Clay	Sand	Sand (Rigid)
Material model	Mohr-Coulomb	Soft soil	Hardening soil	Hardening soil
Identification number	1	2	3	4

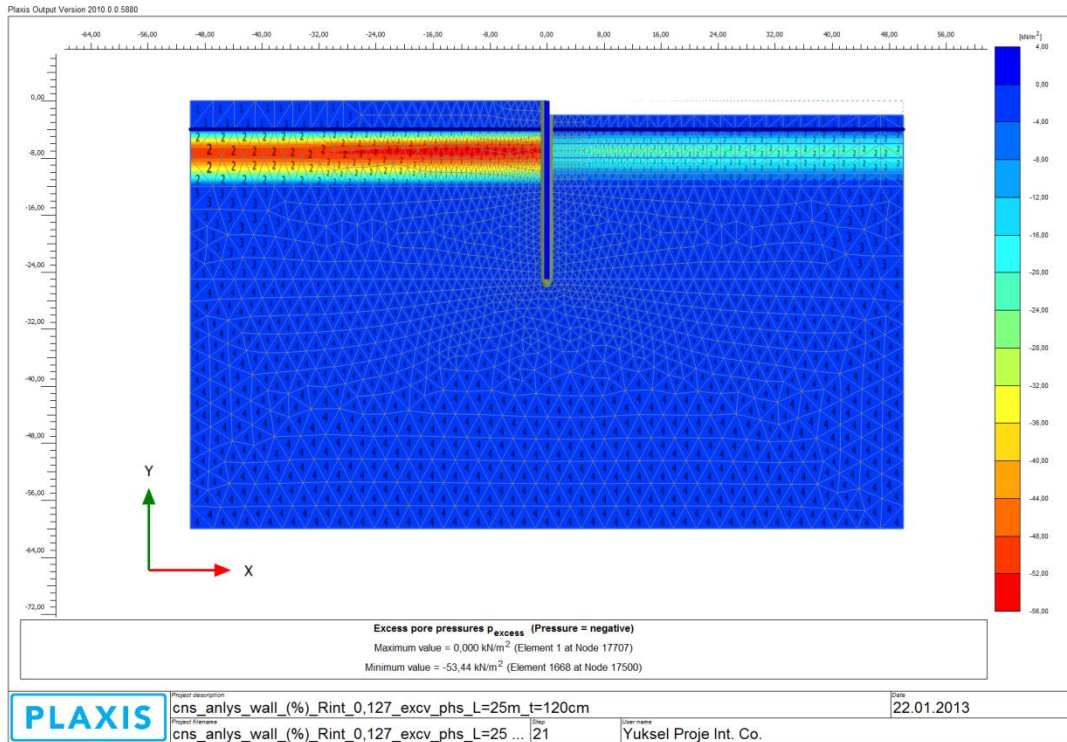


Figure B 18: Average Degree of Consolidation (U) = 25 % (Step 3)

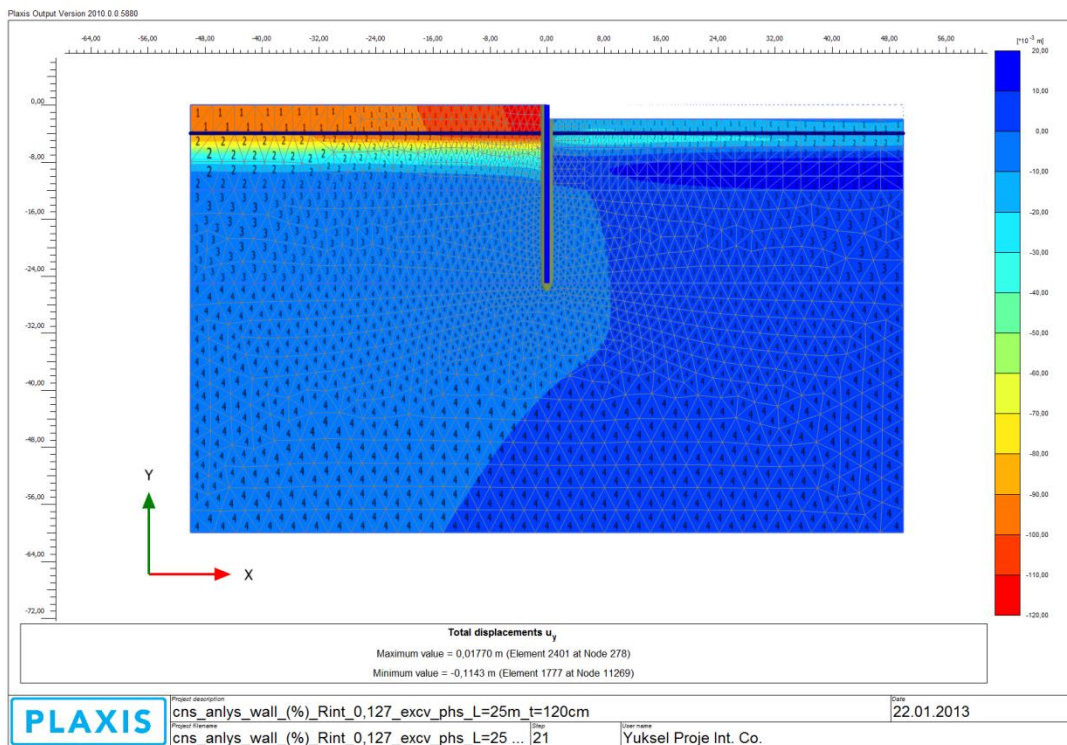


Figure B 19: Total Displacements (u_y) (Step 3)

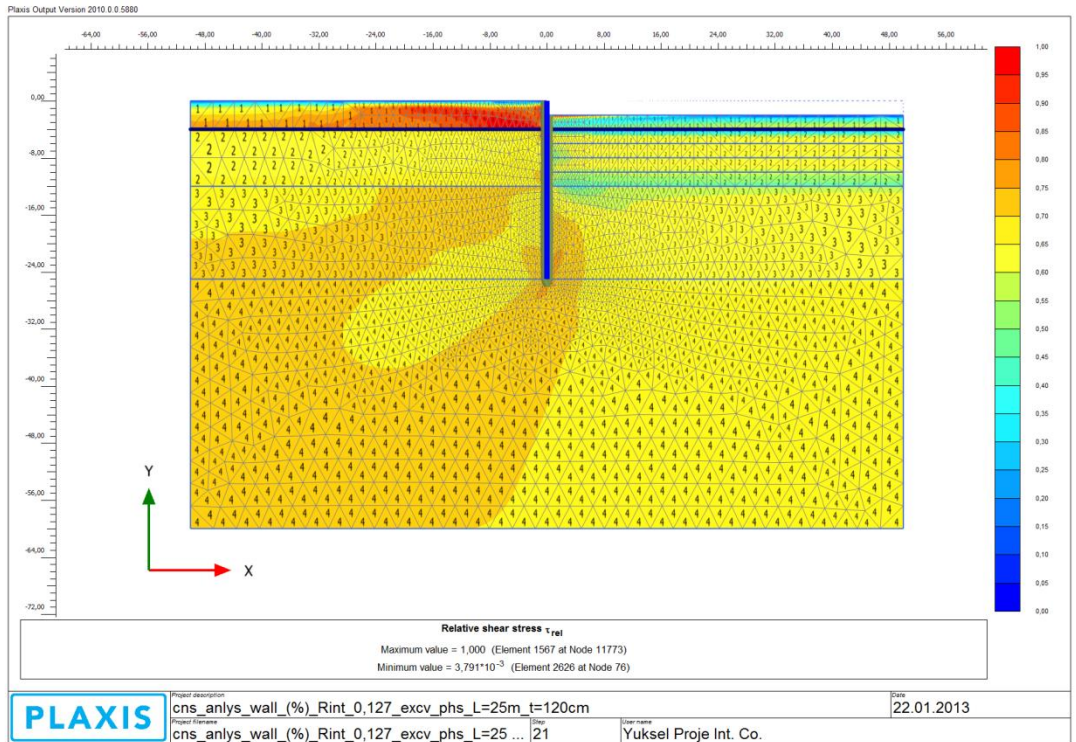


Figure B 20: Relative Shear Stress (τ_{rel}) (Step 3)

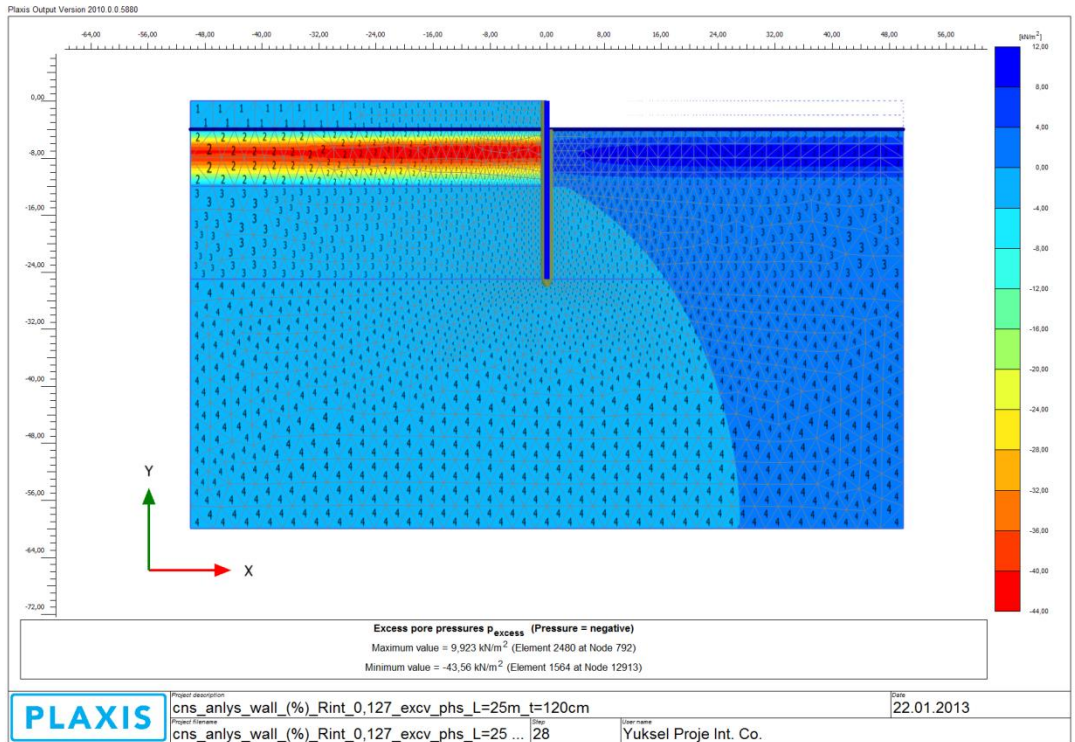


Figure B 21: Average Degree of Consolidation (U) = 40 % (Step 4)

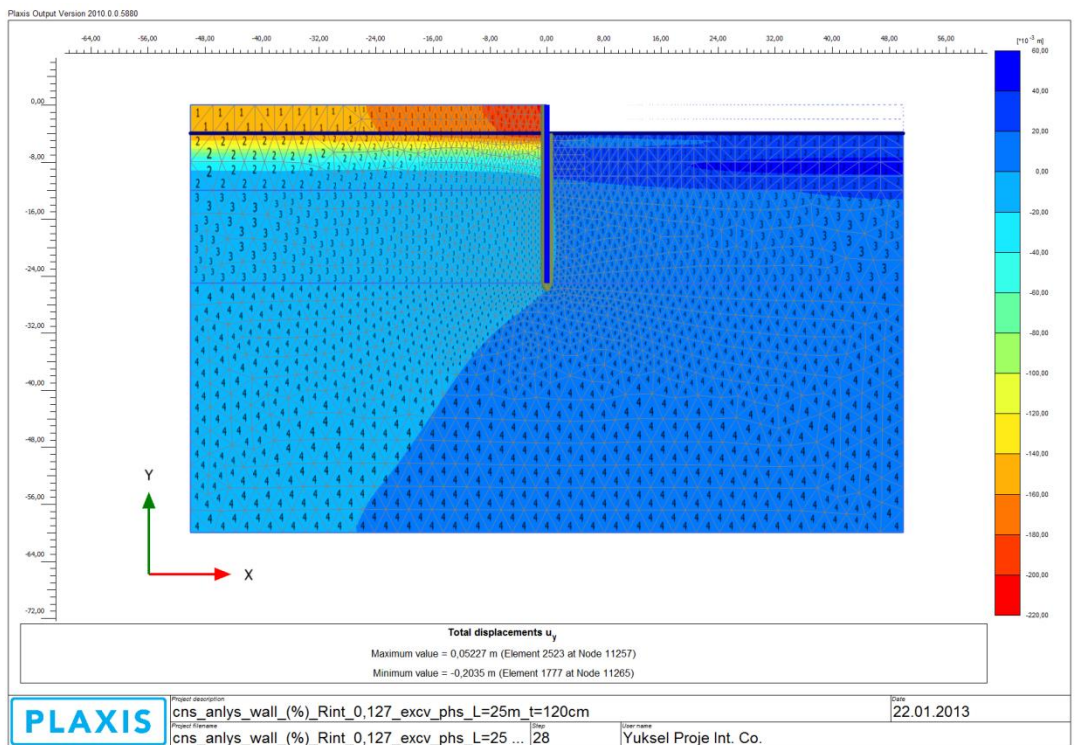


Figure B 22: Total Displacements (u_y) (Step 4)

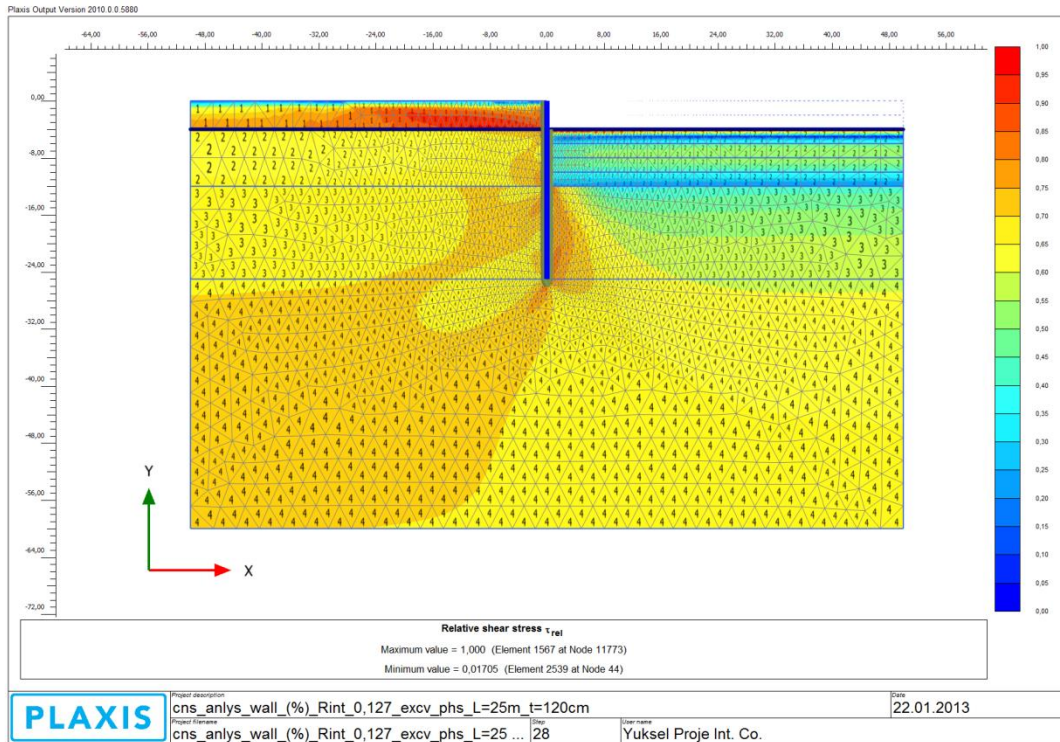


Figure B 23: Relative Shear Stress (τ_{rel}) (Step 4)

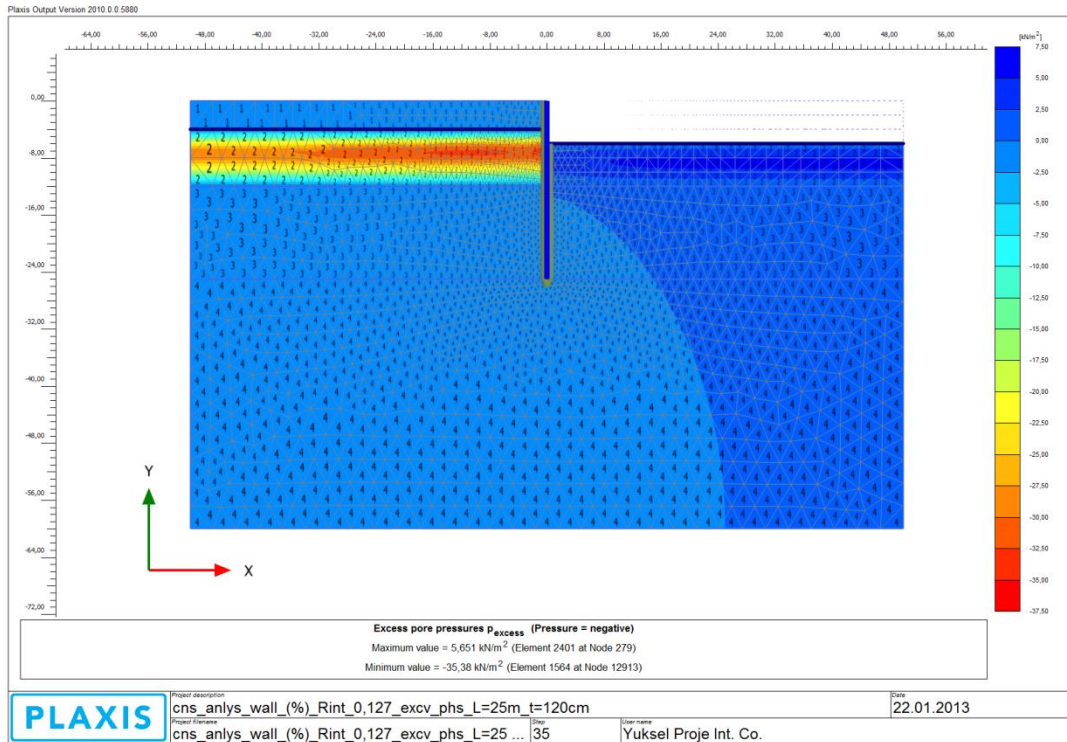


Figure B 24: Average Degree of Consolidation (U) = 55 % (Step 5)

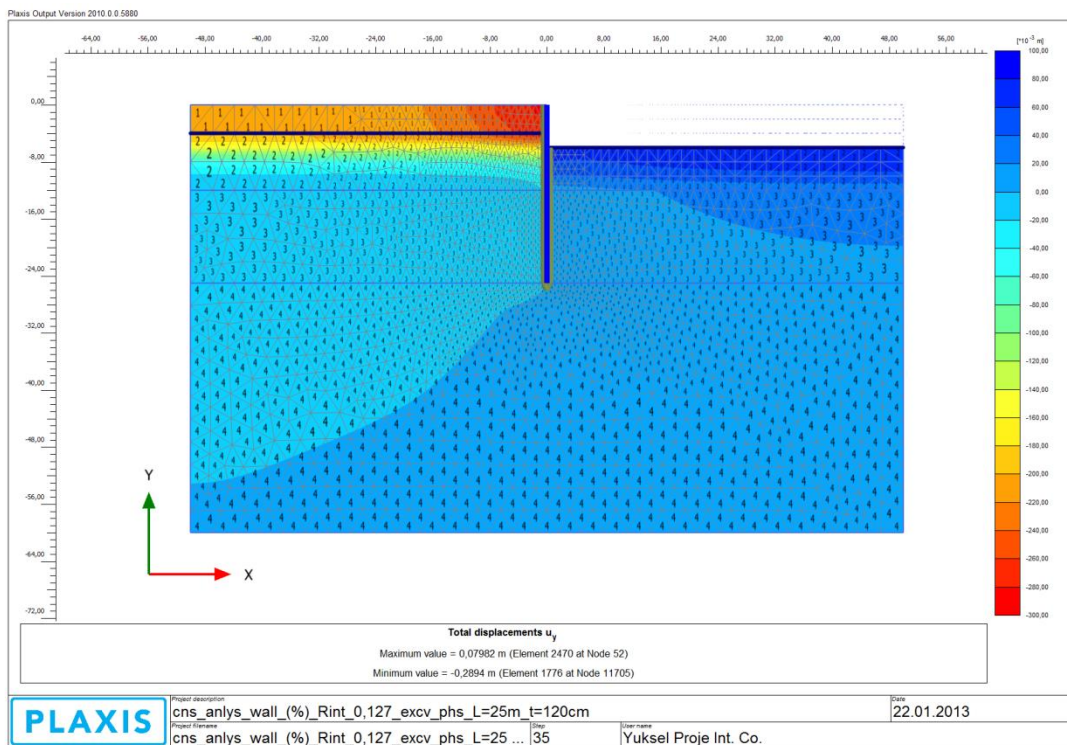


Figure B 25: Total Displacements (u_y) (Step 5)

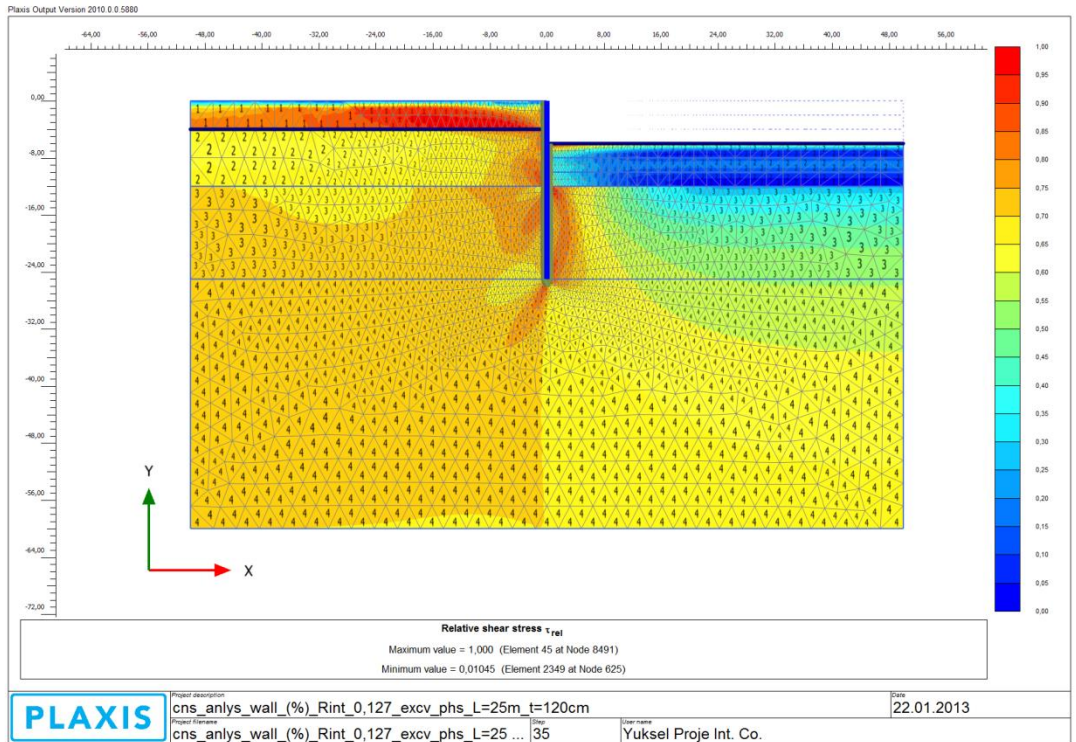


Figure B 26: Relative Shear Stress (τ_{rel}) (Step 5)

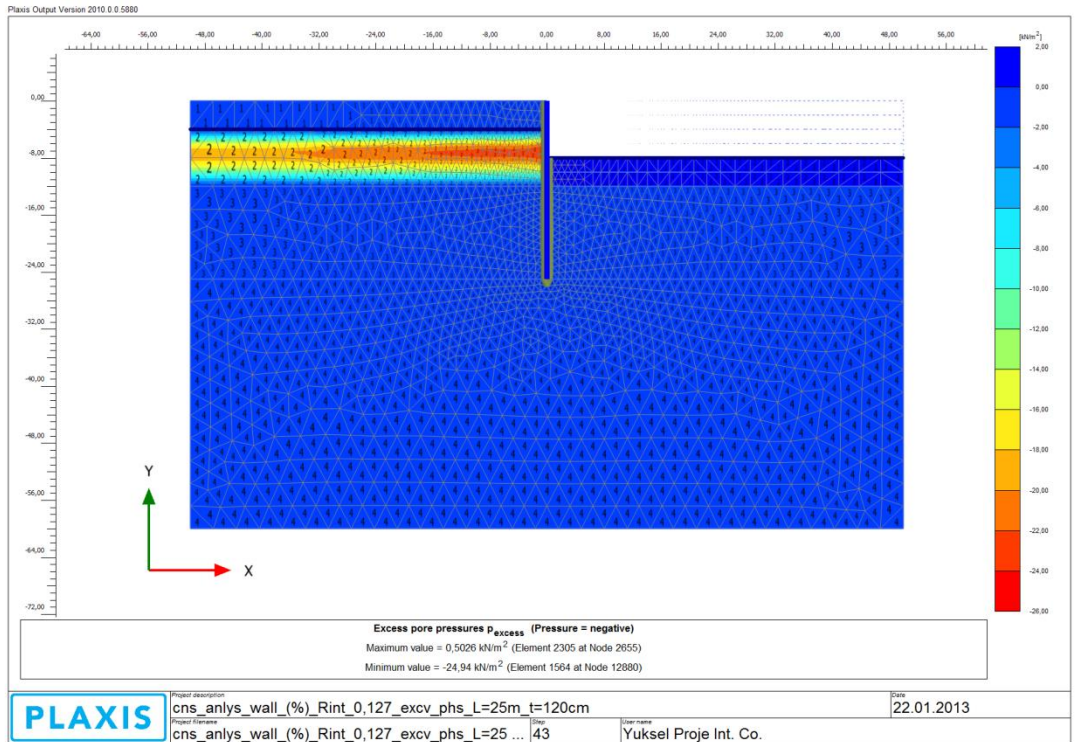


Figure B 27: Average Degree of Consolidation (U) = 70 % (Step 6)

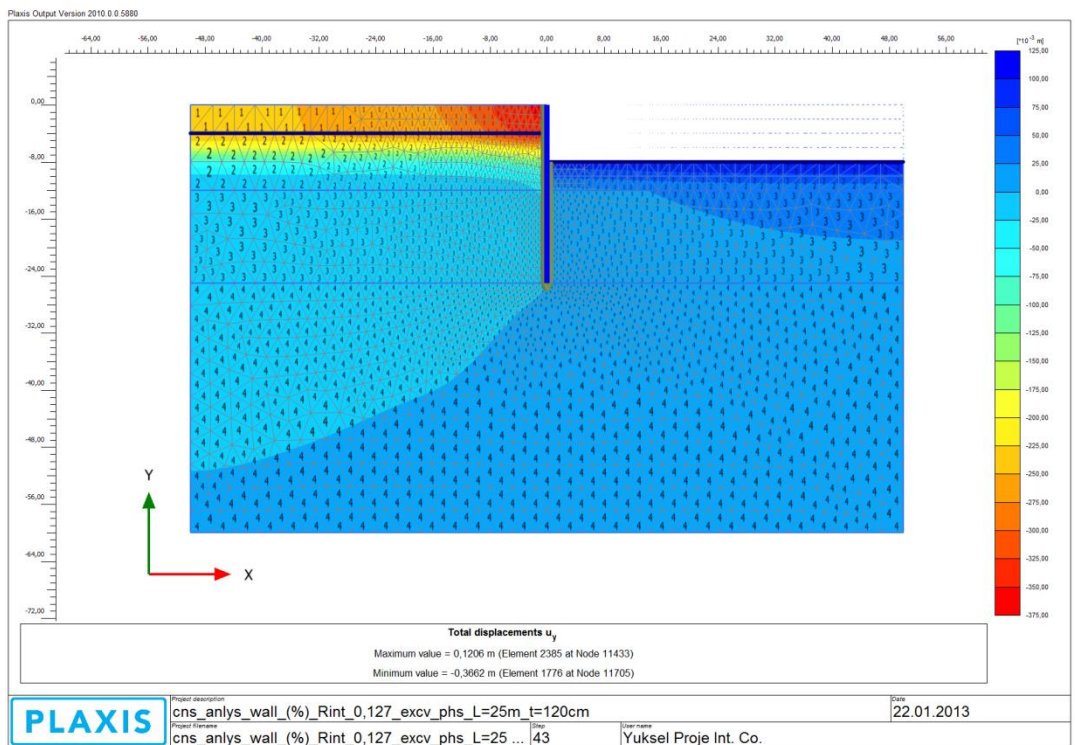


Figure B 28: Total Displacements (u_y) (Step 6)

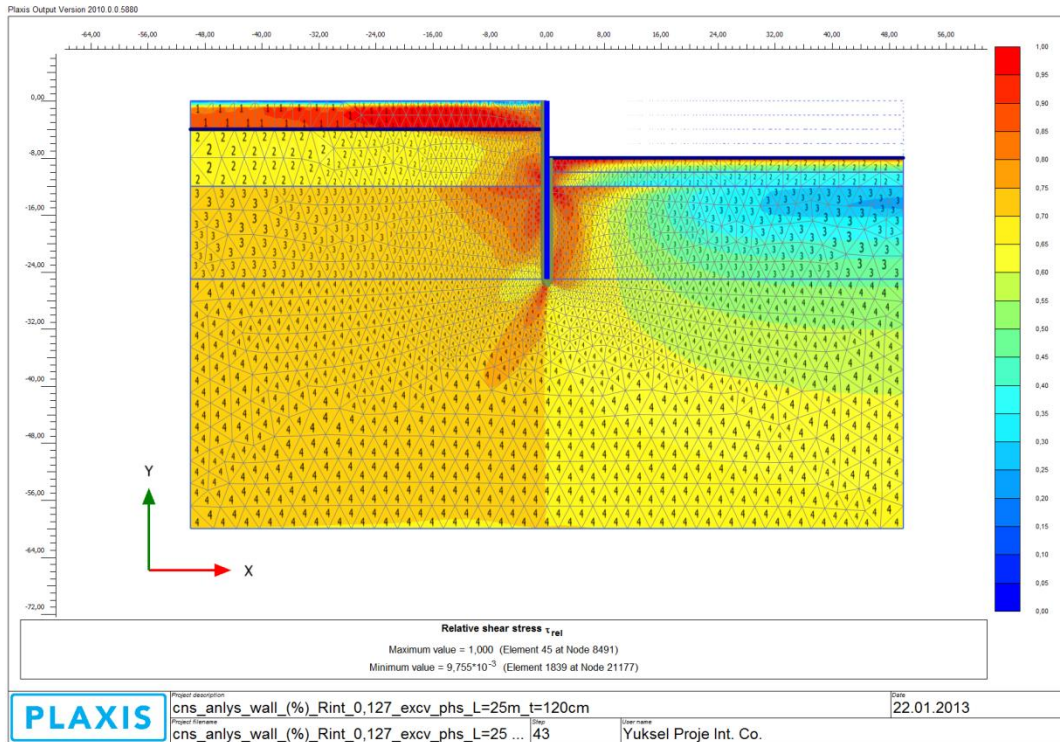


Figure B 29: Relative Shear Stress (τ_{rel}) (Step 6)

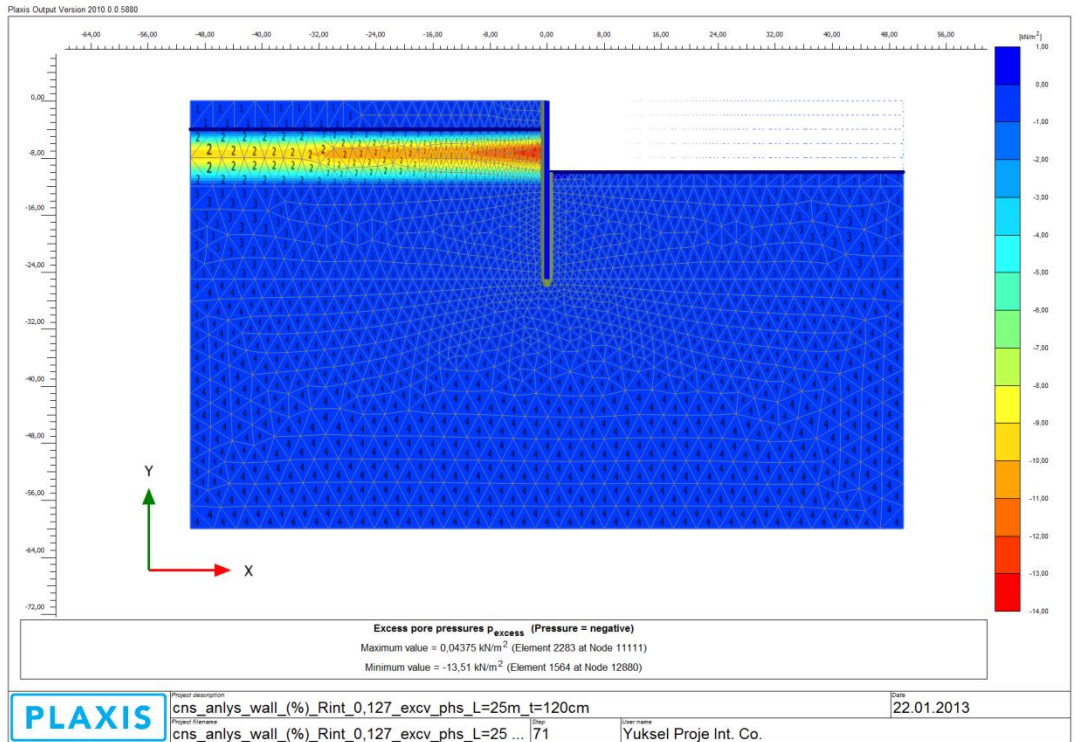


Figure B 30: Average Degree of Consolidation (U) = 85 % (Step 7)

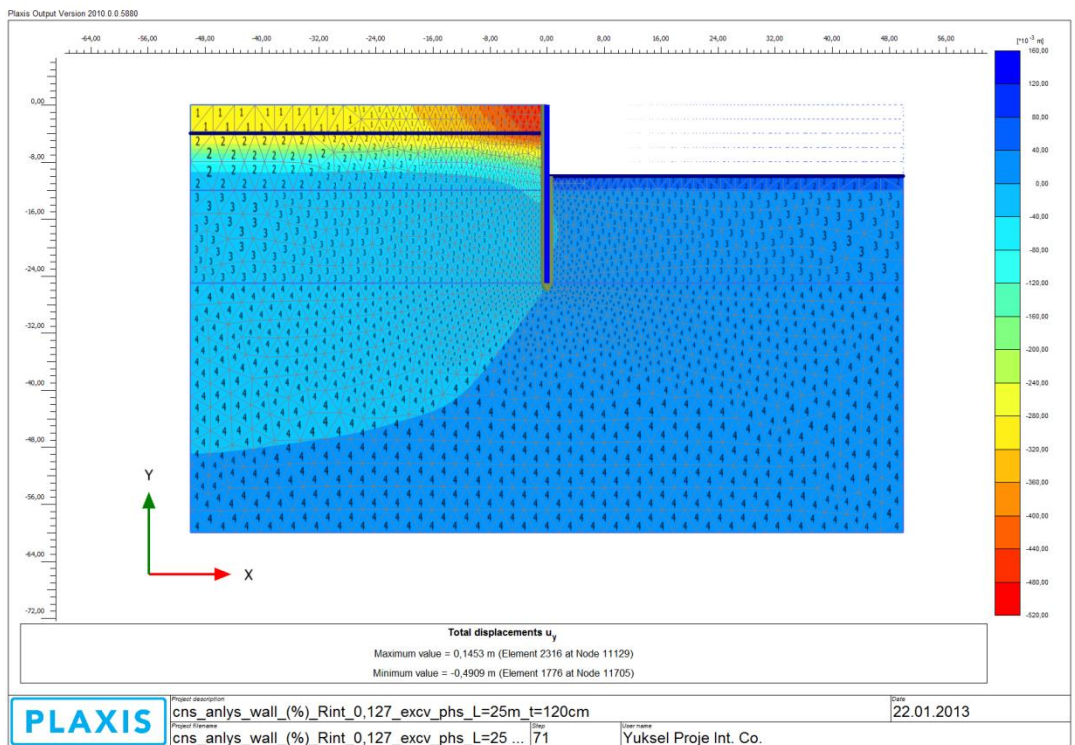


Figure B 31: Total Displacements (u_y) (Step 7)

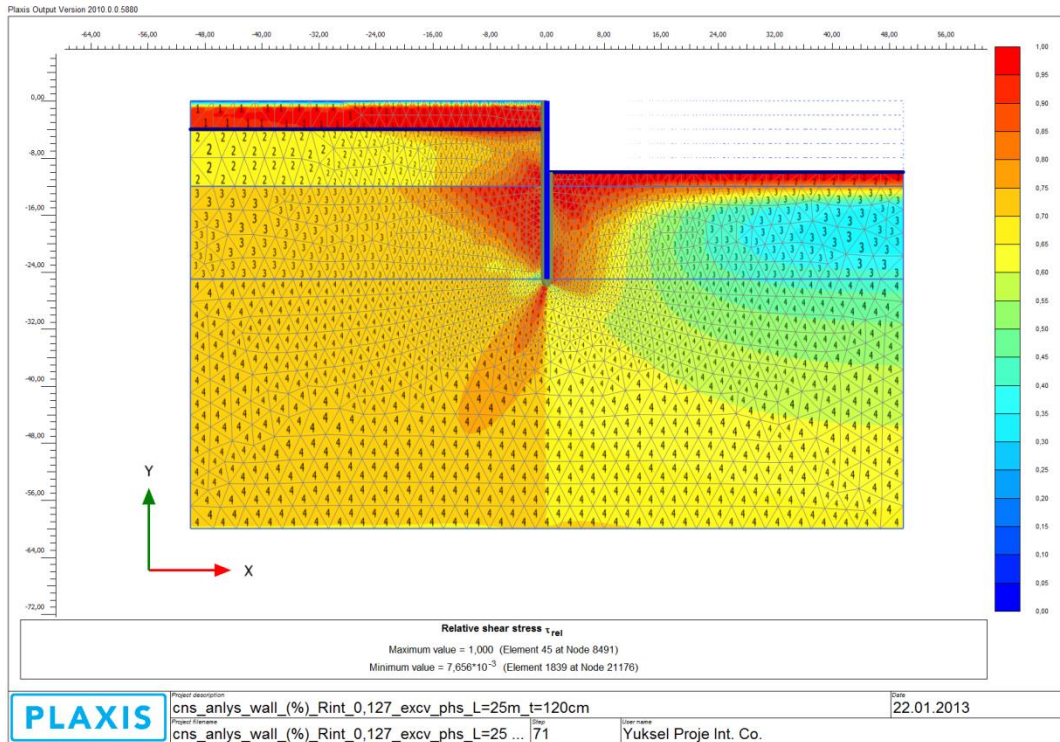


Figure B 32: Relative Shear Stress (τ_{rel}) (Step 7)